UNIVERSITY OF OKLAHOMA

GRADUATE COLLEGE

TARGETING SINGLE-WALLED CARBON NANOTUBES FOR THE TREATMENT OF BREAST CANCER USING PHOTOTHERMAL THERAPY

A DISSERTATION

SUBMITTED TO THE GRADUATE FACULTY

in partial fulfillment of the requirements for the

Degree of

DOCTOR OF PHILOSOPHY

By

LUÍS FILIPE FERREIRA NEVES

Norman, Oklahoma

2012

Downloaded from SHAREOK. Persistent Handle URL: https://hdl.handle.net/11244/319444

TARGETING SINGLE-WALLED CARBON NANOTUBES FOR THE TREATMENT OF BREAST CANCER USING PHOTOTHERMAL THERAPY

A DISSERTATION APPROVED FOR THE
DEPARTMENT OF BIOENGINEERING

BY

_____

Dr. Roger Harrison, Chair

_____

Dr. Wai Yip

_____

Dr. David Schmidtke

_____

Dr. Edgar O'Rear

_____

Dr. Vassilios Sikavitsas

© Copyright by LUÍS FILIPE FERREIRA NEVES 2012
All Rights Reserved.

I dedicate this dissertation to my mother for all of the support and help provided during my years abroad.

ACKNOWLEDGMENTS

An endeavor of this magnitude cannot be completed without the support of and encouragement from my advisor, Dr. Roger G. Harrison. I would like to express my sincere gratitude to him for offering his help and guidance throughout the entire Ph. D. program. I also want to acknowledge all of the members of the committee for their collaboration in being part of my advisory conference and the oral defense.

The work in this thesis was carried out with helpful contributions from some collaborators: Dr. Daniel E. Resasco, Dr. Naveen R. Palwai, Dr. David E. Martyn, Dr. Yongqiang Tan, Dr. Samina Azad, Wesley Tennyson, Mr. Scott Zerger and Dr. Stanley Kosanke. I would like to express my appreciation to the University of Oklahoma International Student Services. I would also like to express my appreciation to Dr. Naveen Palwai who helped me in the lab at the beginning of this research study. I also would like to thank all of the lab mates that I interacted with and provided me with some kind of help.

I am so thankful for the support I received from all my family and friends, in particular my mother for all the motivation that she provided me every single day. Finally, my special thanks go to the Portuguese Foundation for Science and Technology for their support (Grant SFRH/BD/38742/2007).



TABLE OF CONTENTS

ACKNOWLEDGMENTS iv

TABLE OF CONTENTS v

LIST OF TABLES xi

LIST OF ILLUSTRATIONS xii

ABBREVIATIONS xvi

ABSTRACT xix

CHAPTER I 1

INTRODUCTION 1

1. Cancer 2

2. Annexins 5

2.1. Annexin V 5

3. Phosphatidylserine 7

4. Single Walled Carbon Nanotubes (SWNTs) 11

5. Photothermal Ablation for Cancer Therapeutics 16

6. Mechanisms of Attachment of Annexin V to SWNTs using Intermediate Linkers 19

7. Tumoral Morphology and Implications for the Current Therapies 20

8. *In vivo* Studies 22

9. Immunostimulation Therapy of Cancer using Cyclophosphamide 24

10. Experimental Hypotheses and Experimental Design 25

CHAPTER II 29

MATERIALS 29
Bacterial Strains and Plasmids 30
Enzymes 30
E. coli cell Culture Medium 30
Cell Transformation 30
Cell Expression 30
Protein Purification 31
SDS-PAGE 31
Cell Culturing and Cell Counting 31
Binding Assay using Human Endothelial Cells 32
SWNT Suspension Preparation 32
Two-step Coupling of the Protein Annexin V and SWNTs using EDC and NHS. 33
Conjugation of the DSPE-PEG-Maleimide linker to Annexin V Protein 33
Visualization of the SWNT-annexin V Conjugates using Atomic Force Microscopy 33
Labeling of the SWNT-annexin V with FITC 34
Cell Staining and Confocal Microscopy 34
Laser Treatment of Endothelial Cells with SWNT-annexin V on the Cell Surface 34
Assessment of Sterility 34
In Vivo Studies 35
Dissection Studies 35
Histology Studies 35
Biodistribution Study 35

CHAPTER III 36
METHODS 36
Expression, Cell Lysis and Purification of the Recombinant Protein Annexin V .. 37
SDS-PAGE and Amino Acid Sequencing 41
Cell Culturing and Cell Counting 41
Binding Assay using Human Endothelial Cells 43
SWNT Suspension Preparation 43
Two-Step Coupling of the Protein Annexin V and SWNTs using EDC and NHS 45
Conjugation of DSPE-PEG-Maleimide linker to Annexin V protein 46
SWNTs Conjugates Characterization 48
Visualization of the SWNT-annexin V conjugates using Atomic Force Microscopy 48
Labeling of the SWNT-annexin V with FITC 48
Cell Staining and Confocal Microscopy 49
Laser Treatment of Endothelial Cells with SWNT-annexin V on the Cell Surface 50
Optical pictures 53
Assessment of sterility 53
In vivo Studies 54
Dissection Studies 57
Biodistribution study 58
CHAPTER IV 61
RESULTS AND DISCUSSION 61
Overexpression and Purification of Annexin V 62

Binding Assay using Human Endothelial Cells 63
Characterization of SWNT Suspensions 65
Two-step Coupling of the Annexin V and SWNTs using EDC and NHS 71
Conjugation of the DSPE-PEG-Maleimide linker with the SWNT-annexin V 72
Visualization of the SWNT-annexin V Conjugates using Atomic Force Microscopy (AFM) 73
Visualization of Binding of SWNT-annexin V to Proliferating Endothelial Cells 75
Laser Treatment of Endothelial Cells with SWNT-annexin V on the Cell Surface 76
Optical Pictures 80
Assessment of Sterility 81
Effect of Sonication on the Optical Absorption of SWNTs 81
In vivo Studies 82
Biodistribution Study 94
CHAPTER V 99
CONCLUSIONS AND FUTURE STUDIES 99
Conclusions and Future Studies 100
LIST OF REFERENCES 105
APPENDICES 114
APPENDIX A 115
A.1. Laboratory Protocols 115
A.1.1. Luria Bertani (LB) medium 115
A.1.2. LB agar 115
A.1.3. Additives: 116

A.1.4. Kanamycin preparation 116
A.1.5. IPTG preparation (10 mg/ml) 116
A.1.6. Sonication buffer preparation 117
A.1.7. Sonication protocol (4 ºC) 117
A.1.8. HRV 3C protease 118
A.1.9. Tris-HCl 118
A.1.10. Acrylamide (29%) Bis (1%) 119
A.1.11. Electrophoresis buffer 119
A.1.12. Ammonium persulfate preparation 119
A.1.13. Cell Medium Preparation 119
A.1.14. PBS preparation 120
A.2 Experimental Protocols 121
A.2.1. Transformation Protocol 121
A.2.2. Bradford protein assay 125
A.2.3. SDS-PAGE analysis of proteins 127
A.2.4. Freeze dryer protocol 131
A.2.5. Determination of the SWNT calibration curve 134
APPENDIX B 136
APPENDIX C 137
APPENDIX D 138
APPENDIX E 140
APPENDIX G 146
APPENDIX H 151

APPENDIX I 155
APPENDIX J 156
APPENDIX K 159
APPENDIX L 162
APPENDIX M 165
APPENDIX N 168
APPENDIX O 169
APPENDIX P 172
APPENDIX Q 174
APPENDIX R 176
APPENDIX S 178
APPENDIX T 180

LIST OF TABLES

CHAPTER IV

RESULTS AND DISCUSSION

1. Data generated by Graphpad software in the determination of K_d for the binding of annexin V to endothelial cells ……..…… 64

2. Mean length of SWNT after sonication for different time periods … 69

3. Histogram distributions for the SWNTs length ……. 70

4. Protein and SWNTs concentrations after conjugation using the linker containing FMOC ……..…….. 72

5. Protein and SWNT concentrations after conjugation using the linker containing DSPE ……..…… 73

6. Summary of the *in vivo* safety test ……. 83

7. Metastatic nodules evaluation …… 89

8. Histological analysis obtained for specimens collected from six animals ……... 92

APPENDIX

A.1. LB medium composition ……..……. 115

A.2. LB Agar / SOC medium composition (per Liter) ……....… 115

A.3. Kanamycin properties ……..…….. 116

A.4. Reagents required for the casting of mini-SDS-PAGE (sodium dodecyl sulfate-polyacrylamide gel electrophoresis) gels ……. 128

A.5. Marker molecular weights ……..……...…… 130

LIST OF ILLUSTRATIONS

CHAPTER I

INTRODUCTION

1. Leading sites of new cancer cases and deaths ……...…… 3

2. *Homo sapiens* annexin V crystal structure ……. 6

3. Molecular organization of phosphatidylserine (PS) …….. 8

4. Fitting of the S_{11} absorption spectrum for SWNT sample ……. 14

5. A single walled carbon nanotube wrapped with PEG ……... 16

6. SDS structure ……. 19

7. FMOC-NH-PEG-NHS linker structure …….……..…… 20

8. Chemical structure of the DSPE-PEG-Maleimide linker ....……..... 20

9. Chemical reaction between a maleimide group and a cysteine ……. 20

10. Picture of a BALB/cJ mouse …… 22

11. Body weight information for the JAX® mice strain BALB/cJ ….. 23

12. Schematic diagram showing the global mechanism of this study ... 28

CHAPTER III

METHODS

13. Protein purification flow diagram …… 40

14. SWNTs suspended in sodium cholate …….. 44

15. The disposition of the samples within the 24-well plate …….. 51

16. Chemical mechanism illustrating the reduction of the resazurin dye …….. 53

17. General view of a dissected mouse prior to organ extraction …….. 57

IV. RESULTS AND DISCUSSION

18. SDS-PAGE analysis using a 12 % gel of purified annexin V ……. 63

19. Total, specific and non-specific binding of biotinylated annexin V to human endothelial cells *in vitro* on a 24-well plate with 1 mM H_2O_2 added to expose PS on the cell surface …….. 64

20. NIR absorbance spectra (normalized) …….. 67

21. Absorbance at 800 nm vs. SWNT concentration plot …….. 68

22. Raman spectrum of the SWNT-annexin V conjugate, where it is visible the characteristic peak at 1590 cm^{-1} ……... 69

23. AFM analysis ……... 74

24. Endothelial cells stained with the CellMask™ Plasma Membrane stain …… 75

25. Assessment of the "safe region" to operate the laser system without the presence of cytotoxicity effects induced by the laser itself. 77

26. Effect on cell viability of incubation for 2 h of non-confluent endothelial cells with the SWNT-annexin V conjugate prepared with either 1 h or 6 h of sonication time …… 79

27. Optical pictures of human endothelial cells taken before and after a laser treatment of cells that had been incubated with SWNT-annexin V ……. 80

28. UV-Vis-NIR absorbance spectra (normalized at 780 nm) ……... 82

29. Treatment of BALB/cJ mice with implanted 4T1 mouse mammary

tumors …… 86

30. Survival curve for the in vivo study…….. 87

31. Pictures of two mice from the *in vivo* study ……..... 88

32. Histological images for different specimens collected from one of the animals from the untreated and treated groups …… 91

33. Raman spectrum for a SWNT suspension with a known nanotube concentration …….. 95

34. Raman spectrum acquired for a liver sample ……... 96

35. Biodistribution of SWNT-annexin V 24 hours post administration evaluated by FT-Raman spectroscopy…… 98

APPENDIX

A.1.1. Sonication process …….. 117

A.2.2.1. Bradford protein assay ……..... 127

A.2.2.1. Bradford protein assay ……. 127

A.2.5.1. SWNT calibration curve …….. 135

D.1. EDC reacts with carboxylic acids to create an active-ester intermediate …… 139

J.1. Photograph of hemacytomer …..……. 156

J.2. Photograph of hemacytomer ..……. 157

J.3. Neubauer Ruling …….. 158

R.1. Illustration showing the method used for the i.p. injections …….. 177

S.1. Mouse tail anatomy …….…… 179

T.1. Standard curve as a function of the G band peak intensity at 1,590

cm^{-1} vs. nanotube concentration ……..... 181

ABBREVIATIONS

AFM – Atomic force microscopy

ANOVA – Analysis of variance

BSA – Bovine serum albumin

CCD – Charge-coupled device

CT – Computer tomography

CTLA-4 – Cytotoxic T lymphocyte-associated antigens 4

CY – Cyclophosphamide

DMF – Dimethylformamide

DSPE – 1,2-Distearoyl-phosphatidyl ethanolamine

DNA – Deoxyribonucleic acid

E. coli – *Escherichia coli*

EDC – 1-Ethyl-3-[3-dimethylamonopropyl] carbodiimide hydrochloride

EDTA – Ethylenediaminetetraacetic acid

FDA – Food and Drug Administration

FITC – Fluorescein isothiocyanate

FMOC – Fluorenylmethyloxycarbonyl

FT – Fourier transform

GC – Glycated chitosan

Ge – Germanium

H_2O_2 – Hydrogen peroxide

His – Histidine

HRP – Horseradish peroxidase

HRV – Human Rhinovirus

IMAC – Immobilized metal affinity chromatography

i.p. – Intraperitoneal

IPTG – Isopropyl-beta-D-thiogalactopyranoside

i.v. – Intravenous

$\mathbf{K_d}$ – Dissociation constant

LB – Luria-Bertani

mAbs – Monoclonal antibodies

MES – 2-(N-morpholino)ethanesulfonic acid

MWNTs – Multiple walled carbon nanotubes

NHS – N-hydroxy-succinimide

NIR – Near-infrared

OPD – O-phenylenediamine

PBS – Phosphate buffer saline

PEG – Poly(ethylene glycol)

PET – Positron emission tomography

pH – Potential hydrogen

PMSF – Phenylmethylsulfonyl fluoride

PS – Phosphatidylserine

RES – Reticuloendothelial system

RFP – Red fluorescent protein

RFU – Relative fluorescence units

SCID – Severe combined immune deficiency

SDS – Sodium dodecyl sulfate

SDS-PAGE – Sodium dodecyl sulfate polyacrylamide gel electrophoresis

SWNT – Single walled carbon nanotube

TNFα – Tumor necrosis factor-alpha

Treg – Regulatory T cell

UV – Ultraviolet

Vis – Visible

TARGETING SINGLE-WALLED CARBON NANOTUBES FOR THE TREATMENT OF BREAST CANCER USING PHOTOTHERMAL THERAPY

LUÍS FILIPE FERREIRA NEVES

ABSTRACT

To develop a therapeutic system with cancer cell selectivity, the present study evaluated a possible specific and localized tumor treatment. Phosphatidylserine (PS) exposure on the external face of the cell membrane is almost completely exclusive to cancer cells and endothelial cells in the tumor vasculature. The human protein annexin V is known to have strong calcium-dependent binding to anionic phospholipids such as PS. This protein was studied for targeting single-walled carbon nanotubes (SWNTs) to the vasculature of breast tumors.

The synthesis of the protein annexin V, by a pET vector in *Escherichia coli*, constitutes the first phase of this study. Recombinant annexin V was purified from the cell lysate supernatant by immobilized metal affinity chromatography. The overall production of purified annexin V protein was 50 mg/L.

The binding ability of the protein annexin V was evaluated by determining the dissociation constant when incubated with proliferating human endothelial cells *in vitro*. The dissociation constant, K_d, was measured to be 0.8 nM, indicating relatively strong binding. This value of K_d is within the range reported in the literature.

Single-walled carbon nanotubes (SWNTs) were functionalized with annexin V using two intermediate linkers (containing FMOC and DSPE) resulting in stable suspensions. The SWNT and protein concentrations were 202 mg/L and 515 mg/L, respectively, using the linker with DSPE (average of nine preparations). The conjugation method that used the DSPE-PEG-maleimide linker allowed to successfully conjugate the SWNTs with final concentrations approximately five times higher than the linker containing FMOC. The conjugation method used has a non-covalent nature, and therefore the optical properties of the nanotubes were preserved.

The conjugate was also visually observed using atomic force microscopy (AFM), allowing to verify the presence of the protein annexin V on the surface of the nanotubes, with an height ranging between 2.5 to 5.0 nm. Confocal microscopy was used to prove the binding of the conjugates to human endothelial cells grown *in vitro*.

Proliferating endothelial cells were used to determine the optimal near-infrared (NIR) laser irradiation settings (energy density = 200 J/cm^2), which would not induce cell cytotoxicity from the laser itself. A 2 hour incubation with the conjugate followed by a washing step and NIR irradiation (wavelength = 980 nm, power = 1 W/cm^2, time = 200 seconds) was enough to induce significant cell death (≈ 55 %), without significant damage to the control samples.

Administration of the same conjugates i.v. in Balb/cJ female mice resulted in detectable accumulation of the SWNTs in the tumor tissues, with minimal retention in the kidneys 24 hours post-administration. A dosage of 0.82 mg/kg of SWNTs administered i.v. and followed one day later by a NIR irradiation (wavelength = 980 nm, power = 1 W/cm^2, time = 175 seconds) led to complete disappearance of implanted

4T1 mouse mammary tumors for the majority of the animals from the treatment groups, within a few days. The combination of the photothermal therapy with a low dosage (50 mg/kg) of the immunoadjuvant cyclophosphamide, given 2 days before NIR irradiation, was also evaluated; this resulted in increased survival. Histological findings revealed the complete obliteration of the tumors treated from the original site, with complete regeneration of the skin epithelial layer and absence of cancer cells.

In conclusion, this research was successful in demonstrating that SWNTs could be targeted to the tumor vasculature *in vivo* and then could be heated by NIR irradiation to completely kill mouse mammary tumors implanted in immune-competent mice. There is evidence that the co-administration of the immunostimulant cyclophosphamide caused increased survival of the mice. It is recommended that future work be directed to exploring methods to increase the concentration of the SWNT-annexin V conjugate in the tumor and to evaluate the co-administration of other immunostimulants, either alone or in combination.

CHAPTER I

INTRODUCTION

1. Cancer

Cancer can be defined as a group of diseases characterized by an uncontrolled cell division, invading the adjacent or distant tissues (metastasis) [2]. Being considered the world's most complex disease process, it is related to 100 or more single diseases [3]. There are several possible environmental factors that can induce cancer, such as exposure to radiation, hereditary factors, viruses, smoke, alcohol, dietetic habits, contributing to approximately 80 % of cancers [3, 4]. Cancer can exhibit different symptoms, although it can be asymptomatic until advanced stages. Risk factors include geography, ethnicity, dietary habits, age, and hereditary genes that increase the predisposition for cancer.

Based on the statistics, the frequency of a specific cancer may depend on gender [5]. According to the American Cancer Society 1,639,000 new cancer cases are expected to be diagnosed in 2012, excluding carcinoma *in situ* (noninvasive cancer) of any site (except urinary bladder) and basal and squamous cell skin cancers. Being considered the second leading cause of death in the U. S., statistics confirm that there are more than 1,500 persons dying per day as victims of cancer [6]. The most common types of cancer in the U.S. are the prostate cancer and breast cancer (Figure 1).

Leading New Cancer Cases and Deaths – 2012 Estimates

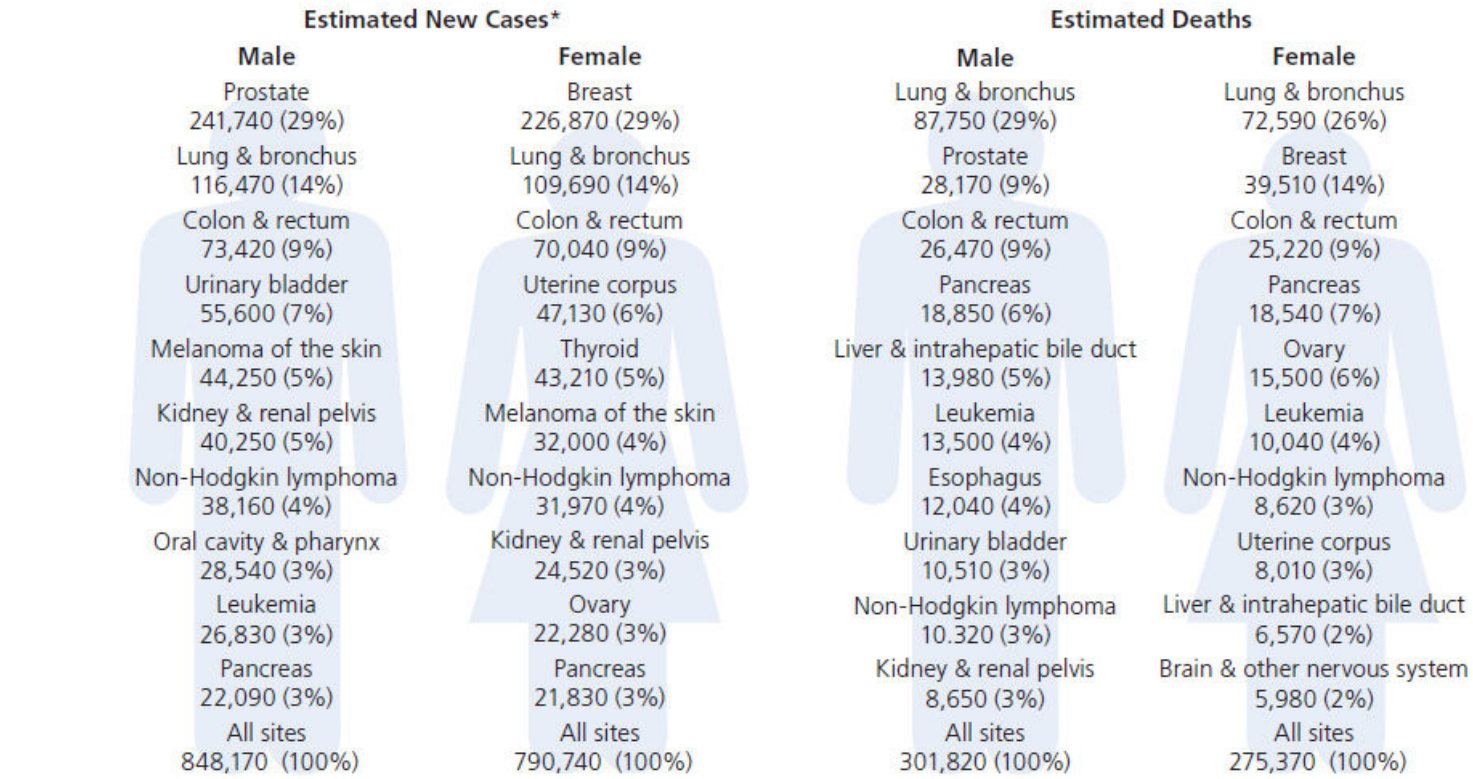


Figure 1: Leading sites of new cancer cases and deaths. *Excludes basal and squamous cell skin cancers and in situ carcinoma except urinary bladder [6].

In order to perform cancer treatment, there is an inherent difficulty in distinguishing malignant cells from normal cells. Both of them share the same origin, which helps explain the fact that cancer cells are not significantly recognized by the immune system.

Generally, the treatment results from the combination of different therapeutic techniques, such as surgery and chemotherapy [2]. According to some studies, these techniques can be very efficient; however, they carry associated-side effects for the patient [2]. A specific case is chemotherapy, based on the introduction of chemical substances in the bloodstream in order to control cell processes. The side effects associated with this therapy are related to the collateral destruction of normal cells [2]. When manifested, examples of these effects are anxiety, anemia and fatigue due to the red blood cells decreasing, diminution of white cells and platelets, renal perturbations, digestive system alterations and loss of appetite, and increase in weight, alopecia, in addition to other symptoms.

Because of the need for an improved system to treat cancer, the general goal of this study is to eradicate all cancer cells in the body, while not affecting healthy cells. By specifically targeting cancer cells, the side effects associated with the conventional therapeutic methods are avoided. The development of a system with intra-venous administration allows a global spread through the entire body, eliminating the conventional problems of localization and treatment of metastatic regions [2]. In this study, the protein annexin V which has PS-binding properties is used as targeting moiety. It is a very important marker for cancer cells, since cancer cells and endothelial

cells in the tumor vasculature expose PS on the external leaflet of the plasma membrane.

2. Annexins

The annexins are a group of proteins with similar properties [7, 8] that were initially named by Geisow [7, 9]. This name is derived from the Greek *annex* meaning "bring/hold together" [10]. The annexins are different proteins, with a common C-terminus attached to an amino acid repeated domain, although presenting a unique N-terminal domain [7, 8, 10, 11].

Discovered by Pazoles, Creutz and Polland approximately 34 years ago at the National Institute of Health [12], the annexins are a protein family comprised of 12 different proteins with a common important characteristic – the affinity binding of a phospholipid to Ca^{2+} [7, 8, 10, 11, 13-15]. These calcium-dependent membrane binding proteins [8, 16] are involved in the membrane-related processes of exocytosis [11], adhesion, fusion and remodeling of the plasma membrane [16, 17], phospholipase regulation, cytoskeletal organization [11], cell growth, and transformation [8]. Adhesion mechanics, membrane traffic [8, 11, 15], signal transduction [11] and/or developmental process are other proposed functions [18].

2.1. Annexin V

Annexin V, a monomeric protein [19], has a structure with four homologous repeated domains. It is a non-glycosylated protein, although it has potential O-glycosylation sites (without N-linked glycosylation sites) [20], and it has a single

cysteine four residues from the C-terminus. *In vitro* studies show that annexin V reveals an ion channel activity, binding in a calcium-dependent manner to acidic phospholipids (e.g., phosphatidylserine [12, 21-23]).

The annexin V molecule is believed to have three Ca^{2+} binding sites (Ca1 to Ca3) [24], situated at the convex face of the molecule as possible phospholipid binding sites [15], which have structural similarity to the calcium site present on phospholipase A_2. Huber et al., concluded that membrane-bound and soluble annexin V present very similar structures, since the membrane-anchoring region is located on the convex face [24]. It has been proposed that it is involved in exocytosis [12, 15, 25], anti-coagulation [10, 25, 26], anti-inflammation [25], anti-thrombotic processes [10, 16], and cell differentiation or replication [15, 25].

Annexin V has a single polypeptide chain that is 320 amino acids long (Appendix B) [15, 27] (including the first methionine) with an evaluated molecular mass of 35,935 Da [27] and dimension of 64 x 40 x 30 $Å^3$ [16], folded into four domains of similar structure arranged in an almost planar cyclic array [10, 24]. Each domain is composed of five α-helices with an approximately 18 Å diameter (Figure 2).



Figure 2: *Homo sapiens* annexin V crystal structure. The ribbon drawing illustrates the highly α-helical folding of the protein core that forms a slightly curved disk. Different colors were chosen to highlight the four annexin repeats that are given in green (repeat

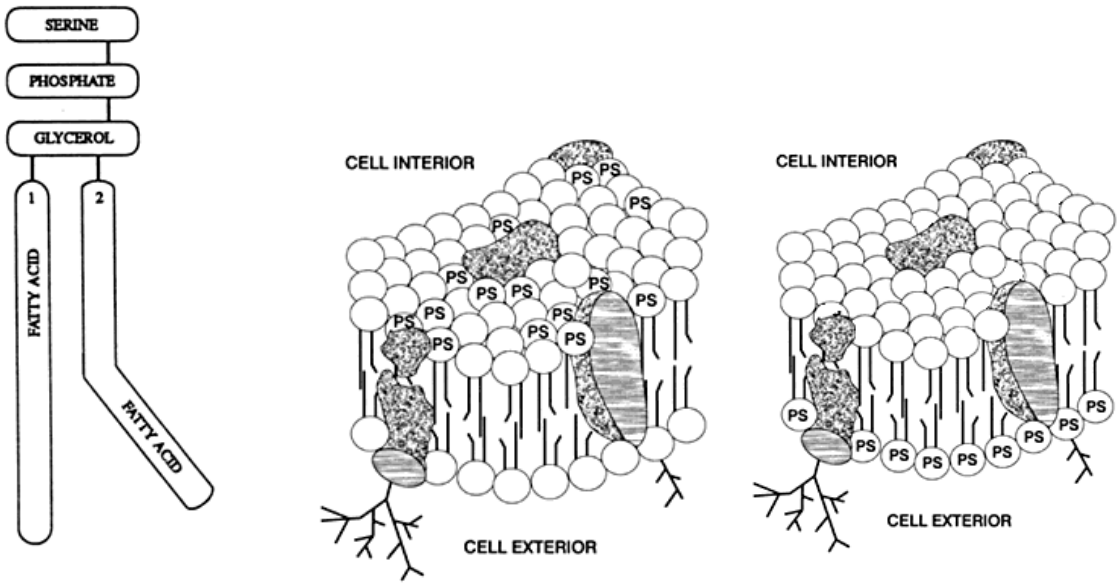
I), blue (repeat II), red (repeat III), and violet/cyan (repeat IV). The NH_2-terminal domain appears unstructured and extends along the concave side of the molecule (green). The high and low Ca^{2+} forms are shown in a superposition revealing the conformational change in repeat III, which leads to an exposure of Trp-187 (violet for the low and cyan for the high Ca^{2+} form). Bound Ca^{2+} atoms are depicted as yellow spheres [10].

Annexin V is a member of calcium-dependent phospholipid binding proteins [13, 22, 28] with a high binding affinity (K_d = 0.5-7 nM - dissociation constant) [26] to PS-containing phospholipid bilayer [26, 29-33]. According to its intrinsic properties, annexin V can be used as an apoptotic cell marker. When combined with a radioisotope or fluorochrome [28], it constitutes a powerful imaging system [28, 33, 34]. Annexin V constitutes the basis for a sensitive flow cytometric assay for cells undergoing apoptosis [21, 34]. Diseases and mechanisms, such as heart failure, aplastic anemia, or transplant rejection, involve high apoptosis occurrence; therefore, it is possible to image them using annexin V [21]. In this study, we used *E. coli* in order to express annexin V, since in that system annexin V can be very easily expressed in a soluble form with the great advantage of non-fusion with another protein [15].

3. Phosphatidylserine

Phospholipids are a major structural component of the cell membrane and can be involved with some cancer signaling [17]. Phosphatidylserine (PS) is an anionic phospholipid that, in normal cells, is exclusively present and tightly segregated in the

internal leaflet of the plasmatic membrane [11, 35-40]; i.e., it presents an asymmetric and heterogeneous distribution [41, 42] (Figure 3). That characteristic asymmetry [35] is maintained by a particular enzyme – aminophospholipid translocase – that transports PS to the cytoplasm [35, 41, 43, 44]. When the cell is under certain conditions, the PS is transported from the cytoplasm to the external leaflet of the membrane [28], by activation of a Ca^{2+}-dependent enzyme scramblase (responsible for the bi-directional lipids transport) or by inhibition of the aminophospholipid translocase [41, 43].



(a) **(b)** **(c)**

Figure 3: (a) Molecular organization of phosphatidylserine (PS). **(b)** PS is preferentially distributed in the inner leaflet of the cell membrane in normal cells. **(c)** PS is externalized on the cell surface of endothelial cells in tumor vasculature [45].

When normal cells are exposed to some stress conditions, they undergo oxidative stress that can be caused by the presence of cancer cells. It is known that hypoxia/reoxygenation conditions and the presence of activating cytokines [46], leukocytes and metabolites [47] are preponderant factors of cell stress. This specific stage induces the production of reactive oxygen species. The ensuing oxidation of membrane phospholipids and the generation of calcium fluxes [35] will also provoke the inhibition of aminophospholipid translocase and/or activation of PS exporters [48].

The exposure of the cells to reactive oxygen species can contribute to the activation of several factors that promote the occurrence of apoptosis [4, 49]. Therefore, it is possible to conclude that the PS can be considered abundant, accessible [47] and a marker of apoptosis [36, 49], being a facilitator of macrophage phagocytosis of apoptosis cells [28, 33, 42, 47]. Research has proven that when the cell is exposed to necrosis factors, the PS is also exposed on the external leaflet of the plasma membrane [36]. PS plays an important role in aging, blood coagulation, cell-cell recognition, and apoptosis [34, 41, 49].

The evidence that endothelial cells present in the tumor vasculature externalize PS [36, 46] is an important and basic idea to the development of this study. The notion that exclusivity, i.e. the exposure of PS, does not occur in normal cells contribute to the development of an efficient and localized therapeutic and imaging system [46] that allows for precise tumor localization.

In mammalian cells, a higher concentration of PS–an excellent marker of tumor vasculature [36, 46]–is observed in the plasma membrane in comparison with the other cell organelles, also being the most abundant lipid of the plasma membrane [36]. The

increasing platelet procoagulant response verified in certain tumors is considered one contributing factor in the translocation of PS to the external leaflet of the membrane [50-52]. The presence of thrombin [35, 36, 53], viral infection [54], hyperlipidemia [55], inflammatory cytokines [36], hydrogen peroxide [35], and docetaxel [36] contacting endothelial cells promotes PS externalization. Cell degranulation [56], cell aging [57], malignant transformation, cell activation [35, 36], cell migration [58], cell injury [35], programmed cell death [23, 49, 59, 60], intracellular fusion of trophoblasts [61] and myoblasts [62] and activation of platelets [10, 50] are other factors associated with the induction of PS externalization. These stimuli when combined may amplify the PS externalization [35]. In some cases, spontaneous appearance of PS can also occur in malignant cells in the absence of cell injury or exogenous activators [63, 64].

There are several characteristics pertaining to PS in cells: they are abundant (PS is present at more than 10^6 molecules per cell); they are on the luminal surface of tumor endothelium, which can be directly accessible for binding by vascular targeting agents in the blood; they are present in a significant percentage of tumor endothelial cells in diverse solid tumors; and they appear to be absent from endothelium in all of the normal tissues [35]. *In vivo* studies have shown that the exposure of PS occurs on tumor endothelial cells in various solid tumors, including metastatic tumors and drug-resistant tumors, and are on the luminal side of tumor endothelium, which is freely accessible for binding by targeted drugs [2, 65].

A detailed analysis [66] has shown that tumor vessels present structure deficiencies showing thin, leaky and tortuous walls, irregular shape, dilatation [2], insufficient supportive pericytes, and can have dead ends [2]. This anomaly increases

the sensitivity to radiotherapy, vascular targeting agents (VTA), and chemotherapeutic drugs [2]. Another important aspect is that endothelial cells present in normal vasculature are quiescent and nondividing, whereas tumor vascular endothelial cells are active and proliferative [4].

Because of annexin V's high affinity and specificity for phospholipids (particularly PS) [36], it can be used for targeting or the imaging of tumor blood vessels (target molecule) [49]. More sophisticated systems include the possibility of annexin V being used to deliver a radionuclide, a cytotoxic drug [2] or coagulant to tumor vessels [35]. This affinity property permitted the use of annexin V to image activated platelets [31] in thrombi apoptotic cells in cardiac allografts undergoing rejection, cyclophosphamide-treated lymphomas, and anti-Fas antibody-treated livers in rodents [67].

4. Single Walled Carbon Nanotubes (SWNTs)

In order for the annexin V-PS *in vivo* binding to be possible, it is necessary to use an efficient carrier that, when injected in the bloodstream, will not cause significant side effects. Single walled carbon nanotubes (SWNTs) are a relatively new type of nanoparticles that are explored in this research for targeting by annexin V to the tumor vasculature. SWNTs have very high absorption of heat when they are exposed to near-infrared light at a specific wavelength, and this property can be used in a photothermal treatment of tumors.

Because of their high hydrophilicity, water-solubilized nanotubes do not present toxicity, even at high concentrations. *In vivo* biodistribution and tumor targeting studies,

using animals, showed that there is a specific elimination profile for SWNTs – being eliminated in the urine with a small accumulation at the liver and reticuloendothelial system (RES) [68].

Carbon nanotubes present a very defined structure, showing a cylindrical structure with dimensions that can vary between several hundred nanometers to a few centimeters (length) [69] and 0.4-2 nm (diameter) for SWNTs [70]. In the present study, (6,5) nanotubes were used with diameter of 0.9 nm [71]. Carbon nanotubes have several optical, mechanical, electronic and thermal properties of interest [72, 73] such as high electrical conductivity, high aspect ratio (length is approximately equal to 1000 times the diameter), low thermal expansion coefficient, high thermal conductivity, very high tensile strength, high elasticity (approximately 18 % to failure), good electron field emitters and high flexibility (can be bent considerably without damage) [74, 75]. The high aspect ratio is an important property, since it is possible to incorporate several types of molecules with different sizes from small molecules to proteins [76].

Those properties of the nanotubes constitute a promising field with potential technological applications [77]. SWNTs are "rolled-up" artificial nanostructures [72] of a unique layer of graphene [70, 72]. Carbon nanotubes are cylindrical carbon allotrope molecules that can be used in several different fields of study (e.g., nano-electronics, optics, materials applications, biological and biomedical systems [70] and biosensor and bioreactor systems).

Biochemical sensors, diagnostic imaging contrast agents, targeted chemotherapeutics, *in vitro* cell markers, and photoablative therapy agents [72] are examples of SWNT biomedical applications. The use of nanotubes in biotechnology is

possible since specific molecules, such as enzymes or proteins, can be immobilized on the surface or in the hollow cavity of nanotubes [70, 73]. The fact that nanotubes present two distinct surfaces (inner and outer surface) shows they can be functionalized, presenting different properties from the inner surface to the outer surface [73, 76]. Nanotube-protein conjugates can afterward be integrated into biological systems. Generally, because of their properties, nanotubes constitute an excellent mean of transportation *in vivo*, allowing the delivery of a specific compound (e.g., drugs, peptides, nucleic acids [73]) into a concrete region, including the possibility of performing gene and protein therapy [77]. The delivery of genetic material into living cells–transfection [76]–is another example of a nanotube application. Antigen recognition, DNA hybridization, enzyme-catalyzed reaction [70], use as vehicle for enzyme encapsulation, DNA transfection, biosensors and drug delivery [73, 76] are some examples of how nanotubes can be used.

Different types of nanotube functionalization are available, being possible to adjust the nanotubes to a specific desired property. For example, the functionalization with PEG (PEGylation) allows nanotube solubilization, increasing the biocompatibility [68, 73, 76] that is an important factor to perform some biological studies [70, 77]. Generally, the nanotube suspension is required to be highly water-soluble, presenting a dark-colored aqueous suspension [78]. High bioavailability, biocompatibility, nontoxicity [79] and target ability are important properties present in functionalized nanotubes.

It is known that biological systems have a high transparency in the near-infrared (NIR) light window (700-1100 nm) [73, 79]. The characteristic of strong optical

absorbance of SWNTs in this wavelength range–a property related with the electronic band structures of nanotubes–can be evaluated by analysis of an S_{11} absorption spectrum. The spectrum of (6,5) SWNTs shows the presence of a characteristic peak at 980 nm [80] (Figure 4).

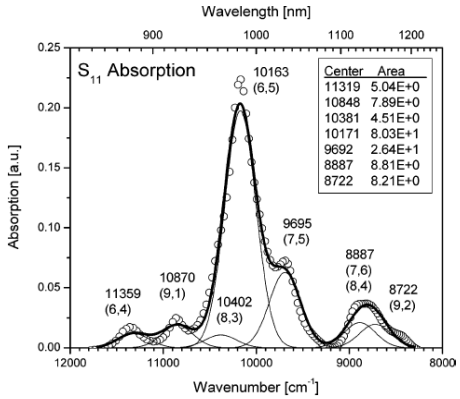


Figure 4: Fitting of the S_{11} absorption spectrum for SWNT sample synthesized on $CoMo/SiO_2$ at 750 ºC [80]. The nanotube chirality is shown on the top of each absorption peak. The (6,5) SWNTs have an absorption peak at 980 nm.

The strong optical absorbance makes it possible to perform optical stimulation of the nanotubes, when injected into the organism [79]. When the SWNTs are bound to specific receptors *in vivo*, the continuous irradiation with NIR light on a specific region can promote cell death because of a local temperature increase [73, 79]. However, the cells not expressing those receptors will not be injured.

Generally, the nanotubes produced are typically interassociated, forming bundles showing an extremely low solubility in the presence of organic solvents or water [81]. In order to solve this particular problem (dispersion and solubility of single walled carbon nanotubes), different methods have been proposed such as high-shear-

flow mixing, milling, and ultrasonication [81] combined with the use of dispersing agents and surfactants [81].

Chemical functionalization is another method that demonstrates a high potential of use. This method can involve covalent or noncovalent bindings. The high reactivity of the carbon atoms present at the ends of the nanotube structure allows the performing of several reactions that seek the establishment of a covalent-binding type. However, this method is not reliable since just a small fraction of the carbon atoms in the nanotube structure becomes functionalized.

Side-wall covalent functionalization is another available covalent attachment method that provides a high carbon atom functionality. This method gives alterations in the optical properties of the nanotubes (loss of optical absorption and photoluminescence) caused by changes induced in the graphene original structure, constituting a severe disadvantage [81].

Adsorption of the protein and adsorption of an inert macromolecule followed by covalent attachment of the protein to the macromolecule are possible methods to form a protein-SWNT complex [81]. The adsorption of biomolecules to SWNTs does not induce any significant change in the intrinsic properties of the SWNTs, with the UV-Vis-NIR absorption of the SWNT´s property conserved [79]. Figure 5 shows a schematic diagram of the mode of attachment of a phospholipid to the surface of the NTs.

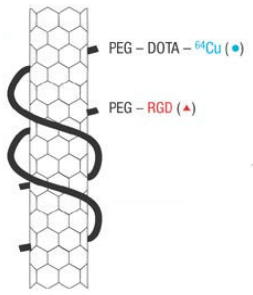


Figure 5: A single walled carbon nanotube wrapped with PEG. PEG molecules have a radioisotope molecule attached to them and others have the RGD peptide [73].

The use of some dispersing agents and surfactants [81] allows for a good distribution and individually nanotube separation from each other. The use of a low concentration of sodium dodecyl sulfate [82], sodium cholate [83], or low-viscosity sodium carboxymethylcellulose [80] as dispersants is encouraged because they are considered good nanotube dispersants.

5. Photothermal Ablation for Cancer Therapeutics

During the last few years, the number of scientific publications published involving the usage of SWNTs combined with a NIR laser for cancer therapeutic applications has greatly increased. The first successful attempt to eradicate cancer cells using nanotubes combined with a photothermal treatment was reported by Kam et al. in 2005 for an *in vitro* study [79]. The SWNTs were non-covalently attached to targeting moieties which bound to cells of interest. After NIR irradiation, cell death was achieved for the treatment groups using an energy density of 168 J/cm^2. Shao et al. [84] performed another *in vitro* study using breast cancer cells that were targeted by mAbs attached to SWNTs. NT internalization was verified and after NIR irradiation at 144

J/cm^2 there was a significant cell killing ratio. Chakravarty et al. [85] published a research article where SWNTs were incubated *in vitro* with lymphoma cells causing thermal ablation by photothermal therapy, using an energy density of 2,100 J/cm^2. Other groups have also evaluated this therapeutic approach using *in vitro* models and different cell lines such as neuroblastoma cells (MWNTs) [86], breast cancer cells (SWNTs) [87] and human prostate cancer (PC3) and murine renal carcinoma (RENCA) cells [88].

In 2009, Zhou et al. [89] published a study that used the same type of carbon NTs used by our group–the (6,5) CoMoCAT SWNTs. The nanostructures were functionalized with folic acid, binding specifically to the surface of certain tumor markers that express folate receptors. The irradiation of those conjugates was done using a NIR light set at 980 nm. Murine mammary tumor line EMT6 cells were used for both *in vivo* and *in vitro* studies. The irradiation profile used contributed to the eradication of a large portion of the cells either *in vivo* or *in vitro*. The injection of the conjugates was intratumoral. Moon et al. also used PEGylated SWNTs to achieve complete eradication of tumors over a 6 month period on mouth carcinoma xenografts (nude mice) [90]. The SWNT conjugates were administered through intratumoral injections which led to a particular accumulation of those structures in the surrounding skin and muscular tissue. Complete tumor eradication was reported to occur by 20 days after the NIR irradiation. The treatment group (SWNTs + NIR) did not reveal toxicity, strange behavior and was mainly in a good and healthy condition over 6 months. There was no tumor reoccurrence on this group. The control group that was irradiated with

NIR light but did not receive SWNTs had an identical behavior when compared with the untreated group.

A later study by Robinson et al. published in 2010 [91] showed *in vivo* complete tumor eradication for more than 6 months using SWNTs conjugated with PEGylated phospholipids. The conjugates were administered intravenously. The group reports that they used the lowest power level to date (P = 0.6 W/cm^2, E = 180 J/cm^2) and a dosage of 3.6 mg/kg. On this study the imaging of the NTs was also studied due to the optical properties inherent to the NTs in the NIR range.

Other studies also used carbon nanotubes to achieve tumor obliteration *in vivo* using intratumoral injections [92, 93]. In 2011, Liu et al. [94] published a successful study where the tumors were treated using an i.v. administration of the conjugates. The SWNTs used were PEGylated in order to achieve a relative long blood circulation half-life (12 h) with a high uptake in the tumor. The irradiation was conducted at 808 nm for 5 minutes using a power density of 1 W/cm^2 (Energy density = 300 J/cm^2). One day after irradiation the tumors disappeared for 5 out of 7 animals in the treatment group, with the generation of black scars on the irradiated area. Three of those tumors did not regrow during the 2 weeks after the treatment. On the other 2 animals the tumors restarted growing approximately a week after irradiation. Two out of seven animals did not see a tumor eradication and the irradiation led to partial burning and consequent slower growth rate.

6. Mechanisms of Attachment of Annexin V to SWNTs using Intermediate Linkers

The use of intermediate linkers to couple proteins to the surface of SWNTs is a common approach [95]. In order to isolate the NTs, they are suspended in SDS (Figure 6)-which is a surfactant and minimizes the interactions between the tubes. The linkers-FMOC-NH-PEG-NHS (Figure 7) and DSPE-PEG-Maleimide (Figure 8) have a hydrophobic group which has the ability to interact with the surface of the NTs due to the establishment of π-π interactions (strong and irreversible binding) [96, 97]. The intermediate poly-ethylene glycol molecule (M.W. = 3,400 Da) will contribute to increase the solubility of the suspension as well as act as a spacer between the surface of the nanotubes and the protein anchorage point (succinimide group). The attachment of the protein to the linker occurs at the other extremity of the linker where there is a succinimide group (FMOC linker) or a maleimide (DSPE linker). During a dialysis step the NHS group undergoes hydrolysis and gets converted into a carboxylic group. This group is then used to react with the N-terminal of the protein through a carbodiimide reaction. The attachment of the DSPE linker to the protein occurs by having a Michael addition, where there is the reaction of a maleimide group with a cysteine (present on the annexin V) (Figure 9).

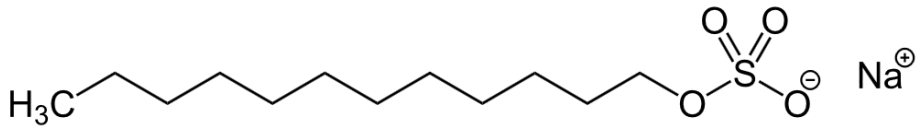


Figure 6: SDS structure [98].

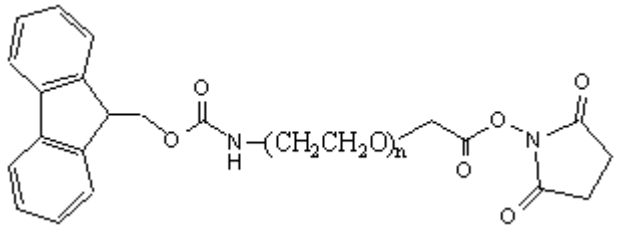


Figure 7: FMOC-NH-PEG-NHS linker structure [99].

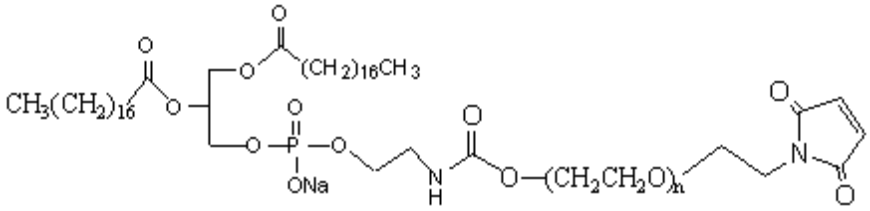


Figure 8: Chemical structure of the DSPE-PEG-Maleimide linker [1].

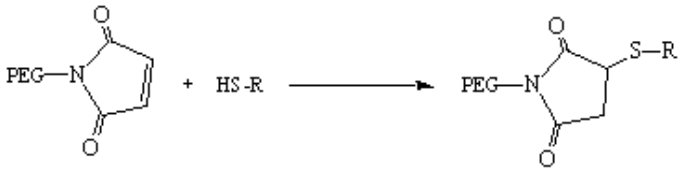


Figure 9: Chemical reaction between a maleimide group and a cysteine [100].

7. Tumoral Morphology and Implications for the Current Therapies

This study aims to overcome the known limitations of the conventional therapies by enhancing the degree of cell death while minimizing the collateral damage of adjacent and viable tissues. In order to evaluate the ability of the photothermal therapy to cause cell thermal ablation, it was required to perform some *in vitro* studies where human endothelial cells were used. This particular cell type was chosen in order to evaluate and mimic the environment and the conditions present at the *in vivo* level.

The vascularization of the tumors is of extremely importance due to the necessity of an appropriate nutrient and oxygen supply and removal of waste metabolites. Angiogenesis plays an extremely important and crucial role on the development of the tumors. For smaller tumors that are under 1 to 2 mm^3 there is no vascularization present since there is diffusion of the oxygen to those cells [101, 102]. However, when the tumors start becoming larger, there is the occurrence of cellular hypoxia in the center of the tumor [101]. This condition results in triggering the process of angiogenesis which will lead to the formation of new vessels. Since, tumors result from the fast and decontrolled replication of the cells, the vasculature that is created and irrigates the tumors is generally abnormal. Those vessels are not allowed to form completely, and therefore the vasculature is usually characterized as irregular and leaky [102]. The existence of large gaps and absence of gap junctions between the endothelial cells explains the leaky nature. This phenomenon is known by the scientific community, and it is commonly used as a way to allow the migration of targeting moieties and/or drugs into the cancer cells. The firm and tight junctions between the endothelial cells on the normal vasculature do not allow relatively large molecules to penetrate into the surrounding tissues. Therefore, we can design conjugates that will be injected into the bloodstream, will travel through the entire organism, and then will selectively bind to the surface of the abnormal endothelial cells but also to the cancer cells that are surrounded by the vasculature in some extent.

Different oncological therapies aim to interrupt the angiogenesis requested by the tumor cells [103]. Also the irregular vasculature is responsible for the generation of enhanced permeation retention effect [104], which is characterized by the lack of an

effective lymphatic drainage. This effect will cause dramatic changes in the fluid transport dynamics at the tumoral level.

8. *In vivo* Studies

In order to test the ablation of tumors using SWNTs and photothermal therapy *in vivo*, it was required to perform some animal studies using BALB/cJ mice (Figure 10), which have a fully functional immune system. The use of immune-competent mice is a much more realistic test of cancer therapy compared to using mice with an impaired immune system, such as athymic mice or SCID (severe combined immune deficiency). This particular strain has a low mammary tumor incidence; however the mice generally develop some tumors when they become older, such as primary lung tumors, reticular neoplasms and renal tumors [105]. These animals belong to an inbred strain, which means that the individuals across the strain are almost genetically identical. The weight distribution across this particular strain is illustrated on the Figure 11.

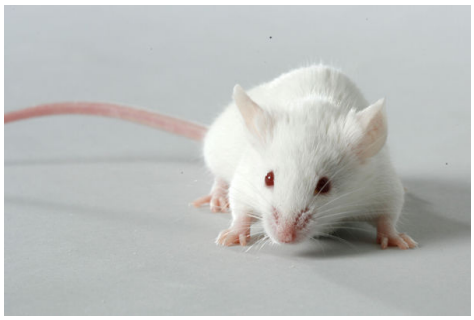


Figure 10: Picture of a BALB/cJ mouse [106].

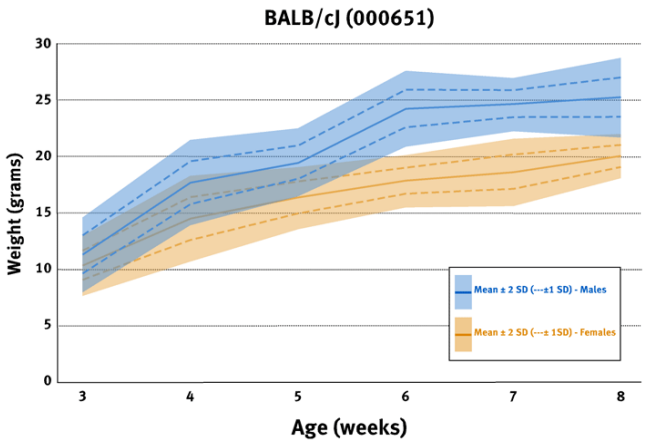


Figure 11: Body weight information for the JAX® mice strain BALB/cJ [107].

Since we were interested in studying the efficacy of this therapy for the treatment of tumors, it was decided to use a cell line that mimics the human breast cancer. For that, the 4T1 metastatic breast cancer model (Appendix M) was chosen due to the fact that these cells grow fast and when inoculated *in vivo* allow for the formation of tumors that will resemble the human breast cancer. This particular cell line was derived from a BALB/c mouse mammary tumor which developed spontaneously [108]. This cell line can be injected orthotopically into the mammary fat pad of the animal or subcutaneously. The cells can also be injected through the bloodstream. The occurrence of metastases in a short time frame is characteristic of this particular cell line, and within few weeks there is the appearance of metastases in the lungs, bone, liver and brain. The metastases found on the lungs can easily be visualized at the naked eye after careful dissection of those organs. They occur as nodules that can be quantitatively determined in order to evaluate the degree of metastasis. The similarity between this model and the human disease defines this model as an excellent candidate to study the metastatic development of breast tumors in humans. The use of a mouse cell line gives

the ability to overcome some of the limitations inherent to the usage of human tumor cell lines which are known to have a slow growth rate and deficient metastasis ability.

9. Immunostimulation Therapy of Cancer using Cyclophosphamide

Cyclophosphamide (CY) is a FDA approved prodrug that has been widely used for the last three decades for treatment of Hodgkin's lymphoma, non-Hodgkin's lymphoma, cutaneous T-cell lymphoma as many other neoplastic pathological conditions [109, 110]. CY is a nitrogen mustard alkylating agent which has the ability to add an alkyl group to DNA [111]. This prodrug is converted at the hepatic level to active metabolites such as 4-hydroxycyclophosphamide and aldophosphamide [112]. CY when administered at low-dosage levels has the ability to suppress Treg cells reinstating antitumor immune responses which lead to an increase on survival rates and prevention of tumoral reappearance [113-115]. Castano et al. [116] combined high- and low-dosage CY with photodynamic therapy in order to evaluate the ability to eradicate the tumors. The use of the photodynamic therapy is known to induce cell damage at the tumoral level leading to the interruption of nutrient and oxygen supply. These conditions ultimately culminate in the occurrence of apoptosis and necrosis triggering the formation of tumor antigens that are released into the bloodstream. When recognized by the immune system, an immune response will be generated. Castano et al. showed that combining CY at a low-dosage level with the photodynamic therapy was successful and resulted in a 70 % survival rate over 4 months. The CY or the photodynamic therapy when administered in separate contribute to an increase on the survival time, however did not impede the animal death.

10. Experimental Hypotheses and Experimental Design

The studies discussed from the literature led to the generation of the following hypothesis for this study:

(1) Human annexin V would be successfully expressed in a soluble and functional form in the *E. coli* bacterial strain;

(2) The produced annexin V binds selectively to human vascular endothelial cells grown *in vitro* that express PS on their surface;

(3) The annexin V produced can be conjugated with SWNTs, which will act as carriers of the protein and also as heat transducers when irradiated;

(4) The SWNT-annexin V conjugate (SWNT-Anx V) binds to non-confluent human endothelial cells (expressing PS) grown *in vitro* and these cells with conjugate bound can be killed after washing and then laser treatment with no effect on cells that were laser-treated with no conjugate present. When injected i.v. in mice, the conjugate will accumulate in the tumor, and subsequent NIR irradiation will lead to a localized thermal ablation effect and consequent cell killing / tumor regression.

(5) When the immunostimulant cyclophosphamide is injected prior to administration of the conjugate and NIR irradiation, there will be more killing of the tumor and increased survival, compared to when there was only conjugate and NIR irradiation administered.

In order to verify and confirm our hypotheses, experimentation was done based on the experimental design presented below:

(1) The expression of the human protein annexin V was performed using a prokaryotic expression system – *E. coli* – due to the fact that is simple to handle, cost effective and allows for the production of large amounts of heterologous proteins [117]. The presence of a His-tag as the affinity tag allowed for the separation of the desired product from any impurities by immobilized metal affinity chromatography. The His-tag was removed before the final purification step. Storage of the pure protein is done after having the entire sample aliquoted and lyophilized. The purity and solubility of the protein was evaluated through a SDS-PAGE and Bradford analysis.

(2) The protein annexin V was biotinylated and incubated with proliferative, non-confluent human endothelial cells expressing PS on the outer leaflet of the cell membrane. After incubation at different concentrations, the unbound protein was removed through an extensive washing step. The binding strength was determined using a colorimetric assay.

(3) The attachment of the protein annexin V to the SWNTs was done using an intermediate linker. The linker acts as a spacer between the protein and the surface of the nanotubes (NTs). This approach allows for the non-covalent attachment of the protein to the NTs. The hydrophobicity of the side walls of the SWNTs and the linker allows for the establishment of a strong and irreversible π-π stacking binding. The NTs are first dispersed in an aqueous surfactant solution. The linker molecules are then added and allow for the displacement of the majority of the surfactant molecules which are removed through an extensive dialysis. The protein is then reacted with the linker through a

particular reaction which is different for each linker. Protein and NT concentrations are evaluated spectroscopically. The conjugate showing the protein surrounding the NT is illustrated by atomic force microscopy (AFM).

(4) The incubation of the conjugates with cells and their i.v. administration *in vivo* for a certain amount of time allows for the establishment of binding. The binding of the SWNT-Anx V conjugate to proliferating endothelial cells *in vitro* was observed using Anx V that was labeled with the fluorescence tag FITC. After washing of the cells incubated *in vitro* or allowing time (24 hours) for unbound conjugate injected i.v. to substantially clear from the bloodstream, the cells (*in vitro*) and the tumors (*in vivo*) are then irradiated using a NIR laser. The proposed mechanism for the *in vivo* binding and subsequent irradiation is illustrated in Figure 12. Cell viability or tumor regression is then evaluated using the Alamar Blue assay and manual measurements of the tumors every 2 days, respectively.

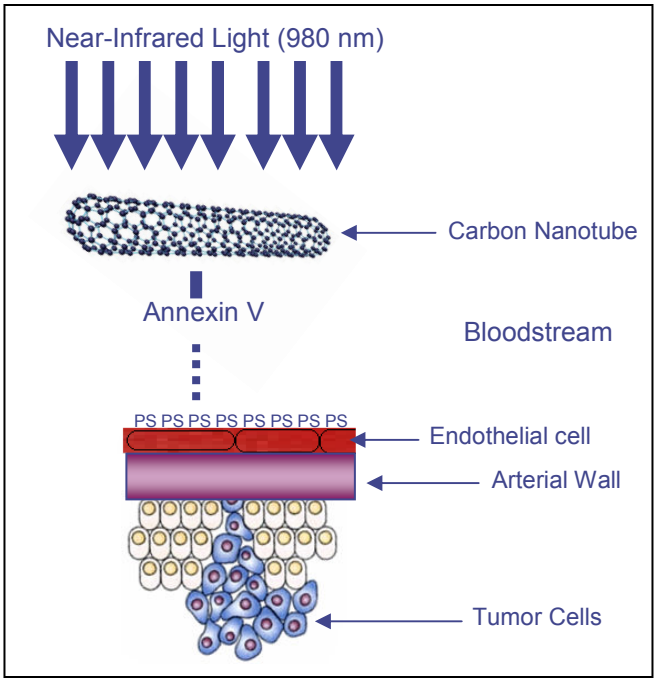


Figure 12: Schematic diagram showing the global mechanism of this study.

CHAPTER II

MATERIALS

Bacterial Strains and Plasmids

The plasmid encoding annexin V, pET-30 Ek/LIC/ANX, was previously constructed in this lab by Ph. D. student Naveen Palwai [118]. The plasmid is designed to express annexin V having an N-terminal $(His)_6$ tag and an HRV 3C protease site next to the N-terminus of annexin V. Host strain *E. coli* BL21 (DE3) (protein expression host) and *E. coli* NovaBlue GigaSingles™ Competent Cells were purchased from Novagen (Madison, WI).

Enzymes

HRV 3C protease and T4 DNA polymerase were acquired from Novagen.

E. coli cell Culture Medium

NaOH, NaCl, tryptone, kanamycin and yeast extract were purchased from Sigma (St. Louis, MO).

Cell Transformation

SOC medium and kanamycin (Sigma) were used.

Cell Expression

Isopropyl-beta-D-thiogalactopyranoside (IPTG), TPCK, PMSF and β-mercaptoethanol were from Sigma. Sodium phosphate was purchased from Mallinckrodt Chemicals (Mallinckrodt Baker, Inc., Phillipsburg, NJ). Imidazole was obtained from Fisher.

Protein Purification

The HisTrap chromatography column (5 ml) was purchased from GE Health Biosciences Corp. (Piscataway, NJ). Flow adapters were purchased from Bio-Rad (Hercules, CA). The 3.5 kDa dialysis membrane was from Spectrum Laboratories (Rancho Dominguez, CA).

SDS-PAGE

Laemmli sample buffer, ladder (marker) and Bio-Rad 10x Tris / glycine / SDS buffer were purchased from Bio-Rad Laboratories (Hercules, CA) and β-mercaptoethanol and Coomassie Brilliant Blue R250 were from Sigma.

Cell Culturing and Cell Counting

Endothelial cells (HAAE-1) were purchased from ATCC (Manassas, VA) (Cat. # CRL-2472) and Coriell Institute Medical Research (Camden, NJ) (Cat. # AG09799). The cell medium Ham's F12K (Appendix G) used for the human endothelial cells was acquired from ATCC (Manassas, VA). The supplements added to the medium were heparin (Polysciences, Warrington, PA), endothelial cell growth supplement (BD Biosciences, Bedford, MA), fetal bovine serum (Atlanta Biologicals, Lawrenceville, GA), and the antibiotics penicillin and streptomycin (Invitrogen, Grand Island, NY). The cells were grown in T-75 flasks (Fisher Scientific, Pittsburgh, PA), 24-well plates (VWR International, LLC, Radnor, PA), petri dishes (Falcon, BD Biosciences, Bedford, MA), and microscope slide chambers (Fisher Scientific, Pittsburgh, PA). Porcine gelatin

was bought from Sigma. The 4T1 cell line and the corresponding RPMI-1640 cell medium were acquired from ATCC.

Binding Assay using Human Endothelial Cells

Biotin and streptavidin-HRP were purchased from KPL (Gaithersburg, MD), and OPD (Appendix E) was from Sigma. The biotin was received in a solid form and distributed in equal amounts in several aliquots. The biotin was reconstituted with DMF at a concentration of 20 mg/ml and stored at -80 ºC. DMF and H_2O_2 were obtained from Fisher Scientific. Sodium phosphate dibasic was from Mallinckrodt Chemicals (Mallinckrodt Baker, Inc., Phillipsburg, NJ). NaCl was purchased from Macron Chemicals (Avantor Performance Materials Inc., Phillipsburg, NJ). Bovine serum albumin (BSA), $CaCl_2$, EDTA, glutaraldehyde and NH_4Cl were obtained from Sigma. Slide-A-Lyzer dialysis cassettes (3.5 kDa) were from Thermo Scientific (Rockford, IL). The assay was monitored using a BioTek Synergy HT microtiter plate reader (Winooski, VT). The dissociation constant determination was done using the GraphPad Prism software purchased from GraphPad (La Jolla, CA).

SWNT Suspension Preparation

Purified and freeze dried (6,5) CoMoCAT SWNTs (batch #000-0031) (average diameter 0.8 ± 0.1 nm) were provided by Southwest Nanotechnologies, Inc. (Norman, OK). Sodium dodecyl sulfate (SDS, from Mallinckrodt Baker, Inc.), sodium cholate (NaC, from Sigma) and low-viscosity sodium carboxymethylcellulose (CMC, from Sigma) were used as dispersants.

Two-step Coupling of the Protein Annexin V and SWNTs using EDC and NHS

The linker FMOC-NH-PEG-NHS was purchased from Creative PEGWorks (Winston Salem, NC). The intermediate PEG molecule that is present on the linker has a molecular weight of 3,400 Da. The 1-ethyl-3-[3-dimethylaminopropyl]carbodiimide hydrochloride (EDC), hydroxylamine, 2-(N-morpholino)ethanesulfonic acid (MES) and N-hydroxy-succinimide, 98% (NHS), 2-mercaptoethanol, and sodium phosphate were from Sigma. Spectra-Por® dialysis membranes (2 and 100 kDa) (Spectrum Laboratories, Inc., Rancho Dominguez, CA) were used. Bradford protein reagent was from Bio-Rad.

Conjugation of the DSPE-PEG-Maleimide linker to Annexin V Protein

The DSPE-PEG-Maleimide linker was purchased from Creative PEGWorks (Winston Salem, NC). Sodium dodecyl sulfate was from Mallinckrodt Baker, Inc.. A Spectra-Por® dialysis membrane (2 kDa) (Spectrum Laboratories, Inc.) was used. L-cysteine amino acid was acquired from Sigma.

Visualization of the SWNT-annexin V Conjugates using Atomic Force Microscopy

The mica substrate and AFM metal specimen discs were from Ted Pella, Inc. (Redding, CA). The MikroMasch NSC15 cantilevers were purchased from MikroMasch USA (San Jose, CA). The MikroMasch cantilevers have a backside aluminum coating, force constant of 46 Nm^{-1} and characteristic resonant frequency of 325 kHz. The software used to operate the AFM was Picoview 1.10 (Agilent, Santa Clara, CA), and further image processing was achieved using Gwyddion (GNU General Public License).

Labeling of the SWNT-annexin V with FITC

Borate buffer and FITC were purchased from Pierce (Thermo Fisher Scientific). Sodium phosphate dibasic was from Mallinckrodt Chemicals.

Cell Staining and Confocal Microscopy

Microscopic chamber slides were purchased from Thermo Fisher Scientific. Microscopic coverslips were from Corning (Corning, NY). Porcine gelatin was acquired from Sigma. A Precision Scientific-Low Temperature Incubator 815 was also used (Precision Scientific, India). CellMask™ Deep Red plasma membrane stain was from Molecular Probes™ (Eugene, OR). Buffered formalin (10 %) was from Richard-Allan Scientific (Kalamazoo, MI). Fluoro-gel antifade reagent was purchased from Fisher.

Laser Treatment of Endothelial Cells with SWNT-annexin V on the Cell Surface

The $CaCl_2$ and Alamar Blue dye were from Sigma. Zap-it® paper was purchased from Zap-it Corporation (Salisbury, NH). The statistical software used was from GraphPad InStat from GraphPad.

Assessment of Sterility

Agar was from Sigma.

In Vivo Studies

The BALB/cJ mice (Appendix L) were purchased from Jackson Laboratory (Bar Harbor, ME). Cyclophosphamide was obtained from Sigma. Ketamine and xylazine were purchased from Butler Schein (Dublin, OH). Needles (25 and 30 gauge) were purchased from Fisher. The syringes and blue mats were from VWR. Matrigel was acquired from Fisher Scientific (Fair Lawn, NJ). The digital caliper from Pittsburgh (Model 47256, Harbor Freight Tools, Camarillo, CA) and the scale from Ohrus (Model: CS 200, Ohaus Corporation, Pine Brook, NJ).

Dissection Studies

Formaldehyde was purchased from VWR (West Chester, PA). A dissection kit was purchased from the Zoology stockroom.

Histology Studies

The histology studies were performed through the OU HSC and the containers used to store the specimens were provided by them.

Biodistribution Study

The tools used to dissect the animals were purchased from the OU Zoology Stockroom. The 10 % buffered formalin was from Richard-Allan Scientific. SDS (Mallinckrodt Baker Inc.), Triton-X 100 (Sigma), DTT (Fisher Scientific) and tris-acetate-EDTA buffer (Sigma) were used to prepare the lysis buffer. Microscope slides and 1.5 ml plastic cuvettes were acquired from the OU Chemistry Stockroom.

CHAPTER III

METHODS

Expression, Cell Lysis and Purification of the Recombinant Protein Annexin V

BL21 (DE3) cells harboring the pET- 30 Ek/LIC plasmid with the annexin V gene (50 µl) were cultured in 10 ml of fresh LB medium (Appendix A.1.1.) containing 35 µg/ml kanamycin overnight with constant shaking (250 rpm) at 37 ºC in an incubator shaker (VWR 1585 Shaking Incubator, Sheldon Manufacturing, Inc., Cornelius, OR). The overnight cell culture (10 ml) was inoculated into 1 L LB medium, containing the same kanamycin concentration. Cell growth was monitored by measuring the absorbance of the sample at 600 nm (Shimadzu UV-2100PC UV-VIS Scanning Spectrophotometer, Japan). IPTG was added to a concentration of 0.6 mM to induce the expression of recombinant annexin V when the optical density (600 nm) of the culture reached 0.4-0.6. The cells were stirred for an additional 5 h at 30º C in a VWR 1585 Shaking Incubator shaker at 250 rpm and centrifuged at 10,000 *x g* for 10 min in a Beckman J2-21 refrigerated centrifuge (Beckman Instruments, Inc., Palo Alto, CA). The soluble part was resuspended in 20 ml of sonication buffer (0.05 mM N- *p*-tosyl-L-phenylalanine chloromethyl ketone (TPCK), 1 mM phenylmethylsulfonyl fluoride (PMSF), 0.01 % β-mercaptoethanol and 0.02 M sodium phosphate at pH 7.4). A vortex (Model: G-560, Scientific Industries Inc., Bohemia, NY) was used to help resuspending the cells. The cells were then sonicated (Sonic Dismembrator, Fisher Scientific, Springfield, NJ) causing cell lysis. The process was performed at 4 ºC using 4.5 watts/ml of lysate for a total time of 150 sec. In order to remove cell debris, the cell lysate was centrifuged at 12,000 *x g* for 30 min.

At this point, the purification was started with all of the steps being performed at 4 ºC. The loading of the different solutions into the 5 ml HisTrap chromatography

column (GE Healthsciences, UK) was performed by a Gilson Minipulse 3 peristaltic pump (Gilson Medical Electronics, Inc., Middletown, WI). The entire chromatography system was cleaned and calibrated using 25 ml of wash buffer (20 mM sodium phosphate, 40 mM imidazole, 500 mM NaCl at pH 7.4). The cell lysate was mixed with 40 mM imidazole (Fisher Scientific) and 500 mM of NaCl and then loaded onto the chromatography column. Next, the wash buffer was flowed through the column in order to wash it. Elution buffer was added next (20 mM sodium phosphate, 500 mM imidazole, 500 mM NaCl at pH 7.4) to promote the elution of the His-tagged annexin V. Fractions containing the purified protein were detected by an Isco UA-5® UV-Vis spectrophotometer (Isco, Inc., Lincoln, Nebraska) at 280 nm.

In order to extract imidazole and NaCl from the protein solution and establish favorable conditions for N-terminal His-tag cleavage, dialysis was performed [119]. Eluted protein was collected into a 12 kDa dialysis membrane that was immersed in a dialysis buffer (20 mM sodium phosphate at pH 7.4). The dialysis process was performed overnight at 4 ºC using a magnetic stirrer to improve dialysis efficiency. After dialysis, HRV 3C protease was used for the cleavage step, which assures the removal of the N-terminal His-tag. HRV 3C protease (0.5 Units / mg of protein) and HRV 3C protease cleavage buffer (1.5 M NaCl, 0.5 M Tris-HCl, pH 7.5) were added to the protein solution. This reaction was performed at 4 ºC for 8 h.

Imidazole (40 mM) and NaCl (500 mM) were mixed with the cleaved protein solution and this solution was loaded onto the 5 ml HisTrap chromatography column. Pure annexin V was eluted using a linear gradient (Bio-rad, Hercules, CA) of 0-0.5 M imidazole. The pure protein was dialyzed against a dialysis buffer (20 mM sodium

phosphate buffer at pH 7.4 and containing 0.1 M NaCl). The final solution was split into several vials (1 mg of protein / vial), which were then instantaneously frozen by immersing them in a liquid nitrogen tank. These vials were then freeze dried (see Appendix A.2.4) and stored at -20 ºC.

The final yield of the run was determined by evaluating the protein concentration of the final solution using the Bradford protein assay (see Appendix A.2.2). A summary of the steps involved in the purification is illustrated in Figure 13.

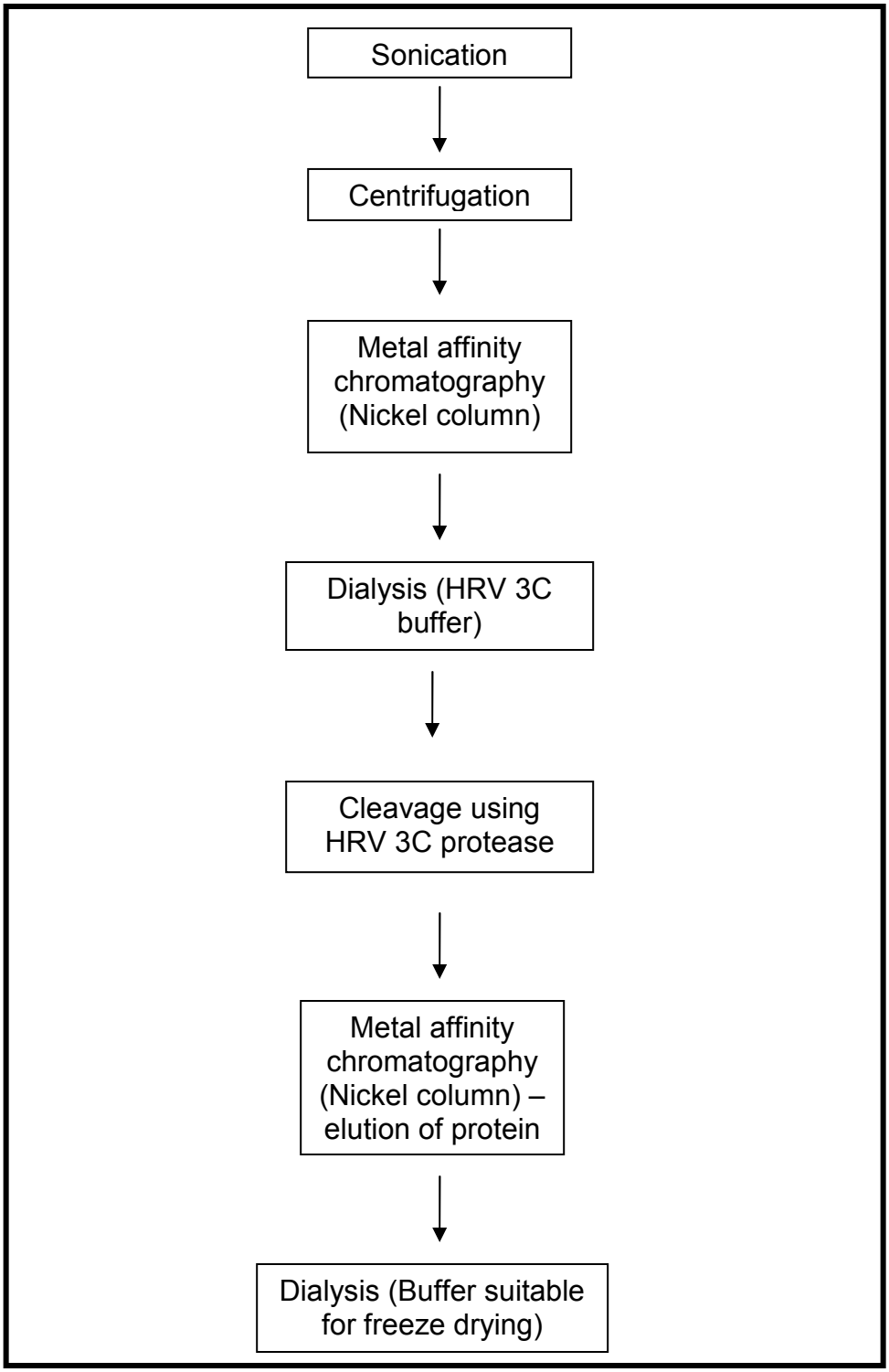


Figure 13: Protein purification flow diagram.

SDS-PAGE and Amino Acid Sequencing

The purity and molecular weight of the recombinant protein annexin V were determined using SDS-PAGE. A Bio-Rad Mini-Protean 3 cell gel electrophoresis unit (Bio-Rad, Hercules, CA) and an Integrated Separation Systems (ISS-emprotech ISS 500) power supply were used for the SDS-PAGE analysis. The SDS-PAGE gel was prepared with 12 % (w/v) acrylamide, 1.5 M Tris-HCl, pH 8.8, 10 % (w/v) SDS. Electrophoresis buffer was prepared using 10 % 10x Tris/glycine/SDS buffer and 90 % deionized water (dH_2O). Each sample (10 µl) was loaded into each individual well of the gel. The gel was run at a constant voltage for about 1 h. The separating gel was stained with 45 % (w/v) dH_2O, 45 % (w/v) methanol, 10 % (v/v) acetic acid, and 0.25 % (w/v) Coomassie Brilliant Blue R250 for 1 h with constant shaking. The SDS-PAGE analysis was done using the UN-SCAN-IT gel™ - Gel Analysis software (Silk Scientific, Orem, UT). The detailed protocol is given in Appendix A.2.3. The amino acid sequencing for the first 6 amino acids of the protein sample was done through OMRF.

Cell Culturing and Cell Counting

Endothelial cells (HAAE-1) (Appendix F) were used for all of the *in vitro* assays in this study. The cell medium used was Ham's F12K cell medium with 2 mM L-glutamine adjusted to contain 1.5 g/L sodium bicarbonate and supplemented with 0.1 mg/ml heparin and 0.03 mg/ml endothelial cell growth supplement, 90 %; fetal bovine serum, 10 %. The antibiotics penicillin and streptomycin were also included in the medium at 100 U/ml and 100 µg/ml, respectively. The cells were grown in T-75 flasks,

24-well plates, petri dishes, and microscope slide chambers. The procedures followed for the cell growth were provided by the American Type Culture Collection. A detailed protocol for the cell growth and passaging is included in the Appendix O. The cell number was determined by cell counting using a hemacytometer (Appendix J). The desired number of cells to add to each T-75 flask after cell passage must be approximately equal to 5 x 10^4 cells.

The *in vivo* studies which were performed at a later stage required the usage of a different cell line in order to mimic and reproduce conditions which are similar to the human breast cancer. The 4T1 cell line is an appropriate line to induce tumors in the BALB/c mice and when injected they produce tumors that are highly metastatic [120, 121]. The main metastatic sites for this cell line are the lung, liver, brain and lymph nodes. This tumor resembles a stage IV for the human breast cancer. When growing the cells, it is important not to let the cells reach confluence, and they should be subcultured when they reach approximately 80 % of confluence. The subcultivation ratio recommended is 1:6 or 1:8. In order to grow this cell line *in vitro*, it is necessary to supply the cells with the appropriate full medium which is composed by RPMI-1640 medium (Appendix N) enriched with 10 % FBS and penicillin/streptomycin antibiotics (100 U/ml and 100 µg/ml, respectively). These cells do not require gelatin as a substrate and can be grown directly in the T-75 flasks. When plating the cells, a frozen vial is allowed to thaw in a water bath for 1 min. and then mixed with 9 ml of warm cell medium. Centrifugation at 1,100 rpm for 5 min. using a Mistral / MSE 3000 E Centrifuge (Leicestershire, England) was performed. The majority of the supernatant is then discarded leaving only 1 ml in the centrifuge tube. Warm medium (9 ml) is then

added to the tube and mixed evenly using a plastic pippetor. The cells are then transferred to the T-75 flask. The subcultivation from one T-75 to eight T-75 flasks was performed on the following day. On the third day, the cell medium was replaced with new one, which had a slightly different formulation. This new cell medium was supplemented with 10 % FBS, but the antibiotics were not added. The cells were grown in a Precision Scientific-Low Temperature Incubator (Model: 815, The Precision Scientific Co., India). A hemacytometer from Hausser Scientific (Horsham, PA) was used for cell counting.

Binding Assay using Human Endothelial Cells

The biotin-streptavidin interaction was used to determine the dissociation constant for the binding of the protein annexin V to the endothelial cells. The use of streptavidin-HRP allowed for the quantification of the binding by using a reducing agent – O-phenylenediamine (OPD) that changes color when in the presence of HRP (horseradish peroxidase). That color change can easily be monitored by measuring the absorbance at 492 nm on a plate reader. The dissociation constant was determined for the specific, non-specific and total binding. A detailed protocol is included in the Appendix Q.

SWNT Suspension Preparation

The SWNTs by themselves tend to aggregate and form bundles. In order to prepare these structures for this study, it was required to suspend them in an aqueous medium. For that, 6 mg of SWNTs were mixed with 7 ml of a 1 % SDS solution. The

suspension was then sonicated for 30 minutes at 19.8 W of power (E = 35,640 J) (Horn Sonic Dismembrator, Model 500 from Fisher Scientific). A 30 min centrifugation was performed at 15,000 rpm (26,000 x *g*) in order to discard any aggregates. Sonication and centrifugation were performed twice in order to enhance the purity of the final samples. The conjugate was then stored in a small glass bottle at room temperature. A characteristic dark-colored aqueous suspension was obtained as result of this sonication process (Figure 14).



Figure 14: SWNTs suspended in sodium cholate.

Part of the suspension (1 ml) was saved for further NIR spectral analysis (note that this was an optional step and it was not always performed). In order to obtain suspensions with shorter nanotubes, the sonication times were increased to 3 h leading to a total of 6 h sonication. The carbon nanotubes size was then measured using atomic force microscope (AFM) (Digital Instruments, Model Dimension 3100 Atomic Force Microscope, Veeco Metrology Group, Plainview, NY).

Two-Step Coupling of the Protein Annexin V and SWNTs using EDC and NHS

The coupling of the protein annexin V using EDC and NHS (Appendices C and D) was done by mixing 779 µl of the FMOC-NH-PEG-NHS linker (using a 1 mg/ml solution) with 7 ml of the nanotube suspension (prepared previously) for 30 min at room temperature and using gentle shaking. An 8 h dialysis followed using a 2 kDa dialysis membrane. The dialysate (2 L of deionized water) was changed after the first 4 h. The main purpose of this initial dialysis was to remove any excess of SDS molecules that were present in the suspension and to replace some of the SDS molecules with the linker molecules. The linker molecules, which have a molecular weight of 3,777 Da, will be retained by the dialysis membrane while the SDS molecules (M.W. = 288.38 Da) will be able to cross the membrane freely. The removal of the excess of SDS will also prevent interactions with the protein annexin V which could eventually cause protein denaturation. At this step, the nanotubes will continue dispersed and in suspension, and each of them will have linker molecules adsorbed on their surface. It is also known that during the dialysis, the succinimide group present on the linker becomes hydrolyzed and it gets converted into a carboxyl group.

The coupling reaction was started by adding one part of an activation buffer to nine parts of the suspension. The activation buffer was prepared using 5 M NaCl and 1 M MES (pH = 6.0) in an aqueous medium. A 1 h centrifugation at 29,600 *x g* (Eppendorf 5424 Centrifuge) was performed in order to remove some possible SWNTs aggregates. EDC and NHS were allowed to equilibrate at room temperature prior to adding them to the suspension. EDC (2 mg, 2 mM) and 3 mg of NHS were added to 5 ml of the SWNT suspension and mixed for 15 min at room temperature. The EDC was

then quenched by adding 7 µl of 2-mercaptoethanol (20 mM). Next, the protein vial was reconstituted by adding deionized water to the lyophilized vial. Protein solution (571 µl, 0.824 mg) was added to 874 µl of the suspension and allowed to mix with gently shaking for 2 h at room temperature. Hydroxylamine was added to a final concentration of 10 mM in order to quench the reaction. This step allows the hydrolysis of the non-reacted NHS present on SWNT-annexin V and results in the regeneration of the original carboxyl groups. A final dialysis step was performed at 4 ºC in order to remove any unbound protein annexin V. The 8 h dialysis was performed using a 100 kDa dialysis membrane. 20 mM sodium phosphate (1 L, pH 7.4) was used as buffer which was replaced after 4 h. The 8 h dialysis requires the use of a 100 kDa dialysis membrane which has pores that are large enough to allow the protein annexin V to migrate. All of the dialysis steps were performed with constant stirrer agitation. A 1 h final centrifugation was performed at 29,600 *x g* in order to remove any SWNTs aggregates. An Orbit water bath shaker (Lab-line Instruments, Inc., Melrose Park, IL) was used to mix the solutions.

The concentration of the protein was determined by Bradford protein assay. The SWNTs concentration was measured by reading the absorbance at 800 nm using a spectrophotometer. Protein and nanotube concentration were measured using a Shimadzu UV-2101 PC UV-Vis spectrophotometer (Shimadzu, Japan).

Conjugation of DSPE-PEG-Maleimide linker to Annexin V protein

In order to perform the conjugation of the DSPE-PEG-Maleimide linker to the protein annexin V, a suspension of SNWTs was prepared using the protocol described

for the FMOC-NH-PEG-NHS linker using 6 mg of SWNTs per 5 ml of 1 % SDS. The linker (M.W. = 4,368 Da) was then dissolved at a concentration of 1.5 mg/ml using a solution of 1 % SDS. The linker was then stored at -20 ºC under a nitrogen atmosphere. Linker solution (1 ml) was mixed with 5 ml of the SWNT suspension. The solution was then mixed at room temperature for 30 min with gentle shaking. After that, the suspension was transferred into a 2 kDa dialysis membrane and allowed to be dialyzed for 8 h against 2 L of deionized water. The dialysate was changed after 4 h. Annexin V (5 mg) was then reconstituted with 1 ml of deionized water. The SWNT-linker (2 ml) suspension was mixed with the reconstituted annexin V at room temperature for 2 h with gentle shaking. Any unreacted linker sites were blocked with L-cysteine (0.048 mg) which was added to the suspension and allowed to react for 1 h at room temperature with gentle shaking. The molar ratio of L-Cys/Linker was equal to 3:1. The suspension was then dialyzed for 8 h against 2 L of 20 mM sodium phosphate buffer at pH of 7.4. The dialysate was changed after 4 h. The dialysis was performed using a 100 kDa dialysis membrane, in order to allow for the removal of any unbound annexin V or L-cysteine present in excess. The final suspension was then centrifuged at 13,000 rpm (15,680 x *g*) for 1 hour in order to remove any aggregates. The nanotube and protein concentrations were then evaluated using the same procedures as for the FMOC-NH-PEG-NHS linker. The conjugate was stored at 4 ºC until use. An Eppendorf 5424 Centrifuge (Eppendorf, Hamburg, Germany) was used.

SWNTs Conjugates Characterization

A Raman analysis was performed using the final conjugate. The sample was analyzed in a Jovin Yvon-Horiba Lab spectrophotometer, equipped with a CCD detector and with a He-Ne laser (excitation of 633 nm). The SWNT-annexin V aqueous suspension was spread on a Si/SiO_2 surface prior to analysis. An optical absorption spectra was also acquired by using a Lambda 950 UV-Vis-NIR spectrophotometer (Perkin Elmer, Waltham, MA).

The Si / SiO_2 substrate was prepared by Verónica (former graduate student working in Dr. Resasco's laboratory). The absorption spectra were acquired at SouthWest NanoTechnologies by Dr. Tan.

Visualization of the SWNT-annexin V conjugates using Atomic Force Microscopy

The visualization of the SWNT-annexin V conjugates was done using AFM. The Agilent 5420 AFM was set up to use the tapping mode. All images were acquired at 512 samples per line at 1 μm and for clearer images 1,024 samples per line at 1 μm were used. The SWNTs suspension was diluted 50 X with deionized water and deposited through slow spin coating (500 rpm) on a freshly cleaved mica surface. Samples were then dried in a vacuum oven at room temperature for 5 h, allowing for water evaporation.

Labeling of the SWNT-annexin V with FITC

The visualization of the endothelial cells after being incubated with the conjugate is our goal, allowing us to verify the binding of this conjugate *in vitro*. In

order to establish a procedure for the visualization of the endothelial cells and the conjugates, it was necessary to label the conjugate with a fluorophore molecule, such as one that emits photons with a characteristic wavelength of green. The green color is conferred by the fluorescein isothiocyanate (FITC) molecules which were previously bound to the conjugate (SWNT-annexin V). The labeling of the conjugate allows for the generation of conjugates that will emit green light when exposed to a laser of a certain wavelength (490 nm). The conjugation of FITC with the SWNT conjugates was done by having the SWNT-annexin V conjugate prepared as described earlier. The conjugate suspension (460 µl) was mixed with 40 µl of borate buffer. FITC solution (50 µl, 1 mg/ml) was then added to the suspension. This was incubated with gentle mixing at room temperature for 1 h. All of the steps involving the dye were done in a controlled environment protected from the light. The excess of FITC was removed by dialysis (using a 3.5 kDa Slide-A-Lyzer dialysis cassette) against 2 L of 20 mM sodium phosphate buffer (pH 7.4) for 7 h, with a change of buffer after 4 h. The conjugate was then stored at 4 ºC protected from light.

Cell Staining and Confocal Microscopy

Endothelial cells were grown to approximately 75-80 % confluence in T-75 flasks as described previously. The cells were then seeded in chamber microscope slides and allowed to growth for 24 h. Partial confluence was achieved after that incubation period, and it is important to verify the confluency level prior to the start of this experiment. Partial confluence allows for the mimicking of active and proliferative cells that are present at the tumoral level *in vivo*. The cells were then incubated for 2 h at 37

ºC with SWNT-FITC-annexin V at a concentration of 6 mg/L. This was followed by an extensive wash step and by staining with CellMask™ Deep Red plasma membrane stain. The entire protocol is described on Appendix P. The acquisition of the confocal microscopy images was done using the procedures established by the confocal microscopy laboratory. The confocal pictures were taken using an Olympus FluoView 500 Microscope at the Electron Microscope facility at OU (Olympus America Corporate, Center Valley, PA). The confocal laser scanning microscope is equipped with different lasers, which we used for green (excitation with blue Argon laser at 488 nm) and red (excitation with green Helium Neon laser at 543 nm) emissions. The images were processed using the Fluoview software (Olympus America Corporate, Center Valley, PA).

Laser Treatment of Endothelial Cells with SWNT-annexin V on the Cell Surface

The laser treatments were conducted using two sets of endothelial cells – confluent and non-confluent. The cells that were previously grown in T-75 flasks were seeded into 24-well microtiter plates. The suspension of the SWNT-annexin V was incubated for 2 h at a concentration of 6 mg/L and at 37 ºC. A washing step (300 µl) followed the incubation using cell medium containing 2 mM $CaCl_2$. Each set had four sample groups which were each evaluated in triplicate. Different controls were studied in order to guarantee the specificity of the assay. Two controls were intended to study the effect of the laser irradiation by itself on the cell viability, and the cytotoxicity of the SWNTs conjugates alone. A final control was composed of cells that were not irradiated or incubated with the conjugate. Each plate subjected to the laser treatment was

irradiated for 120 sec at 2.92 W (energy density = 350 J/cm^2) using a Diodevet-50 NIR laser at 980 nm (B&W Tek Inc., Newark, DE). The distribution of the samples on the plate is illustrated on Figure 15.

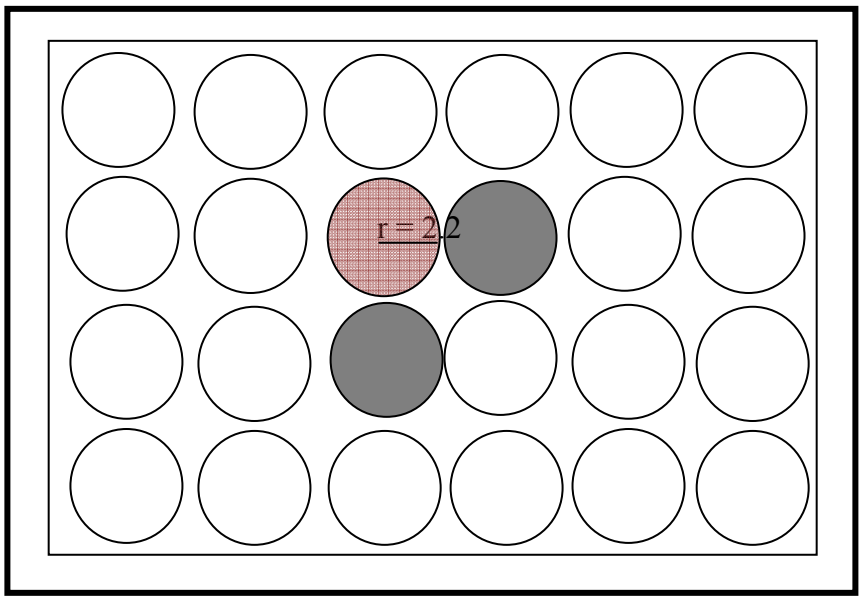


Figure 15: The disposition of the samples within the 24-well plate. The shadowed wells represent the wells that received cells and were subjected to the laser irradiation. The red circle represents the size of the NIR laser beam when irradiating the sample. The irradiation was always performed by having the plate sitting on top of a platform and with the optical fiber placed few centimeters away from the bottom of the plate in order to obtain the desired size beam. The size of the beam was adjusted using a laser sensitive paper (Zap-it® paper) which burns when exposed to a laser beam. The entire irradiation session was conducted by having the cells under a sterile environment by not removing the lid of the plate.

The attenuation of power from the fiber was determined by a power meter (Ophir Optronics Ltd., Israel). The laser beam was delivered by an optical fiber placed a few centimeters from the bottom of the plate below the well. Each well was carefully adjusted in order to be centered with the laser beam. The size of the beam was adjusted using a laser sensitive paper (Zap-it® paper) which burns when exposed to a laser beam and allows the visualization of the intensity of the beam. Cutting a small circle of this paper and placing it on the bottom of the well permits to determine if the entire well is being subjected to the irradiation. After having the fiber completely aligned with the well, the power attenuation inherent to the optical fiber and to the plate was determined by using the power meter. The power meter probe was placed on top of a microtiter plate (without the lid on) and the power was determined. The entire irradiation was done at room temperature keeping the cover of the plates on, maintaining the sterility of the samples. The cell viability was determined by using the Alamar Blue assay. The Alamar Blue evaluates the metabolic activity of the cells, and it is basically a non-fluorescence indicator dye (resazurin) which gets reduced in the presence of metabolically active cells [122]. When reduced, the resazurin gets converted into a bright-pink fluorescent resofurin as illustrated on Figure 16. The Alamar Blue is performed by adding 10 % to the cells followed by a 4 h incubation at 37 ºC. The colorimetric changes are then evaluated by measuring absorbance or fluorescence. The complete protocol is given in Appendix K.



Figure 16: Chemical mechanism illustrating the reduction of the resazurin dye when in the presence of metabolic active cells [122].

The data was further analyzed using a one-way ANOVA in conjunction with the Tukey method. The statistical analysis was performed using the GraphPad InStat software with different confidence intervals.

Optical pictures

The optical pictures were taken using a Nikon D50 (Nikon, Thailand) camera which was directly attached to an Olympus CKX41SF microscope (Olympus, Co., Japan).

Assessment of sterility

The sterility of the SWNT-annexin V conjugate needs to be guaranteed prior to the *in vivo* injection in the mice. This will minimize any immune response or infection in the animal. In order to sterilize the conjugates, the entire suspension was placed in a small petri dish, which allowed the entire suspension to form a thin layer uniformly distributed. The suspension was then subjected to a direct UV (UV-C, shortwave UV at 254 nm) irradiation for 30 min in a sterile environment. The samples were sterilized in a regular laminar flow hood equipped with a Philips UV-C lamp (30 Watts). The

temperature during the sterilization was monitored, and there were no significant increases during the entire process. The samples were then stored in an aseptic vial. Further sterility evaluation demonstrated the absence of microorganisms in the samples. That assay was done by plating tap water, non-sterile, and sterile SWNTs suspensions in a agar plate enriched with LB medium.

In vivo Studies

The BALB/cJ mice received from Jackson Laboratory (Bar Harbor, ME) were 6 weeks of age and female. Animal experimentation was not started until the animals were 9 weeks old. The animals were kept in a dedicated room in the animal facility located in the Zoology building of the University of Oklahoma. All of the protocols used involving animals were previously submitted and approved by the Institutional Animal Care and Use Committee (IACUC). All of the animals were placed in appropriate cages with food and water in an adequate environment. Each cage hosted five animals. The anesthetics used were ketamine (100 mg/ml) and xylazine (20 mg/ml). In order to prepare the anesthetic solution, 1 ml of ketamine (100 mg/ml) was mixed with 0.5 ml of xylazine (20 mg/ml) and 8.5 ml of sterile saline solution (0.9 % NaCl). The dosage used for each animal was equal to 0.1 ml of the stock solution per 10 grams of body weight. Prior to anesthesing the animals, each of them was weighted using a scale. The protocol followed for the anesthesia is shown in the Appendix R. For the tail vein injections, the protocol presented in the Appendix S was followed.

In order to evaluate the ability to eradicate the tumors using this therapy *in vivo*, it was necessary to implant a suitable cancer cell line in the animals. The 4T1 cell line was

chosen for this study, since these cells have the ability to replicate at a fast rate and also develop visible tumors in BALB/c mice in a matter of less than one week after implantation. The methods used to grow these cells *in vitro* were previously described on the Cell Culturing and Cell Counting section of this chapter. After having the eight T-75 flasks growing for 2 days, there are plenty of cells to inject the animals, for each test. The cells are then lifted from the flasks using Accutase (Appendix I, trypsin can also be used–Appendix H), using the same procedure as for human endothelial cells. The cells are then resuspended in 80 ml of cell medium prior to cell counting. Knowing that it is necessary to inject 5 x 10^5 cells / animal (volume = 100 µl), the total number of cells was determined. The cell concentration in the sample was evaluated using the standard cell counting procedure. The required cells per animal were then placed in Eppendorf vials and immersed in a chilled water bath. Matrigel was also placed in Eppendorf vials (volume = 100 µl), and transferred to the water bath. This water bath had the function of keeping the cells and the matrigel cold during the transportation of the materials to the animal facility.

As a basis of our theory, the laser irradiation would be responsible for heating within the tumor. In order to check this hypothesis *in vivo*, the animals were injected i.v. with suitable nanotube suspensions conjugated with the protein annexin V. Before performing those tests, the irradiation safety level had to be determined for the mice. It was important to evaluate the highest energy level tolerated by the animals without compromising their normal functions. For these tests three different energy levels were used: 200 J/cm^2, 300 J/cm^2 and 400 J/cm^2. Prior to the laser irradiation, the three mice used were shaved on the flank using a multipurpose electric razor. The fur must then be

removed in order to eliminate any attenuation of laser energy due to blocking. This will help maximize the amount of energy delivered on the region of interest. The area of the irradiating beam was equal to 1.77 cm^2 for the majority of the animals. When necessary the beam size was adjusted to a larger size in order to make sure that the entire tumoral region was being irradiated. The three animals were anesthetized prior to the irradiation session. The power used was 1 W/cm^2.

Intratumoral injections of the SWNT-annexin V conjugated were also performed in order to evaluate the efficiency of the treatment when comparing with the i.v. injections. For this study four mice were used.

For the main photodynamic therapy study, 36 animals were used. The animals were separated into six different groups: Untreated, SWNTs, Laser, SWNTs+Laser, CY and CY+SWNTs+Laser (CY: cyclophosphamide). The first three groups and the CY group were control groups that were used as comparison with the treatment groups (SWNTs+Laser and CY+SWNTs+Laser). When the average tumors volume was approximately equal to 60 mm^3, the therapy was started. At that point, the CY and CY+SWNTs+Laser groups received the pro-drug cyclophosphamide i.p. at a dosage of 50 mg/kg. Twenty four hours post-administration the animals from the SWNTs, SWNTs+Laser and CY+SWNTs+Laser received an i.v. administration of the SWNT-annexin V conjugates. The laser irradiation of the animals from the Laser, SWNTs+Laser and CY+SWNTs+Laser groups was conducted 24 h later.

After irradiation, the tumor volumes were monitored every two days. This was done in order to verify the efficiency of the treatment and compare the sizes among the different groups. Prior to the measurements, the animals were sedated and then they were also

weighted using a scale. The length and width of the tumors was measured using a digital caliper. The tumor volumes were determined by applying the following formula:

$$V_{tumor} = \frac{(length \times width^2)}{2}$$ [94].

Dissection Studies

In order to perform the histology analysis, it was necessary to euthanize the mice and extract the tumors and also the lungs. Since this particular type of cancer line is known to metastasize to the lungs, it was important to check for the presence of nodules on those organs. The animals after being used in the previous *in vivo* studies were euthanized following the protocol recommended by the OU IACUC. The animals were then dissected using appropriate dissecting tools acquired from the OU Zoology stockroom. The animals were open through the abdominal side and an example of the method used is illustrated on Figure 17.

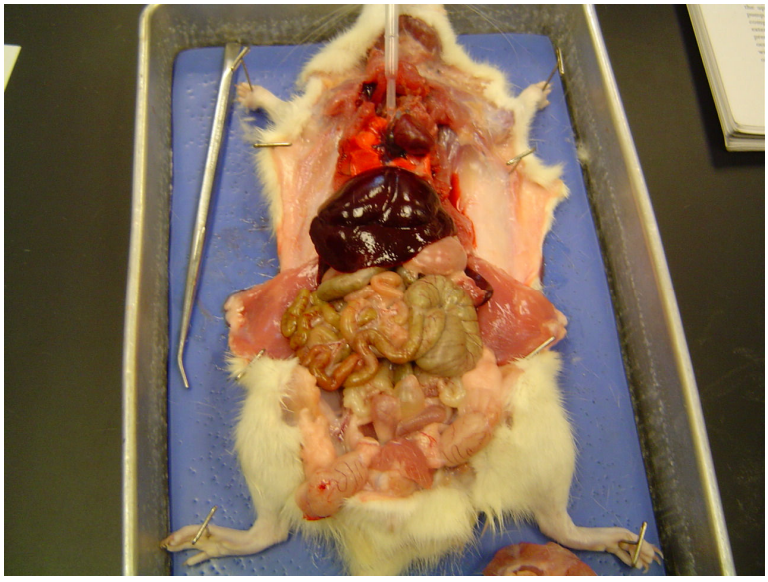


Figure 17: General view of a dissected mouse prior to organ extraction [123].

After exposing the internal organs, the lungs and the tumors (actively grown in the flank region) were carefully extracted and placed in appropriate containers previously filled with 10 % formalin (or 4% formaldehyde solution diluted with PBS). The carcasses of the animals were appropriately disposed of following the OU IACUC guidelines. The containers were appropriately sealed and stored overnight in the refrigerator. The samples can be stored for several weeks under these conditions without major problems.

Biodistribution study

In order to study the biodistribution profile of the SWNT-annexin V conjugate when injected i.v. *in vivo*, two animals were used. The animals were subjected to the same conditions as the other group of animals that were part of the main photothermal study. The animals received a subcutaneous injection of 4T1 breast cancer cells in the flank region. When the average tumors' volume was approximately equal to 60 mm^3, the animals received an i.v. administration of the nanoconjugates (150 μl at a concentration of 109.1 mg/L, average dosage = 0.82 mg/kg). The animals were sacrificed 24 h later, and the organs and tissues of interest were collected. Lungs, livers, and tumors were preserved and stored in 10 % formalin at 4 ºC for further evaluation. Raman spectroscopy was the technique used to quantify the concentration of the single-walled carbon nanotubes present in the organs. The Raman system used was the Nicolet NXR 9610 FT-Raman from Thermo Electron Corporation ($\lambda_{YAG\ Laser}$ = 1,064 nm). The system is property of the Chemistry Department at the Oklahoma State University under the supervision of Dr. Barry Lavine, who kindly evaluated the samples for us. The

Fourier transform Raman (FT-Raman) has the ability to decrease sample's fluorescence that could mask the Raman signals from the SWNTs. The FT-Raman system has an interferometer installed, which generates an interferogram. This set of data contains all of the Raman signal frequencies encoded. The signal is acquired in a very fast and accurate way allowing for the acquisition of 64 scans in less than 2 minutes. The interferogram is then converted into the final Raman spectrum by a computer that is attached to the system.

The characteristic G band seen at 1590 cm^{-1} was our reference. Based on the fact that Raman spectroscopy allows for a qualitative and quantitative evaluation, a calibration curve was obtained using known concentrations for a reference sample (SWNT suspension) in lysis buffer (1% SDS, 1% Triton-X 100, 10 mM DTT, 40 mM tris-acetate-EDTA buffer). While obtaining this curve, it was possible to determine the limit of detection for this particular equipment, which means that below a certain nanotube concentration it is not possible to detect a significant light scattering intensity for the G band region. The Raman system has the ability to evaluate the scattering intensity from the samples using two different modes. The sample can either be placed in a Ge metallic disk (drop deposition method, which is further dried at room temperature) or in a 1.5 ml plastic cuvette (liquid sample). In order to be able to measure the Raman signal from the specimens, the samples were sliced and mixed with a lysis buffer solution (1% SDS, 1% Triton-X 100, 10 mM DTT, 40 mM tris-acetate-EDTA buffer). Each individual sample was then sonicated for 1 minute at 25 % of the total power. The samples were then subjected to heating at 70 ºC for 2 h in a water bath. This resulted in obtaining clear samples as described by Liu et al. [124]. Samples were

also subjected to a 1 h centrifugation step at 15,000 rpm (Eppendorf 5424 Centrifuge) which allowed for the physical separation of the cell debris and the SWNTs suspended in the lysis buffer. Raman evaluation was performed for all of the samples after the centrifugation step. Some of the samples were also further diluted using distilled water.

CHAPTER IV

RESULTS AND DISCUSSION

Overexpression and Purification of Annexin V

Induction of *E. coli* containing the pET-30 Ek/LIC/ANX plasmid using IPTG at 0.6 mM for 5 h at 30 ºC resulted in annexin V being overexpressed in soluble form. Pure annexin V was obtained in the second immobilized metal affinity chromatography (IMAC) near the beginning of the linear 0-0.5 M imidazole gradient. Since any annexin V with the His_6 tag still attached would remain on the column, the annexin V eluted in the second IMAC (after the His_6 tag was cleaved of by HRV 3C protease) does not have the His_6 tag.

The annexin V obtained at the end of the purification was analyzed by SDS-PAGE gel electrophoresis followed by Coomassie Blue staining in order to quantify the protein purity. For comparison, bovine serum protein was also analyzed. Figure 18 shows the purity of the annexin V obtained after the expression, purification, and freeze drying processes. The markers indicate that the purified annexin V is close to its theoretical molecular size (36 kDa). The purity of annexin V was estimated to be greater than 99 % using UN-SCAN-IT gel densitometry software (Silk Scientific, Orem, UT). The average yield from 1 L of culture for the different runs was 49.9 ± 10.3 mg (n=4).

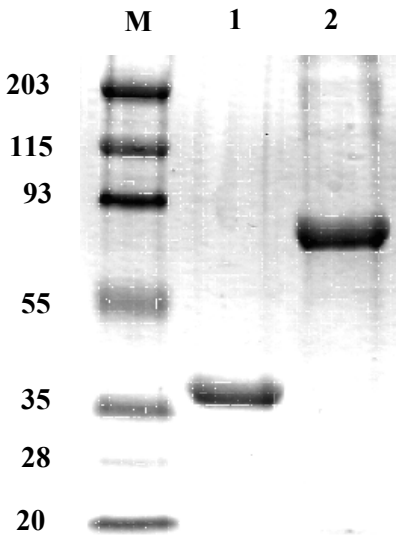


Figure 18: SDS-PAGE analysis using a 12 % gel of purified annexin V. Coomassie Brilliant blue was used for staining. The sample size was 10 µl. Lane M, marker ladder (Bio-Rad, Hercules, CA) with the indicated molecular masses. Lane 1, annexin V prepared at 1 mg/ml after the freeze drying step; Lane 2, bovine serum albumin prepared at 1 mg/ml.

Binding Assay using Human Endothelial Cells

The specific binding of biotinylated annexin V to human endothelial cells *in vitro* was evaluated using a colorimetric assay. HRP reacts with H_2O_2 (substrate), and then reacts with a chromogenic substrate (OPD) which gives a soluble colored product. The non-specific binding, obtained in the absence of Ca^{2+}, is subtracted from the total binding to obtain the specific binding, as shown in Figure 19. The dissociation constant value for the specific binding was determined to be equal to 0.8 nM. The dissociation constant is defined as an equilibrium constant for a reversible binding. The K_d represents the concentration of the annexin V (ligand) that is needed to have half of the

binding sites occupied (PS). The K_d is inversely proportional to the degree of binding strength. The value obtained for the dissociation constant is characteristic of a strong binding capacity, and it is within the expected range [125]. The plot (Figure 19) suggests the existence of a plateau for high concentrations of annexin V, which can be interpreted as where the PS binding sites are saturated. This information is of our interest for the development of the tests of laser treatment of endothelial cells with SWNT-annexin V bound on the cell surface, allowing for the use of a concentration that is high enough to saturate all of the binding sites. The data generated by the software is shown in Table 1. The dissociation constant value was on the lower side of the range found in the literature [26], which is characteristic of a strong binding.

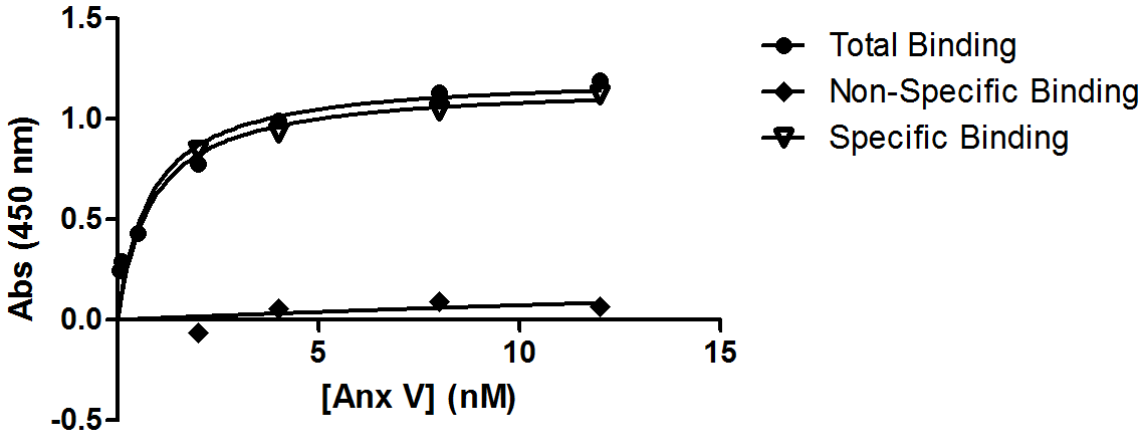


Figure 19. Total, specific, and non-specific binding of biotinylated annexin V to human endothelial cells (80-85% confluence level) *in vitro* on a 24-well plate with 1 mM H_2O_2 added to expose PS on the cell surface. For the non-specific binding data, no calcium was present in the medium. The dissociation constant value for the specific binding was determined to be 0.8 nM.

Table 1: Data generated by Graphpad software in the determination of K_d for the binding of annexin V to endothelial cells.

Nonlin fit	A	B	C
	Total Binding	Non-Specific Binding	Specific Binding
One site -- Specific binding			
Best-fit values			
K_d	0.800	64.4	0.846
Std. Error			
K_d	0.316	1120	0.189
95% Confidence Intervals			
K_d	-0.013 to 1.612	-4760 to 4890	0.032 to 1.660
Goodness of Fit			
Degrees of Freedom	5	2	2
R^2	0.928	0.418	0.941
Number of points			
Analyzed	7	4	4

Characterization of SWNT Suspensions

The centrifugation of the solution containing the nanotubes in suspension with sodium dodecyl sulfate gave a solution with nanotubes largely dispersed (individually), because of the high *g* force used for centrifuging. The SWNTs suspensions obtained had a homogeneous and non-translucent appearance. There was no visible difference between the suspensions that were sonicated for 1 h and 6 h. They were stable for several days without major aggregation when stored at room temperature. Figure 20 shows NIR absorbance spectra for a sample of suspended nanotubes that were conjugated with the protein annexin V compared to SWNTs suspended only using SDS (control). The control sample shows an absorption peak at 980 nm as expected for this type of nanotubes [126-128]. The conjugate gave a slight change in the peak (red shift effect) due to the protein attachment. The red shift can be attributed to a stronger

interaction of the hydrophobic part of the linker compared to that of the surfactant. Similar shifts have been observed for suspended SWNTs with protein [129] or DNA [130] adsorbed compared to those suspended with surfactant only. In order to determine the NT concentration for a particular sample, it was necessary to generate a calibration curve based on the optical density at 800 nm (Figure 21).

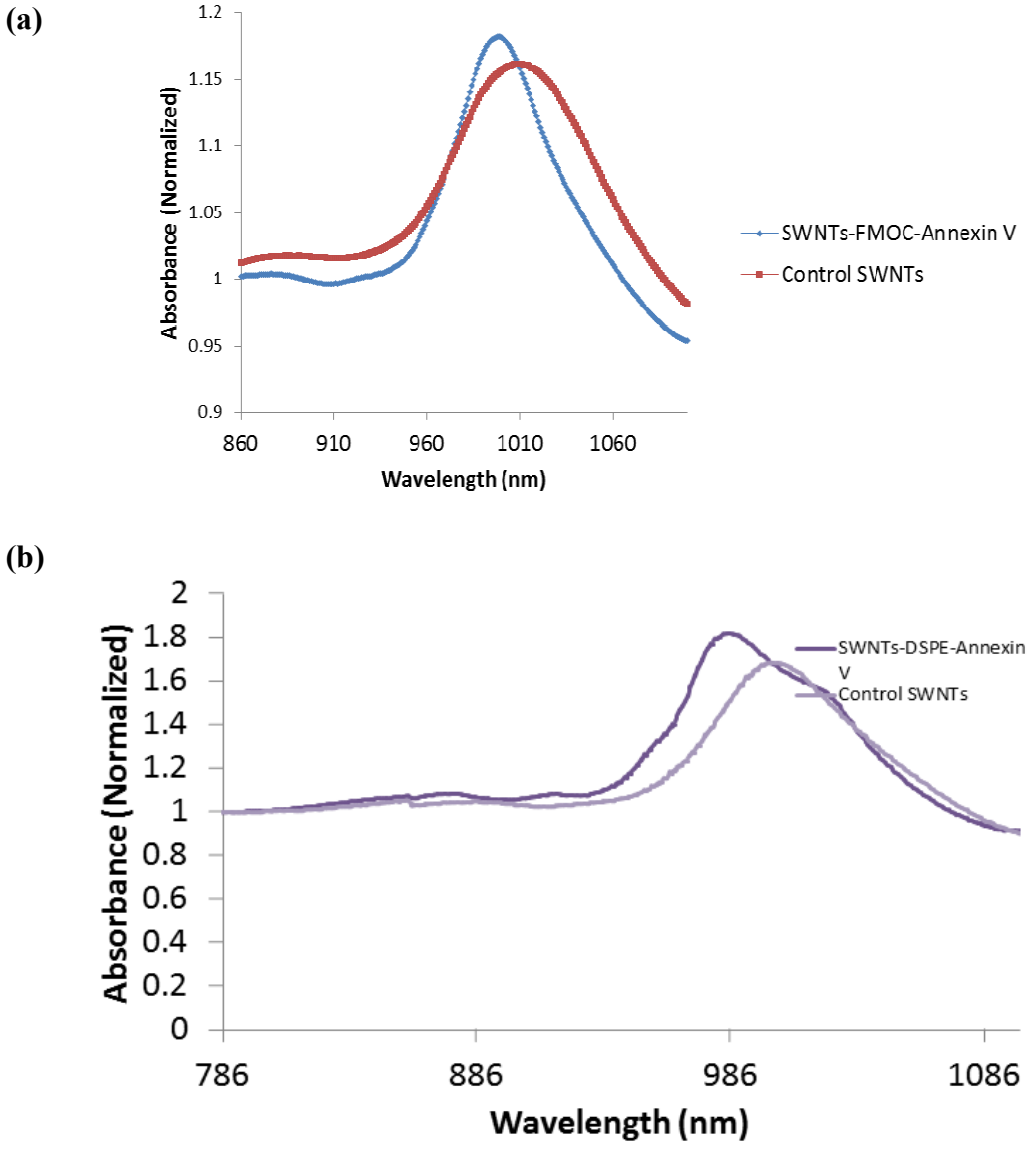


Figure 20: NIR absorbance spectra (normalized) for SWNTs with annexin V attached via the **(a)** FMOC linker or the **(b)** DSPE linker, and SWNTs only suspended using SDS (control).

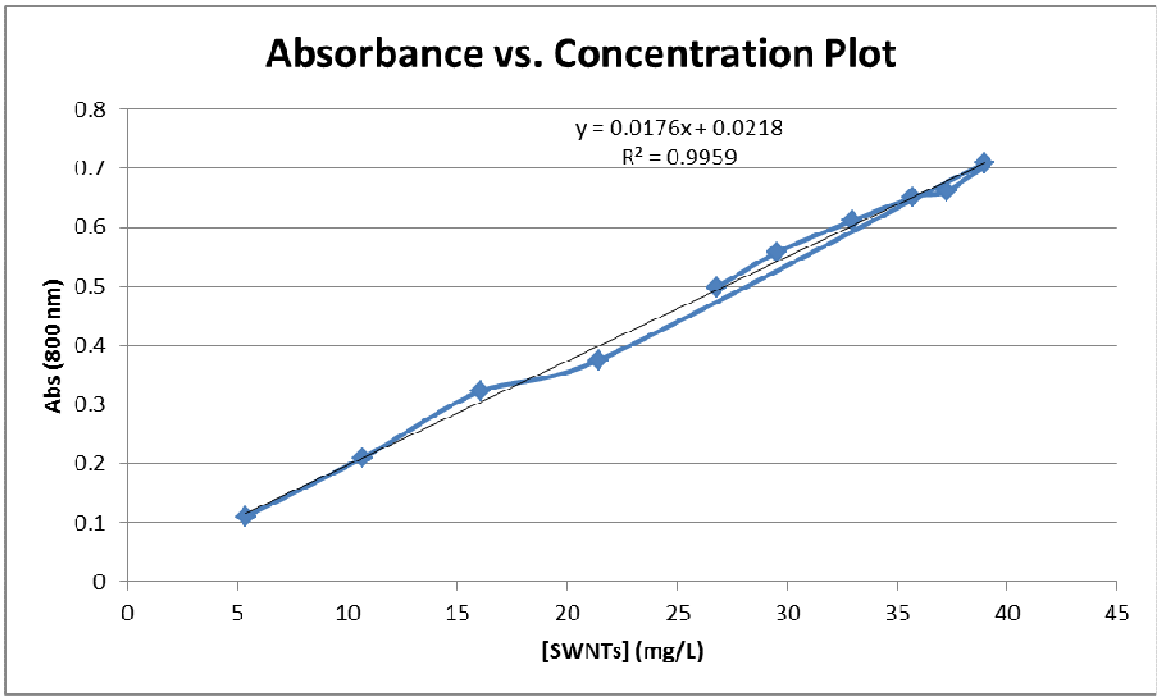


Figure 21: Absorbance at 800 nm as function of SWNT concentration. SWNTs were suspended in 1 % SDS.

The characterization of the SWNT-annexin V suspension by Raman spectroscopy (Figure 22) showed a characteristic spectrum for this type of SWNTs. All of the characteristic peaks were present, which means that the useful properties of the nanotubes were preserved.

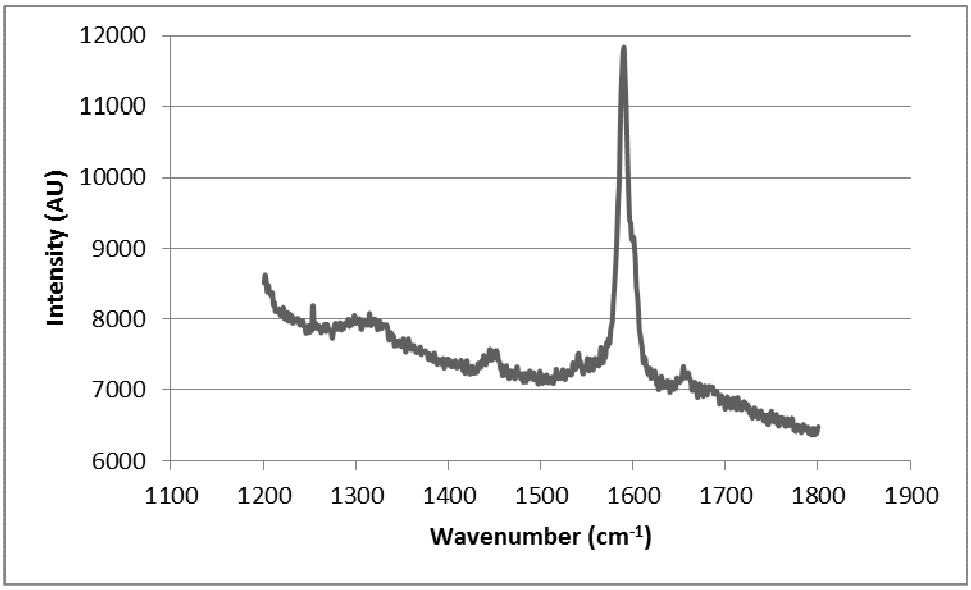


Figure 22: Raman spectrum of the SWNT-annexin V conjugate, where the characteristic peak at 1590 cm^{-1} is visible. The conjugate was prepared using the FMOC linker.

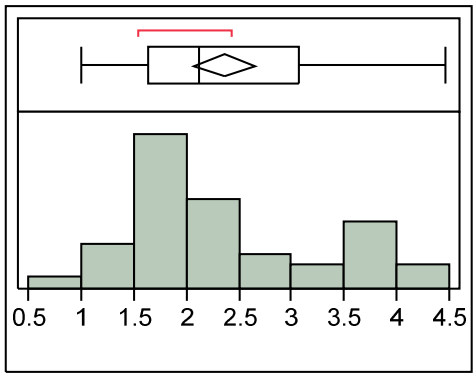
AFM analysis was used in evaluating the length of the carbon nanotubes after the sonication. The extended periods of sonication contributed directly for the shortening of the nanotubes. The results are summarized on Table 2. In Table 3, the detailed data for each sample is plotted in histograms, which allows to understand the distribution of sizes within the samples.

Table 2: Mean length of SWNT after sonication for different time periods.

Material	Number of Measurements	Mean Length (microns)
1 hour sonication	40	2.4
6 hour sonication	52	1.4

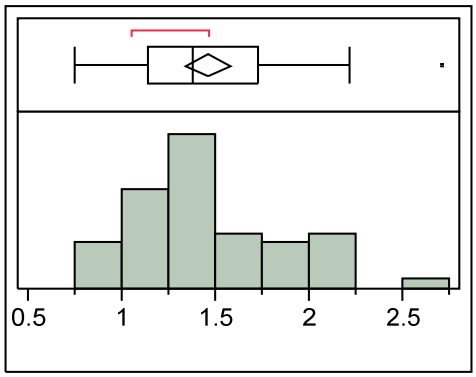
Table 3: Histogram distributions for the SWNTs length. This data was acquired from AFM images.

1 h Sonication



100.0%	maximum	4.5
50.0%	median	2.1
0.0%	minimum	1.0
Mean		2.4
Std Dev		0.9
Std Err Mean		0.1
Upper 95% Mean		2.7
Lower 95% Mean		2.1
N		40

6 h Sonication



100.0%	maximum	2.7
50.0%	median	1.4
0.0%	minimum	0.7
Mean		1.4
Std Dev		0.4
Std Err Mean		0.1
Upper 95% Mean		1.6
Lower 95% Mean		1.3
N		51

The fact that the suspension of SWNTs was prepared using DMF instead of a surfactant, led to obtaining samples with low degree of nanotube isolation. This was an important factor that we attempted to avoid by trying to use a known surfactant, which would allow for obtaining a well dispersed suspension. However, the methods required to deposit the sample on the substrate were not compatible with any of the surfactants (SDS or sodium cholate). DMF is a solvent that is compatible with the deposition method (spin coating or evaporation) allowing for a successful deposition. The use of surfactants in an aqueous medium was not successful due to the fact that the angle of contact was too high and when combined with the fast spinning speed would not allow for the particle deposition to occur. There were therefore some repulsive effects between the suspension and the substrate. The use of a solvent allows to decrease the

angle of contact between the substrate and the sample. The evaporation method is also not recommended for aqueous suspensions due to the existence of high surface tension forces, which will induce the formation of bundles within the suspension.

Even though this method is not giving data for the length of individual nanotubes but of nanotubes that are partially aggregated, the data in Table 3 for length is the same order of magnitude of the length reported for individual nanotubes by Southwest Nanotechnologies, which is 0.8 μm based on a few seconds of sonication [131]. Assuming the nanotubes in the AFM test are aggregating along their length, the individual length would be proportional to the length of aggregates. Thus, for this assumption and according to the data in Table 3, the length of nanotubes after 6 h of sonication is 58% of that after 1 h of sonication (= 100 x 1.4/2.4).

Two-step Coupling of the Annexin V and SWNTs using EDC and NHS

The coupling of annexin V with the SWNTs using the linker FMOC-NH-PEG-NHS was successful. The protein and SWNTs concentrations obtained after conjugation are shown on Table 4.

Table 4: Protein and SWNTs concentrations after conjugation using the linker containing FMOC. The data shown is the average and the standard error of the mean for multiple runs (n=9).

Linker	[SWNTs] (mg/L)	[Annexin V] (mg/L)	SWNTs yield (%)	Protein yield (%)	Protein loading (mg/mg)
FMOC	37.0 ± 7.3	176.2 ± 57.1	7.1	42.8	4.76

The concentrations achieved were high enough to perform all of the *in vitro* studies. However, for *in vivo* studies in mice, the SWNT concentration shown in Table 5 would give a dose of 0.28 mg/kg for the maximum injection volume of 150 µl and mouse weight of 20 g. This is lower than was used for studies where the SWNTs were injected directly into the tumor (0.6-1.0 mg/kg) [89, 90] or into the bloodstream (3.6 mg/kg) [91]. Due to this limitation, it was necessary to redesign the approach in order to increase the final concentration of the SWNTs, which would assure the desired dosage for *in vivo* administration.

Conjugation of the DSPE-PEG-Maleimide linker with the SWNT-annexin V

The conjugation of the SWNTs with the protein annexin V using the DSPE-PEG-maleimide linker was also successful. This method was facilitated by the fact that annexin V contains only one cysteine residue that is five amino acids from the C-terminus. This cysteine is in a random coil configuration [16], so linking it to maleimide would not be expected to interfere with the binding of annexin V to PS

exposed on the surface of the tumor vasculature. This protocol resulted in a substantial increase in both the SWNT and annexin V concentration as shown in Table 5. Therefore, this method was adopted for preparing SWNT-annexin V conjugates used in the *in vitro* and *in vivo* tests.

Table 5: Protein and SWNT concentrations after conjugation using the linker containing DSPE. The data shown is the average and the standard error of the mean for multiple runs (n=9).

Linker	[SWNTs] (mg/L)	[Annexin V] (mg/L)	SWNTs yield (%)	Protein yield (%)	Protein loading (mg/mg)
DSPE	202.0 ± 30.1	515.0 ± 107	25.3	30.8	2.55

Visualization of the SWNT-annexin V Conjugates using Atomic Force Microscopy (AFM)

The visualization of the SWNT-annexin V conjugates using AFM was successful, and the following image (Figure 23) shows a SWNT surrounded by the protein annexin V. The topographic image shows a color gradient that represents the height of the structures present on the sample, whereas the light areas correspond to tall structures and dark areas to low level features, respectively. The height distribution across the middle of the tube was determined using profile extraction through the Gwyddion software to be between 2.5 to 5.0 nm which is within the expected range seen in the literature for a protein bound to SWNTs [129]. In the study by Choi et al.

[132], there are two AFM images that display SWNTs deposited on a mica substrate. For those images, the height distribution profile was evaluated, and it was determined that the height of the SWNTs was 0.85 nm.

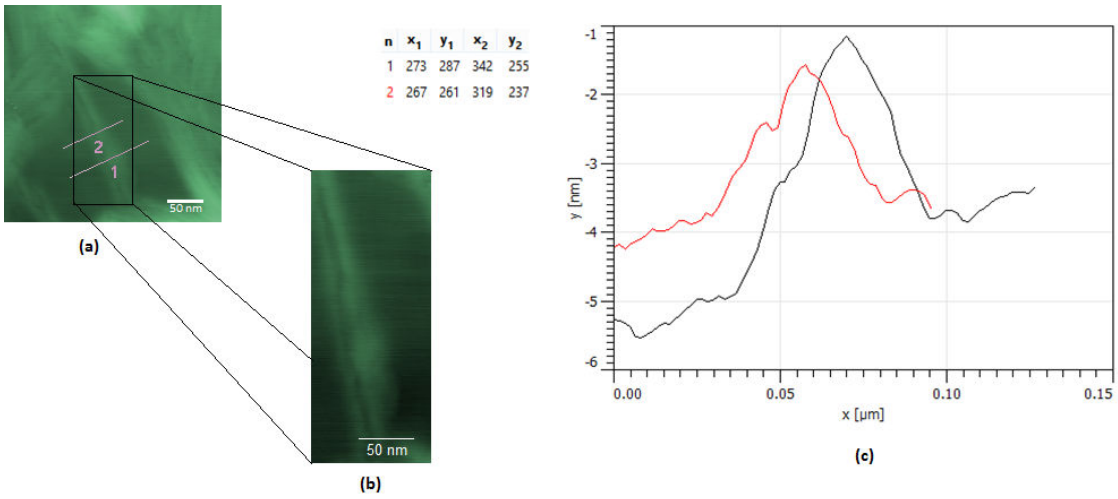


Figure 23: AFM analysis. **(a)** Tapping mode AFM topography image of a SWNT-annexin V conjugate and deposited on a mica substrate (scale bar = 50 nm). Lines 1 and 2 correspond to cross-sections evaluated using the height profile function of the Gwyddion software. **(b)** Detailed AFM image showing a SWNT with the protein annexin V surrounding its surface. The SWNT is surrounded by the protein, which is represented with brighter pixels. **(c)** Cross-section height profiles for two different regions of the SWNT. The profile plotted with a black line corresponds to the cross-section #1, while the red line represents the region defined by the cross-section #2. From the plot, the height of the protein was determined to be between 2.5 and 5.0 nm.

Visualization of Binding of SWNT-annexin V to Proliferating Endothelial Cells

The labeling of the SWNT-annexin V conjugates with the FITC was successful, resulting in a fluorescent conjugate that emitted a bright green color when visualized under the fluorescent microscope. The stability of the dye allows for the detection of fluorescence for at least a week.

The CellMask™ Plasma Membrane stain is a red stain that stained the cell membrane of each endothelial cell. The FITC was helpful to identify the SWNT-annexin V conjugates on and within the cells. The need for determination of the exact location of the carbon nanotubes on or within the cell led us to visualize the samples with a confocal microscope. The confocal microscope analysis showed that the SWNT-annexin V conjugates were present in several cells in the microscope field (Figure 24). Some cells showed a uniform distribution of the conjugates across the entire cell, while others had a well-defined distribution around the cell boundaries. The use of the different dyes allowed for the differentiation between the structures.

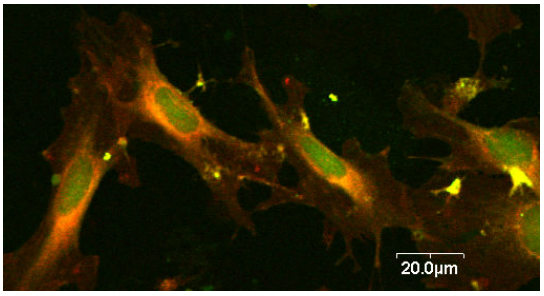


Figure 24: Proliferating endothelial cells stained with the CellMask™ Plasma Membrane stain show the presence of FITC-labeled SWNT-annexin V conjugates bound to the surface. The image displays a plane located above the cell surface. The image results from the merging of the red channel with the green channel. Structures

represented with a yellow coloration correspond to structures that evidenced bright pixels for both color channels. Cells were incubated 2 h at 37 ºC with SWNT-annexin V at a concentration of 6 mg/L. The conjugates were previously prepared using the DSPE-PEG-Mal linker.

Laser Treatment of Endothelial Cells with SWNT-annexin V on the Cell Surface

Before starting studying the effect of the conjugates when incubated *in vitro* with the endothelial cells, it was necessary to establish a safety limit where we could operate the laser without causing cytotoxicity to the cells. The maximum energy density had to be determined in order to evaluate the tolerance of the cells to this source of energy. As shown in Figure 25a, the highest allowed energy level without significant induction of cytotoxicity was 200 J/cm^2. Increasing the waiting time between the irradiation and the Alamar blue assay did not contribute to significantly different cell viability (Figure 25b).

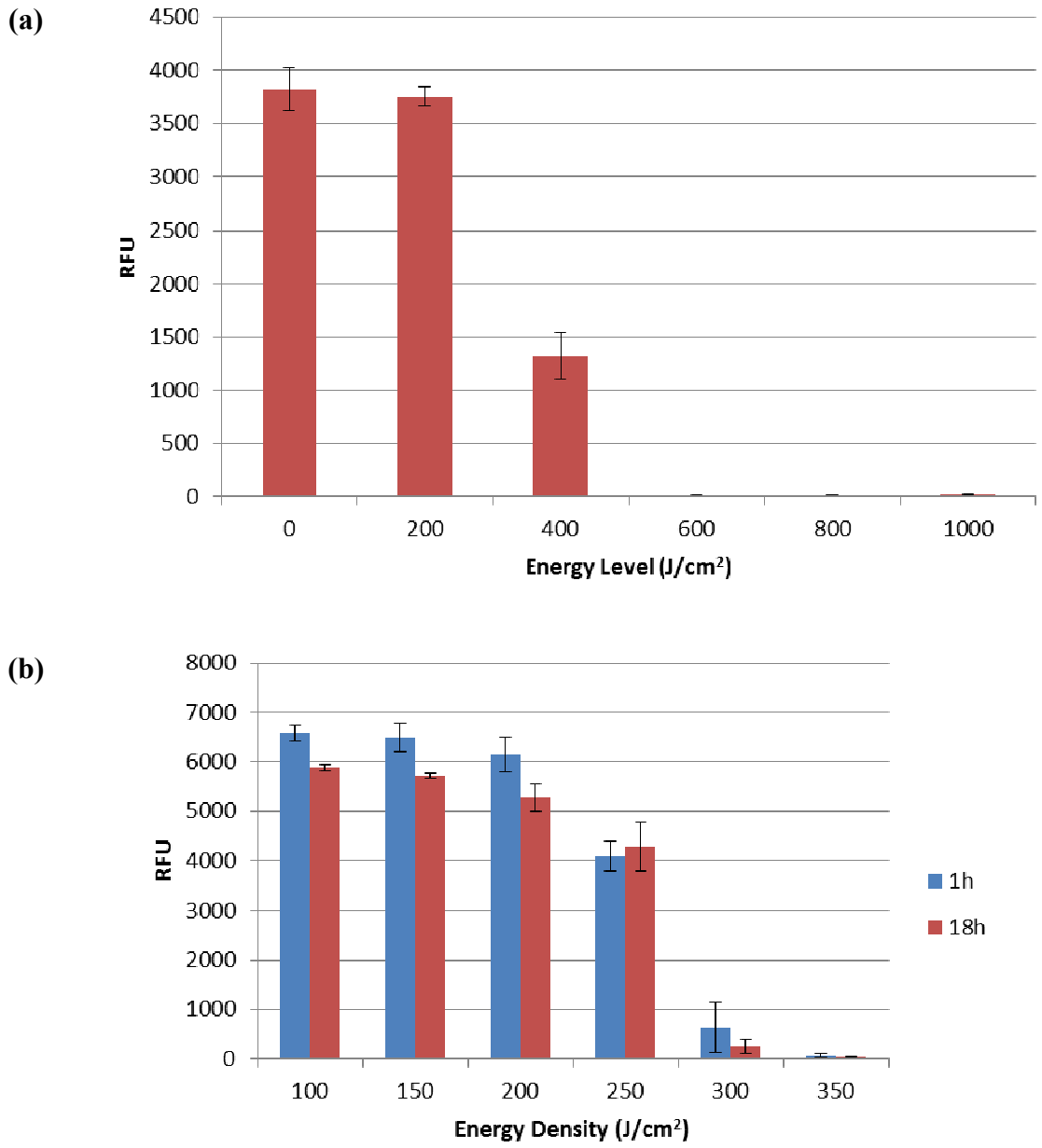


Figure 25: Assessment of the "safe region" to operate the laser system without the presence of cytotoxicity effects induced by the laser itself. Non-confluent endothelial cells were used. The laser irradiation times were 120 s for the 200 J/cm^2 energy density and 130 s for the other energy densities. Data are presented as the mean ± SE (n=3). RFU stands for relative fluorescence units, and it correlates with the percent cell viability. **(a)** The Alamar Blue evaluation was started 1 h after the irradiation of the

cells. **(b)** A lower energy density range was used for this evaluation, which aimed to evaluate the difference between performing the Alamar Blue assay 1 h vs. 18 h after the irradiation.

Cytotoxicity tests were performed *in vitro* on non-confluent endothelial cells with the laser energy density at 200 J/cm^2. Non-confluent cells were used since they actively express the PS molecules on the surface when growing *in vitro*, which does not happen when they reach a total confluence [133]. Since proliferating cells express PS naturally when grown *in vitro* there is no need to add H_2O_2 as a promoter of PS externalization. Because it was thought that shortening the SWNTs might make the i.v. injections easier in the *in vivo* tests, for the *in vitro* tests the SWNTs were prepared using the normal 1 h of sonication and also with the sonication time extended to 6 h. The results are shown in Figure 26. Treatment with only the laser or only with either of the two SWNT preparations did not cause a significant change in cell viability compared to untreated cells. When the cells were incubated with either SWNT preparation prior to laser treatment, compared to untreated cells the cell viability was reduced by 57% and 54% for SWNTs sonicated for 1 h and 6 h, respectively, which are statistically significant ($p < 0.001$). The SWNTs sonicated for 1 h resulted in slightly more cytotoxicity than those sonicated for 6 h, but this difference was not statistically significant.

Since the cells were washed thoroughly after incubation with the SWNT-annexin V conjugate, it is clear that the cell death was caused by the SWNT-annexin V being bound to the endothelial cells and then being heated by the laser. Earlier work in

this laboratory showed that a cytosine deaminase-annexin V fusion protein bound only on the surface of MDA-MB-231 breast cancer cells grown *in vitro* [133]; the specific binding of this fusion protein to these cells was relatively strong (K_d = 4 nM). Therefore, it is likely that the SWNT-annexin V conjugate, much larger than the cytosine deaminase-annexin V fusion protein, was also bound to the cell surface of the endothelial cells, and not internalized, in the tests with the laser.

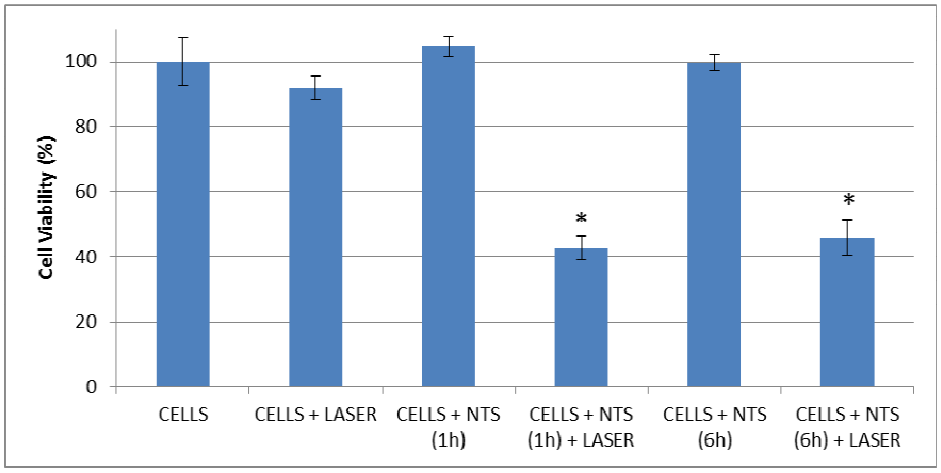
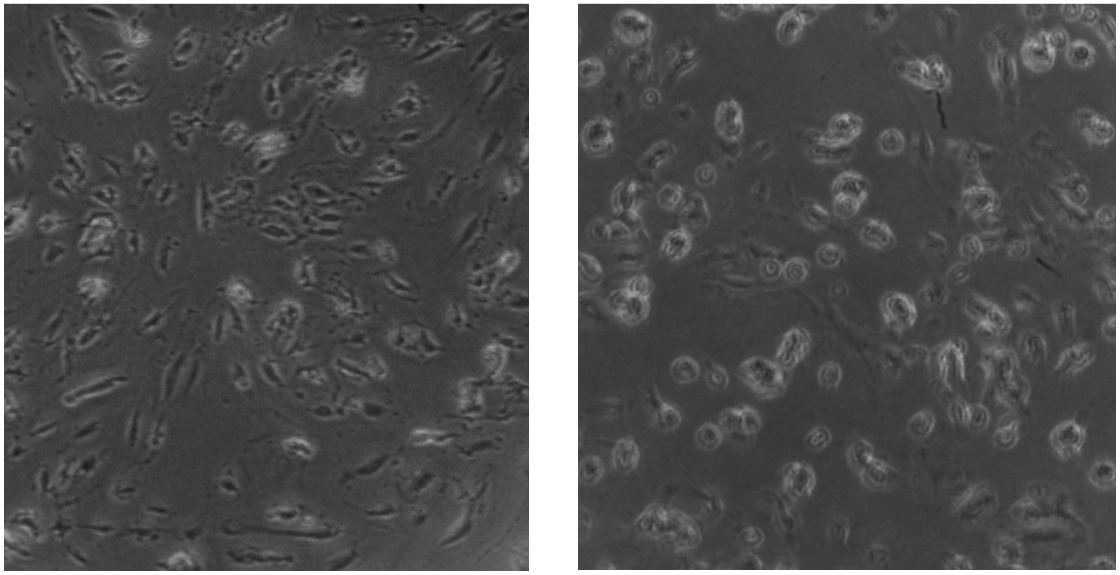


Figure 26: Effect on cell viability of incubation for 2 h of non-confluent endothelial cells with the SWNT-annexin V conjugate prepared with either 1 h or 6 h of sonication time. The laser energy and power density were 200 J/cm^2 and 1 W/cm^2, respectively. Data are presented as the mean ± SE (n = 3), and statistical significance compared to untreated cells is denoted by * ($p < 0.001$). Cell viability was calculated by using data from Alamar blue assay.

Optical Pictures

Optical pictures show human endothelial cells (HAAE-1) grown *in* vitro, before and after a laser treatment of cells that had been incubated with SWNT-annexin V (Figure 27). The elongated morphology of cells before treatment is characteristic of this type of cells. There is a difference in the cell morphology before and after the laser irradiation. The elongated shape is lost for the majority of the cells after laser irradiation, which suggests the occurrence of thermal ablation.



BEFORE LASER TREATMENT **AFTER LASER TREATMENT**

Figure 27: Optical pictures of human endothelial cells taken before and after a laser treatment of cells that had been incubated with SWNT-annexin V. The cells were in a non-confluent state.

Assessment of Sterility

The sterilization of the SWNTs suspensions was successful resulting in the absence of visible colonies on the agar plates after incubation at 37 ºC.

Effect of Sonication on the Optical Absorption of SWNTs

Due to the fact that there was some difficulty injecting the SWNTs conjugates during the second *in vivo* study, it was necessary to evaluate if would be feasible to use shorter carbon nanotubes to facilitate the administration of those i.v.. It is possible that shorter nanotubes would lead to less clogging in the veins than the longer nanotubes upon injection. The shortening of the single-walled carbon nanotubes was attempted by performing extended sonication using different time intervals. From Figure 28 it is possible to conclude that there is a relationship between the sonication time used and the intensity of the absorption peak at 980 nm. The sonication time used is inversely proportional to the peak intensity at 980 nm. Also, the conjugation of the protein annexin V leads to a reduction on the peak intensity, which was not seen when sonication was for 1 h and the NTs were conjugated using the FMOC linker (Figure 20). Due to the diminishment on the peak intensity, it was decided not to use conjugates that were sonicated longer than 1 h.

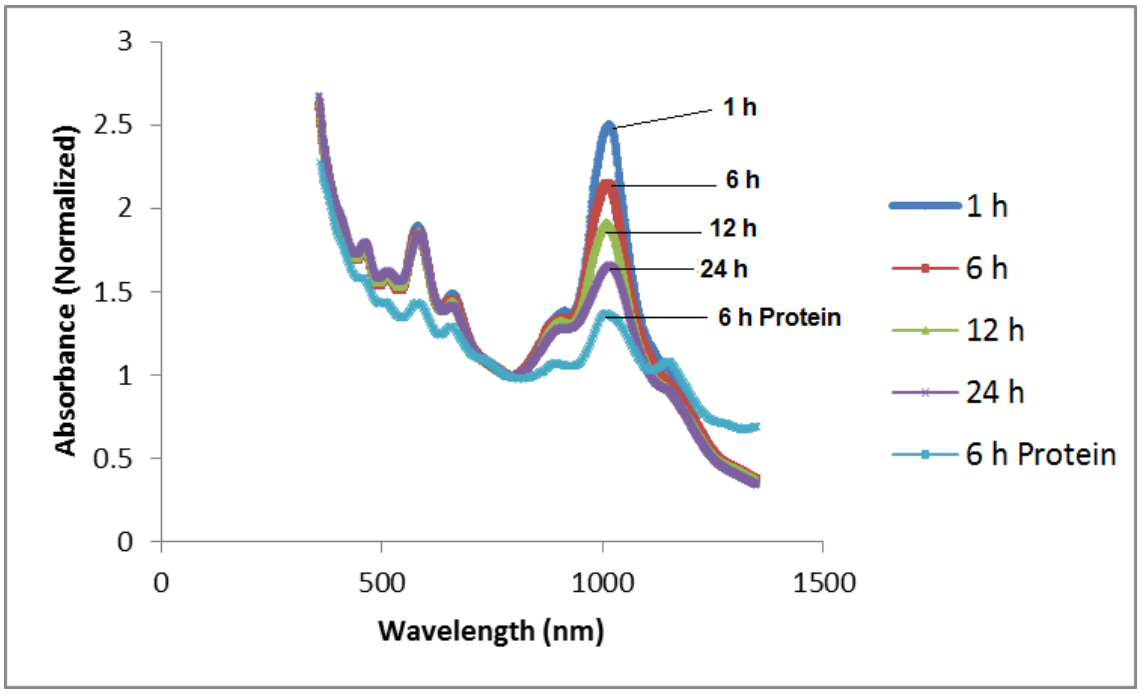


Figure 28: UV-Vis-NIR absorbance spectra (normalized at 780 nm). This spectra compares five different suspensions prepared using SWNTs that were sonicated for different times (1, 6, 12 and 24 h). None of these suspensions were reacted with the protein annexin V, except for the last spectrum (6 h protein) that was sonicated for 6 h and then reacted with the protein annexin V using the DSPE-PEG-Mal linker.

In vivo Studies

During the safety test, some animals were irradiated at certain energy density levels in order to evaluate their response to the NIR irradiation. The results obtained are summarized on Table 6.

Table 6: Summary of the *in vivo* safety test.

Number of animals	Power density (W/cm^2)	Time (s)	Energy density (J/cm^2)	Results
2	1	400	400	Suggested pain during the procedure evidenced by animals moving while under the anesthetic effect. Tails were lifted after the irradiation session. No visible skin damage. Formation of black scars occurred within the 48 h after the irradiation. Revealed walking anomalies few days after irradiation.
2	1	300	300	Suggested pain during the procedure evidenced by animals moving while under the anesthetic effect. Tails were lifted after the irradiation session. No visible skin damage. One of the animals was dead on the following day. Formation of black scars occurred within the 48 h after the irradiation. Revealed walking anomalies few days after irradiation.
2	1	200	200	No visible skin damage. Formation of black scars occurred within the 48 h after the irradiation. Revealed walking anomalies few days after irradiation.
2	1	175	175	No visible skin damage. Formation of black scars occurred within the 48 h after the irradiation. Irradiation level was well tolerated by the animals.
1	1	120	120	No visible skin damage. Formation of black scars occurred within the 48 h after the irradiation. Irradiation level was well tolerated by the animals.

It was found that when the SWNT-annexin V conjugate that was prepared using 1 h sonication was centrifuged just before injection, the suspension flowed out of the tail vein when injected. Thus, the difficulty associated with the injection was likely due to aggregates developing while the conjugate was stored at 4^{o}C. Therefore, the SWNTs were prepared using a 1 h sonication time, and the suspension containing the conjugate was centrifuged just before being injected in the tail vein.

Besides having a group of mice treated with injection of the SWNT-annexin V conjugate followed the next day by laser treatment, a group was added that had the SWNT-annexin V and laser treatment with the addition of an injection of cyclophosphamide at a low dose (50 mg/kg) 48 h before the laser treatment. Low dose treatment with CY has led to increasing antitumor immunity in mouse models, which is believed to be caused by selective depletion of T-regulatory cells. In one study, high cure rates in mice with a reticulum cell sarcoma were achieved with treatment with low dose CY and photodynamic therapy [116]. T-regulatory cells protect the body from autoimmune disease by suppressing self-reactive T cells and may also block antitumor immune responses mediated by tumor-specific T cells.

The *in vivo* test results for BALB/cJ mice with 4T1 mouse mammary tumor implants are shown in Figure 29. Using a tagging system, changes in each animal could be monitored. The tumor sizes in the two groups treated with the laser (SWNTs+Laser and CY+SWNTs+Laser) are significantly lower than those in the untreated group from 16 days after cell inoculation ($p < 0.01$). After the laser treatment, the tumors in the two groups treated with SWNTs steadily reduced in size, and 11 days later (at day 26) there were no animals with visible tumors in the SWNTs+Laser and SWNTs+Laser+CY

groups. A few days later, in three animals (two from the SWNTs+Laser and one from the SWNTs+Laser+CY groups) the reoccurrence of palpable tumors was detected. These tumors were growing outside of the area treated with the laser, so it is believed that they did not receive a full treatment. It was decided to re-treat these three animals at day 37, by repeating the same protocol previously used on days 13 through 15. Before that day, one of the animals in the SWNTs + laser group died, possibly due to the high degree of metastasis. During the irradiation conducted on day 37, the other animal from the SWNTs + laser group also died. It is suspected that the animal was too weak to resist the irradiation session. The only animal that was treated ended up dying on day 46 with an average tumor volume of 415 mm^3. It is likely that this animal died because of metastasis, not because of the size of the tumor. Figure 31 illustrates the difference in appearance between an animal from the untreated group and another animal from one of treatment groups.

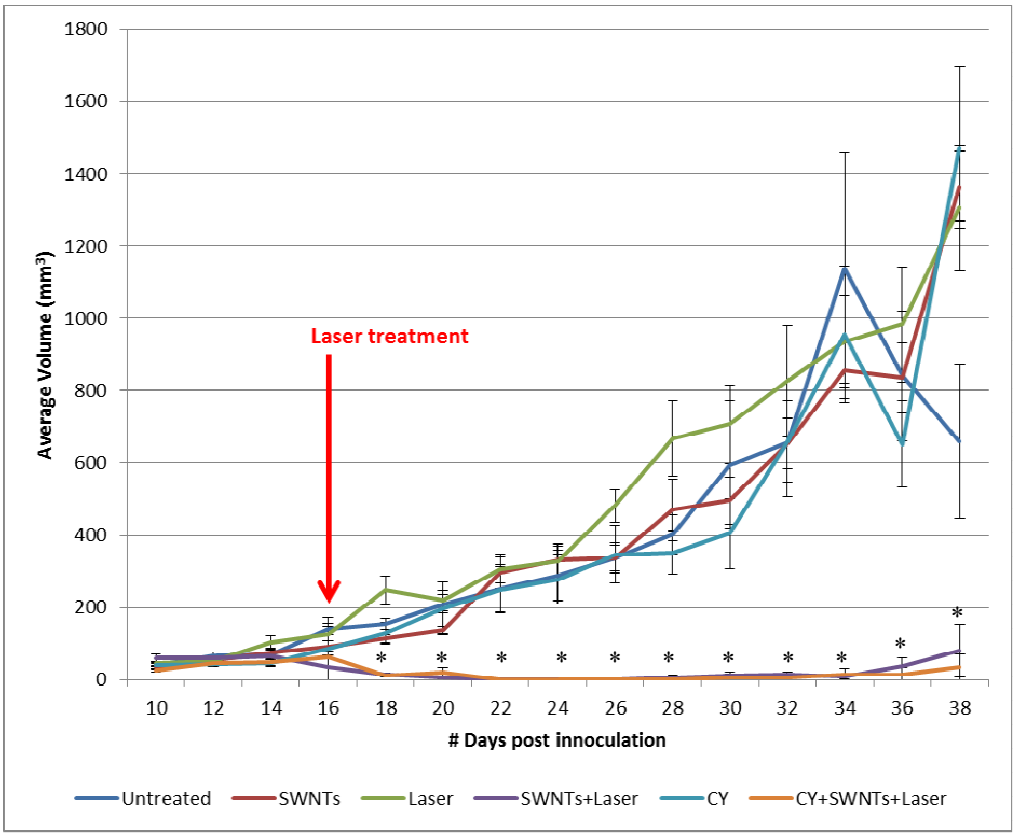


Figure 29: Treatment of BALB/cJ mice with implanted 4T1 mouse mammary tumors. The doses injected i.p. were 50 mg/kg cyclophosphamide (CY) and 0.82 mg SWNT/kg (109.1 SWNT mg/L, 150 µL). The laser energy and power density were 175 J/cm^2 and 1 W/cm^2 (time = 175 s). Data are presented as the mean ± SE (n = 6), and statistical significance compared to untreated cells is denoted by * ($p < 0.01$).

The *in vivo* study was conducted for 60 days since the inoculation of the cancer cells into the animals. The majority of the animals stayed alive until day 38 as shown in the survival curve (Figure 30). Some of the animals died naturally, while some of them were euthanized based on the presence of signs of possible discomfort. It is important to mention that the animals from the CY+SWNTs+Laser had the better survival rate from

the study. One animal had a significantly longer longevity being alive until day 59, which corresponds to a survival of 44 days post-irradiation.

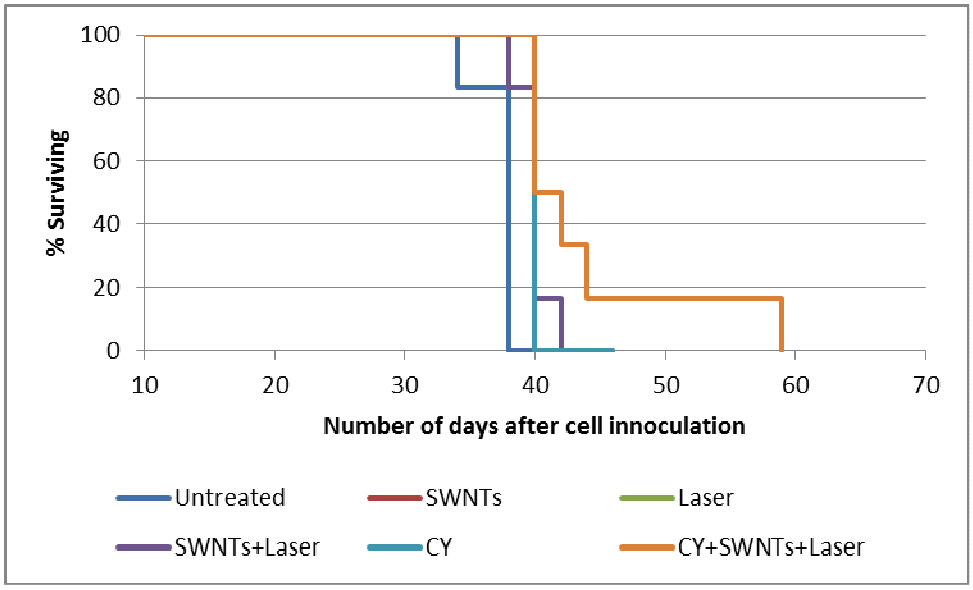
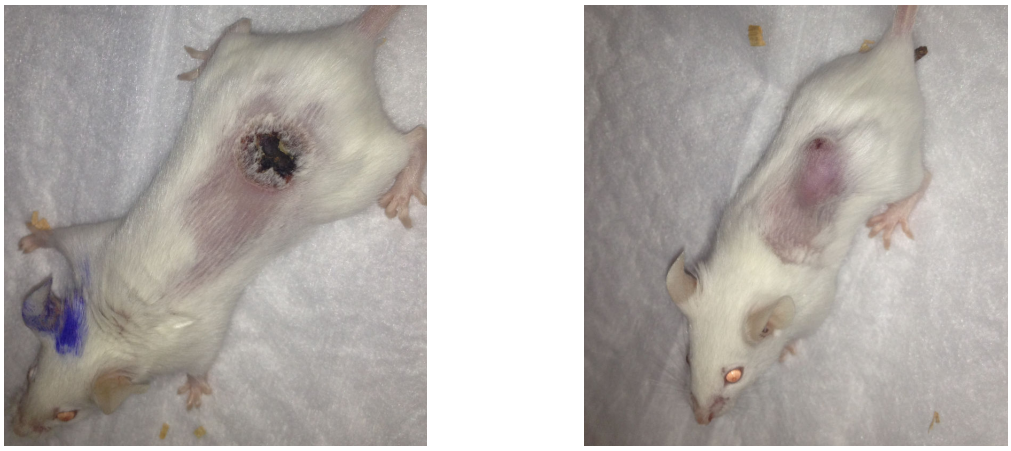


Figure 30: Survival curve for the *in vivo* study. Euthanasia was performed on any animal that showed signs of discomfort. The first animal that died was from the untreated group and that death occurred on day 34. On day 39 and while performing the second irradiation session, one of the animals present in the SWNTs+Laser group did not survive. On this day, the remaining animals from the Untreated group and one animal from the Laser group were sacrificed. By day 42 all of the animals from SWNTs+Laser were dead. There was one animal in the CY+SWNTs+Laser group that had a significantly longer longevity, being alive until day 59, which corresponds to a survival of 44 days post-irradiation.

After euthanizing the animals, a total of six animals were chosen for further evaluation, two from each of the untreated group, SWNTs + laser group, SWNTs +

laser + CY group. For the latter two groups, mice with no visible tumors were chosen. The tumors, lungs, and livers were dissected out and preserved in 10% formalin. The number of metastatic nodules was counted in the lungs, and the results are shown in Table 7. The number of these nodules in the lungs was negligible for 2 animals from the SWNTs+Laser group and for one animal from the CY+SWNTs+Laser. One of the animals from the CY+SWNTs+Laser that was dissected exhibited a relatively small number of visible nodules. It is therefore likely that there were already metastases to the lungs for some animals when the laser treatment was carried out at 15 days from the injection of tumor cells. The injection of CY in conjunction with laser + SWNT treatment, intended to boost the immune response to the tumor, did not lead to fewer metastatic nodules, compared to laser + SWNT treatment alone.



(a) **(b)**

Figure 31: Pictures of two mice from the *in vivo* study. (a) Animal treated with the SWNT-annexin V conjugate and NIR irradiation. The tumor completely regressed after therapy. (b) Animal from the untreated group where there was no tumor regression.

Table 7: Metastatic nodules evaluation.

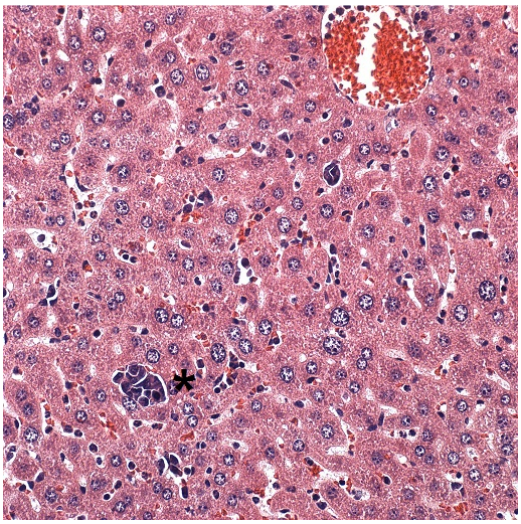
ANIMAL #	GROUP	No. OF VISIBLE NODULES
1	Untreated	16
4	Untreated	18
19	SWNTs + Laser	0
21	SWNTs + Laser	0
31	Cy + SWNTs + Laser	0
32	Cy + SWNTs + Laser	4

The majority of the animals from the treatment groups (SWNTs+Laser and CY+SWNTs+Laser) completely regenerated the epithelial layer on the irradiation site, with absence of the black scar and fur regrowth. This visual observation correlated with the histological analysis as shown in the Table 8. The specimens were sent for histological analysis by the OU Health Sciences Center. The qualitative analysis is shown on Figure 32 and Table 8.

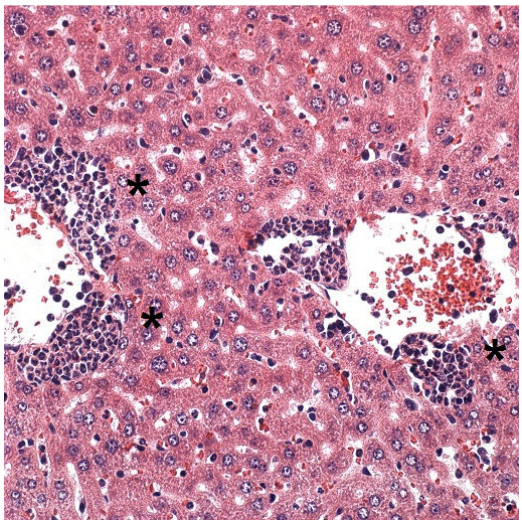
The animals from the untreated group presented multiple micro- and macrometastases in the lungs and liver. There was also the evidence of neutrophils in the liver, which is suggestive of a leukomoid response and may be strain-related. The normal tissue in the lungs was almost absent. The tumor masses presented extensive ischemic necrotic areas, with the presence of an abnormal epithelial cell layer.

On other side, three animals of the treatment group were completely free of metastases, presenting intact morphology in the lungs and liver. The samples collected from the tumoral sites evidenced an epithelial layer with an intact and preserved morphology, without evidence of tumoral cells. However, one of the animals from the CY+SWNTs+Laser had metastases present in the lungs and liver. This result shows the

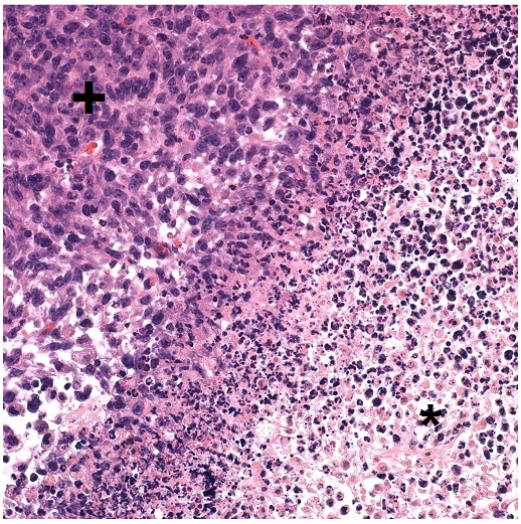
variability among the organisms, which can possibly be explained by having metastases forming prior to the treatment start. The original tumoral site had the same appearance as the other animals from the treatment group, i.e., absence of any evidence of tumor cells.



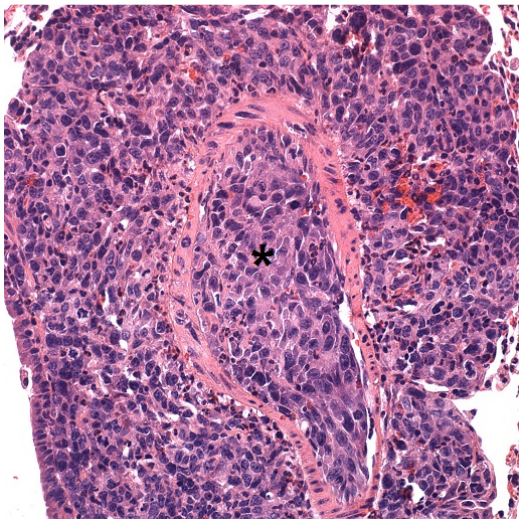
(a)



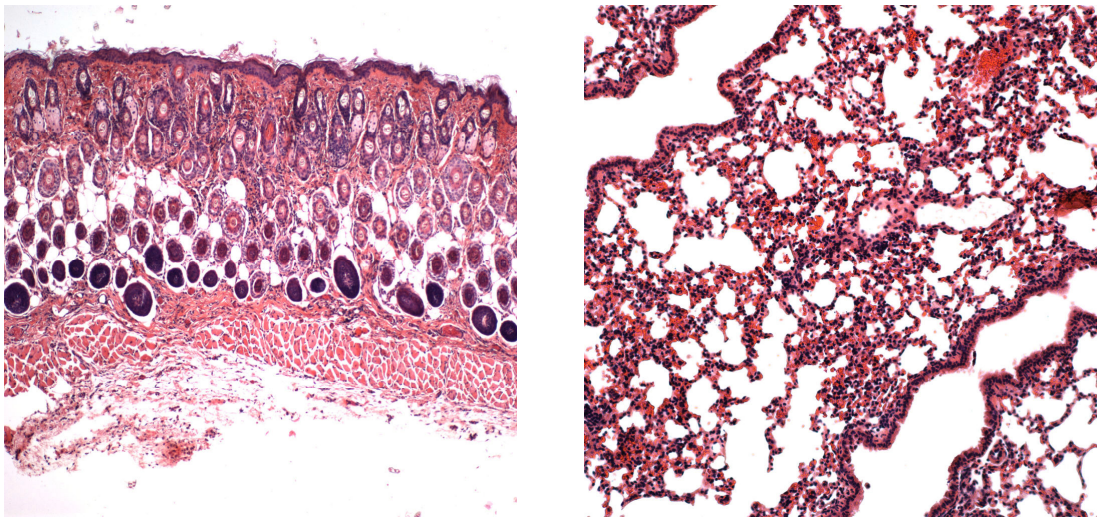
(b)



(c)



(d)



(e) **(f)**

Figure 32: Histological images for different specimens collected from one of the animals from the untreated group (a-d) and treated group (e-f). (a) Sectional image of a portion of the liver (40 X) with evidence of metastases present on the left side of the black asterisk. (b) Sectional image of the liver (40 X) with multiple perivascular focal aggregates consisting mostly of neutrophils evidenced on the left side of the black asterisks. (c) Sectional image of the tumor (40 X) illustrating a large necrotic mass denoted by the black asterisk. The region that surrounds the black + symbol presents a large number of atypical cells that were viable. (d) Sectional image of a portion of the lung (40 X) with evidence of metastases in the blood vessel (denoted by the black asterisk) and also in the periphery. (e) Sectional image of a portion of the skin (10 X), collected from the original tumor *site*, showing an intact epithelial layer without the presence of any atypical cells. (f) Sectional image of a portion of the lung (20 X) displaying a normal morphology with very distinct alveolar sacs.

Table 8: Histological analysis obtained for specimens collected from six animals.

Animal #	Group	Lungs	Liver	Tumor
1	Untreated	Multiple macroscopic metastases present on the surface; evidence of invasion of the chest tissue. Almost complete absence of normal tissue.	Multiple perivascular locations contained a focal aggregate consisting mostly of neutrophils. This is suggestive of a leukomoid response and may be strain-related. Numerous microscopic metastases found in the sinusoids. Almost complete absence of normal tissue.	Extensive ischemic necrosis in the mass. It was comprised of mostly atypical-appearing cells ranging from oval to spindle-shaped
4	Untreated	High degree of macroscopic metastases, with extensive metastatic *foci*. Almost complete absence of normal tissue.	Multiple perivascular locations contained a focal aggregate consisting mostly of neutrophils. This is suggestive of a leukomoid response and may be strain-related. The area occupied by the micrometastases was lower than the animal #1 and not so severe. Almost complete absence of normal tissue.	About 66 % of the mass appeared to be necrotic, probably as result of ischemia. Epithelial cell layer was not viable.
19	SWNTs + Laser	Intact morphology and free of metastases.	Intact morphology and free of metastases.	No evidence of the original tumor. Epithelial layer presents an intact morphology.
21	SWNTs + Laser	Intact morphology and free of metastases.	Intact morphology and free of metastases.	No evidence of the original tumor. Epithelial layer presents an intact morphology.
31	CY + SWNTs + Laser	Intact morphology and free of metastases.	Intact morphology and free of metastases.	No evidence of the original tumor. Epithelial layer presents an intact morphology.
32	CY + SWNTs + Laser	Presence of some metastases.	The incidence of intrasinusoidal atypical cells, suggestive of micrometastasis was lower than the animals from the Untreated group.	No evidence of the original tumor. Epithelial layer presents an intact morphology.

As seen from the histological analyses, there were metastases present in the lungs for some of the animals which is the most suggested cause of death. From a literature analysis, 4T1 cells are known for being poorly immunogenic and highly metastatic inducing metastases even before the tumors are palpable for this particular animal strain [134, 135]. It has been also reported that even if there is complete tumor eradication the most common cause of death is lung failure because of tumor metastases.

These results are very encouraging since we were able to eradicate the tumors in a large fraction of the animals in the treatment groups. Currently there are only two research studies that use a similar approach in terms of using SWNTs administered i.v. for cancer treatment [91, 128]. Both studies used Balb/c mice and the 4T1 cell line.

Robinson et al. [91] used SWNTs conjugated with PEGylated phospholipids at a dosage of 3.6 mg/kg. Those were injected i.v. 5 days after cell inoculation, and irradiation at 808 nm followed 3 days later (180 J/cm^2). The tumor average size when performing the treatment was equal to 22 mm^3, which is approximately five times smaller than the size our animals had when subjected to the irradiation. Their study was successful in terms of reaching complete tumor eradication for all of the animals in the treatment group with no tumor reoccurrences for over 6 months.

Liu et al. [128] using the same administration mode used a higher energy density (300 J/cm^2) and performed laser irradiation at 808 nm 48 h after nanotube administration (dosage not given). The conjugates used were composed of SWNTs with amphiphilic polymers anchored to the surface through an intermediate PEG molecule. Temperature rises were reported in the order of 50 ºC for the animals that were part of

the treatment group versus 1-2 ºC temperature increase for the control groups. Their study was not so impressive as the one by Robinson et al. since they were not able to completely eradicate the tumors for more than 2 weeks. In fact, two out of seven animals only evidenced a reduction on the growth rate, while the other five totally regressed for at least one week, but reoccurred after that time period.

Compared to the *in vivo* studies by Robinson et al. and Liu et al., it is seen that the laser energy density used in our study was similar. The SWNT dose in our study was more than four times lower than in the Robinson et al. study and yet still achieved a high degree of tumor eradication when combined with laser treatment; this is likely because we targeted the SWNTs to the tumor vasculature via annexin V so that SWNTs selectively accumulate in the tumor, instead of being distributed throughout the body. In neither of these other studies were the SWNTs targeted, which could lead to the undesirable side effect of thermal ablation of normal tissue.

Biodistribution Study

Two animals were injected with the SWNT conjugates during the biodistribution study. A standard curve of the Raman G band intensity as a function of SWNT concentration is shown in the Appendix T. The Raman spectrum of a SWNT suspension with a known nanotube concentration is illustrated in Figure 33.

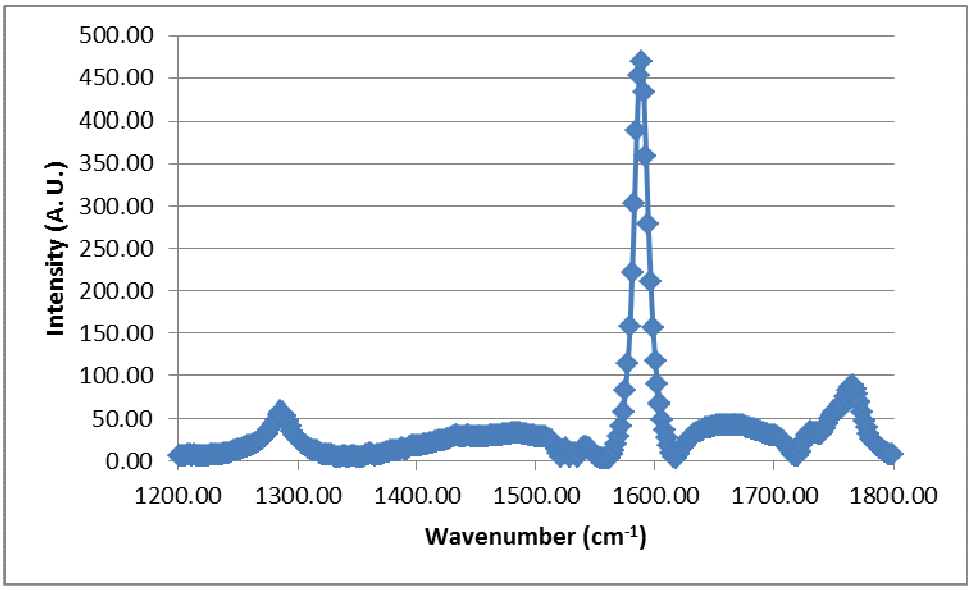


Figure 33: Raman spectrum for a SWNT suspension with a nanotube concentration of 98.6 mg/L. A drop of the sample (previously diluted using a 1 % SDS solution) was allowed to dry. The signal was acquired using 64 scans in a FT-Raman system.

While attempting to evaluate the presence of SWNTs in the tissue samples, different acquisition modes and settings were used in order to optimize the ability to detect those structures. The optimal settings used corresponded to 64 scans / sample and by having a drop placed on top a Ge disk (previously allowed to dry at room temperature). The sample was carefully placed in front of the laser beam.

The majority of the tissues collected from the two animals that were used for the biodistribution did exhibit a characteristic G band at 1,590 cm^{-1} as expected. Each Raman spectrum obtained from those samples exhibited the presence of a characteristic G band associated to the SWNTs. An example of a spectrum obtained for one of the samples is illustrated in Figure 34. The spectrum exhibits a characteristic G band, therefore meaning the presence of single-walled carbon nanotubes in the samples. The

percent injected dose (% ID) was determined for each tissue sample by using the following equation:

$$\%\ ID = \frac{[SWNT]_{tissue\ lysate}\ x\ V_{tissue\ lysate}}{[SWNT]_{injected}\ x\ V_{injected\ SWNT}}\ x\ 100\ \%$$ (adapted from [124]).

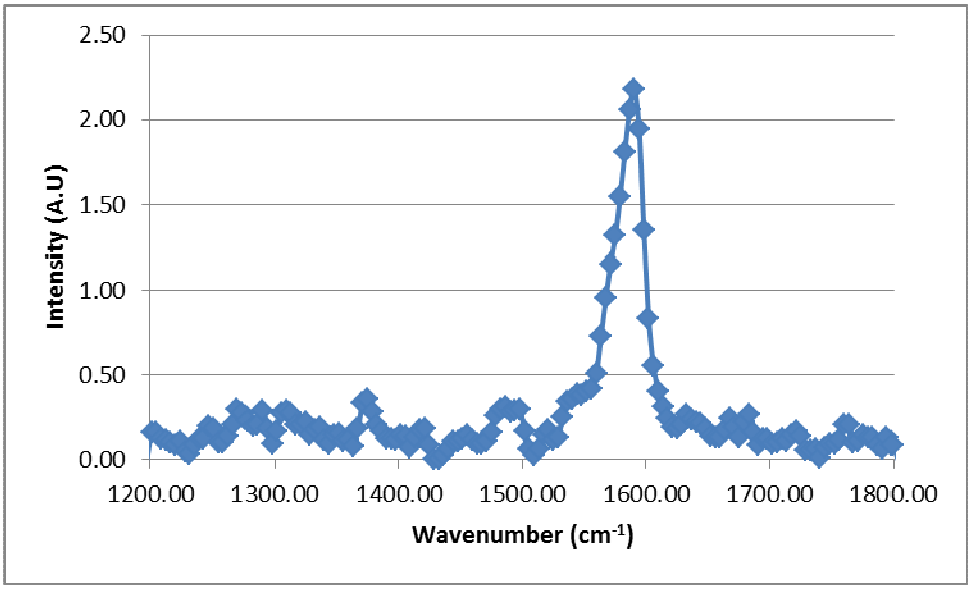


Figure 34: Raman spectrum acquired for a liver tissue sample. The sample was previously deposited on the surface of a Ge metallic disk and allowed to dry at room temperature for 30 minutes. The laser light was then shined directly into the sample in a FT-Raman system.

The data for % ID and % ID/g of tissue is plotted in Figure 35. The tumors had a higher total SWNT accumulation followed by the livers, with much lower accumulation in the kidneys (Figure 35A). From the six samples evaluated, the only one that did not have a detectable amount of SWNTs (i.e., no Raman peak) was in a kidney, which is probably because the clearance rate is relatively low at 24 hours post

administration and also because there could be variable excretion from animal to animal.

A biodistribution study conducted by Liu et al. [124] reported that for a similar administration level (≈ 0.98 mg/kg) there was no Raman signal registered for the majority of the organs. Liu et al. used SWNTs conjugated with DSPE-PEG (with different PEG molecular weights) reporting a minor Raman signal for the kidneys and a strong signal for the livers 24 hours after SWNT administration (with an approximately 70 % ID/g for the conjugates that had a PEG with a M.W. = 2,000 Da). In our study, the average % ID/g for the livers and the kidneys was approximately equal to 6 %/g and 3 %/g, respectively. Therefore, the concentration of SWNTs in the liver in the Liu et al. study was much higher than in our study, even though the SWNT administration level was similar. It is important to note that the length of the carbon nanotubes used in the Liu et al. study was approximately eight times smaller than the nanotubes used in this project, and therefore possibly explaining the higher accumulation in the liver within the same time interval. The successful detection of those nanostructures occurred when the administration dosage was approximately six times higher than that used in our study.

In the study by Robinson et al. [91] where non-targeted, PEGylated SWNTs were injected i.v. at 3.6 mg/kg in mice with 4T1 breast tumors, the concentration of SWNTs was 55 % ID/g and 8 % ID/g after 48 hours in the liver and tumor, respectively. Thus, the concentration of SWNTs in the Robinson et al. study was much greater in the liver than in our study (about nine times higher) but was similar in the tumor to our study.

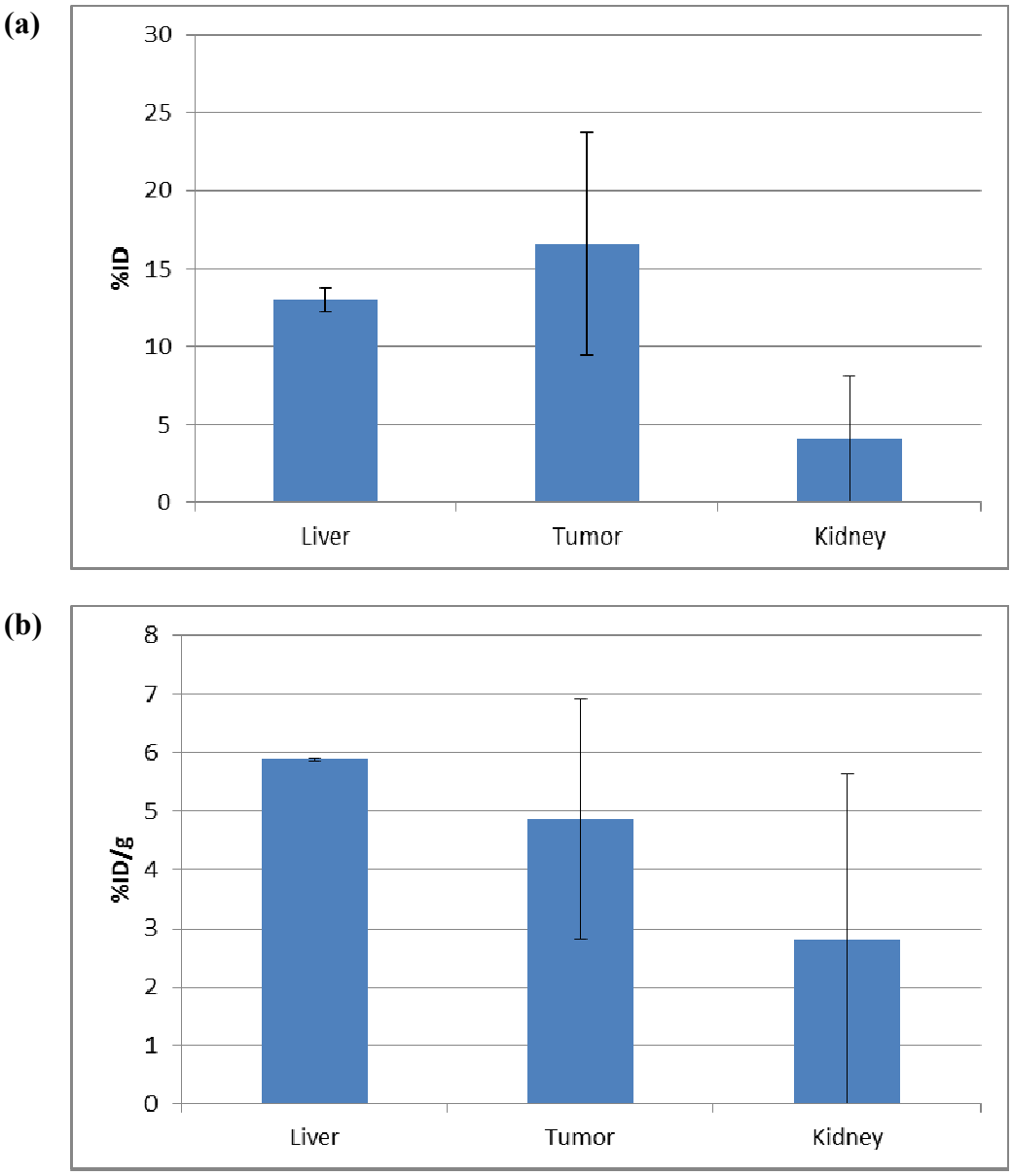


Figure 35: Biodistribution of SWNT-annexin V 24 hours post administration evaluated by FT-Raman spectroscopy. **(a)** % ID stands for percent of injected dose. **(b)** % ID/g stands for percent injected dose per gram of tissue. The data was averaged and the standard error of the mean was determined (n=2).

CHAPTER V

CONCLUSIONS AND FUTURE STUDIES

Conclusions and Future Studies

The present study aims the enhancement of the current and conventional therapeutic approaches to treat neoplasms. The need for more efficient therapies with a higher success rate and a lowering of side effects makes this research project suitable to overcome the current limitations associated with the current treatments. Radio- and chemotherapy along with invasive procedures have been used in current therapeutical procedures for a long time period and their limitations are well known. Based on the hypotheses that define this project, it is foreseen that this research will bring improvements to the actual therapies.

The production of the protein annexin V using recombinant technology allowed for its production in our laboratory which was beneficial in terms of saving time and even more important reducing costs. Also, the ability to have easy access to the nanotube samples was a key component in terms of obtaining nanotube suspensions with the highest purity levels that can be currently obtained. The theory behind the use of carbon nanotubes to the treatment of cancer is not new however, the targeting of cancer cells combined with the excellent properties inherent to the nanostructures is something new that distinguishes this research work from other studies that have been published in the last couple of years. The *in vitro* studies revealed interesting results that helped us design the *in vivo* studies as an approach to confirm this theory in live organisms.

The binding ability for the protein annexin V when incubated *in vitro* with non-confluent endothelial cells was strong, and the dissociation constant value was within the expected range as seen in the literature. Therefore, hypotheses 1 and 2, which

concerned producing annexin V in a soluble and functional form that binds selectively to endothelial cells, were proven.

The use of two different conjugation protocols allowed for obtaining single walled carbon nanotubes with immobilized annexin V at concentrations that were high enough to perform *in vitro* laser irradiation. The need for higher dosage levels of the conjugates used for the *in vivo* administration led to the need of developing a new conjugation protocol which allowed for the immobilization of higher amounts of protein on the surface of the nanostructures. The SWNT-annexin V conjugate prepared using the linker that contains DSPE gave a relatively high concentration of SWNTs in suspension (202 mg/L). The SWNT-annexin V conjugate gave a significantly peak of optical absorption near 980 nm that was similar in intensity and wavelength to when SWNTs were not conjugated to annexin V, which validates hypothesis 3.

A short incubation of endothelial cells with this conjugate followed by laser treatment resulted in significant thermal ablation. The nanotubes or the laser by themselves did not induce cell cytotoxicity, as expected.

The *in vivo* studies were successful in terms of inducing tumor regression within the animals in the treatment groups. One day after the laser irradiation of the animals, there was already a significant difference in the average tumor volumes between the animals from the treatment group and the untreated animals. At one point after laser treatment in the two treatment groups, there were no animals with visible tumors; later in a few animals there was tumor regrowth outside the area of the laser beam. It is important to mention that there was black scar formation specifically on the area where the tumor was; however there was no visible scar on the surrounding area, which was

also subjected to irradiation. Another important finding is that the skin epithelial layer in the area of the tumor was completely regenerated, with the absence of the black scar and tumor regrowth for the majority of the animals in the group treated with SWNTs and the laser. The biodistribution study revealed that there was a SWNT accumulation in the tumor (verifying the predicted accumulation as stated in the hypothesis 4), liver, and kidney 24 hours post administration. Compared to a study by another group that used non-targeted SWNTs and laser treatment of the same tumors in mice (Robinson et al. [91]), tumor eradication was achieved in this study using a much lower dosage of SWNTs (approximately four times lower) while resulting in a similar concentration of SWNTs in the tumor.

It is possible to conclude that this therapeutic approach was successful in terms of achieving partial or complete tumor eradication for the treatment groups, thus confirming hypothesis 4. Also, it is very significant that the epithelial cell layer was intact as observed by the histology analysis in the epithelial area where previously there were tumors in the mice examined in both treatment groups. In addition, the dark scars where the tumors were treated in both treatment groups had returned to a normal skin color by the end of the study for the majority of the animals.

The addition of CY did not translate into a significant difference in terms of tumor volume reduction; however, there was an increased survival of animals in the treatment group that received CY compared to the treatment group that did not, then partially proving hypothesis 5. This difference in survival could not be correlated with the histology studies of the tumor, lungs, and liver.

The results obtained on this study are encouraging, and it is suggested to pursue some additional approaches in future studies that will enhance the efficacy of the current proposed therapy.

1. In order to enhance the externalization of the PS molecules on the surface of the endothelial cells that line the tumor vasculature, it is suggested the administration of docetaxel–a well-known chemotherapeutic drug–at subtoxic dosages. Huang et al. [136] proved that the administration of this drug at those dosages was responsible for significant more externalization of anionic phospholipids *in* vivo.
2. In order to attempt to mount a more efficient immune response against the tumor antigens, it is proposed to explore the possibility of using alternative immunostimulants, both single or in combination. The cytotoxic T lymphocyte-associated antigens 4 (CTLA-4) are involved with the process of downregulation of the immune system by decreasing or suppressing the activation of T-cells. Blocking these antigens (using a CTLA-4 blockade) can be useful to mount an immune response against possible tumor antigens presented to the immune system [134, 137]. Glycated chitosan (GC) is another compound that can be obtained by linking galactose molecules to chitosan molecules. GC has been used in combination with laser phototherapies for cancer treatment and it is known to have immunostimulatory properties [138, 139]. In the study by Zhou et al., the GC when combined with a laser phototherapy had the ability to increase the

secretion of TNFα, which is an effector cytokine produced by mouse macrophages.

3. Tracking any changes within the tumor region is important and beneficial in order to determine if further irradiation therapy is necessary to achieve complete tumor eradication. This can be accomplished by using a tumor transfected with red fluorescent protein (RFP) that will allow to visualize the tumor region using a small animal imaging system [140]. Another alternative would be to use a small PET-CT imaging system [141]. After performing the first irradiation session and waiting 48 h, it would be recommended to perform a visual evaluation in order to check for the need of additional irradiation sessions.

LIST OF REFERENCES

1. http://www,creativepegworks.com.
2. Sanchez, J.-C., Corthals, G. L., Hochstrasser, D. F., *Biomedical Applications of Proteomics*, ed. J.-C. Sanchez, Corthals, G. L., Hochstrasser, D. F. 2004, Switzerland: Wiley-VCH.
3. Fink, D.J., *Cancer Overview.* Cancer Research, 1979. **39**(7): p. 2819-2821.
4. Cooper, G.M., Hausman, R. E., *The Cell - A Molecular Approach*. 2004, Washington, D. C.: ASM Press.
5. http://www.medicinenet.com/.
6. *Cancer Facts & Figures.* American Cancer Society, 2012.
7. Smith, V.L., M.A. Kaetzel, and J.R. Dedman, *Stimulus-Response Coupling - the Search for Intracellular Calcium Mediator Proteins.* Cell Regulation, 1990. **1**(2): p. 165-172.
8. Heizmann, C.W., *Novel calcium-binding proteins - Fundamentals and Clinical Implications*, ed. C.W. Heizmann. 1991, Berlin: Springer-Verlag.
9. Geisow, M.J., *Common domain structure of Ca2+ and lipid-binding proteins.* Febs Letters, 1986. **203**(1): p. 99-103.
10. Benz, J. and A. Hofmann, *Annexins: From structure to function.* Biological Chemistry, 1997. **378**(3-4): p. 177-183.
11. Schlaepfer, D.D. and H.T. Haigler, *Expression of Annexins as a Function of Cellular Growth-State.* Journal of Cell Biology, 1990. **111**(1): p. 229-238.
12. Bandorowicz-Pikula, J., *Annexins-biological importance and annexin-related pathologies*. 2003, Texas: Kluwer Academic.
13. Klee, C.B., *Ca-2+-Dependent Phospholipid-Binding (and Membrane-Binding) Proteins.* Biochemistry, 1988. **27**(18): p. 6645-6653.
14. Barton, G.J., et al., *Amino-Acid-Sequence Analysis of the Annexin Supergene Family of Proteins.* European Journal of Biochemistry, 1991. **198**(3): p. 749-760.
15. Celio, M.R., Pauls, T. L., Schwaller, B., *Guidebook to the Calcium-Binding Proteins*, ed. M.R. Celio. 1996, Switzerland: Oxford University Press.
16. Huber, R., J. Romisch, and E.P. Paques, *The Crystal and Molecular-Structure of Human Annexin-V, an Anticoagulant Protein That Binds to Calcium and Membranes.* Embo Journal, 1990. **9**(12): p. 3867-3874.
17. Sherbet, G.V., *Calcium signaling in cancer*. 2000: CRC.
18. Crumpton, M.J., *The Annexins*, ed. S.E. Moss. 1992, Cambridge: Portland Press.
19. Seaton, B.A., et al., *Purification, Crystallization, and Preliminary-X-Ray Diffraction Analysis of Rat-Kidney Annexin-V, a Calcium-Dependent Phospholipid-Binding Protein.* Journal of Biological Chemistry, 1990. **265**(8): p. 4567-4569.
20. Romisch, J. and E.P. Paques, *Annexins - Calcium-Binding Proteins of Multifunctional Importance.* Medical Microbiology and Immunology, 1991. **180**(3): p. 109-126.
21. Sigel, A. and H. Sigel, *Metal Complexes in Tumor Diagnosis and as Anticancer Agents*. Metal Ions in Biological Systems, ed. A. Sigel and H. Sigel. Vol. 42. 2004, Switzerland: Marcel Dekker, Inc.

22. Ohsawa, K., et al., *Molecular cloning and characterization of annexin V-binding proteins with highly hydrophilic peptide structure.* Journal of Neurochemistry, 1996. **67**(1): p. 89-97.
23. Kling, J., *Flow Cytometry: It's Not Just For Immunologists Anymore.* The Scientist, 1997. **11**(13): p. 14.
24. Huber, R., Berendes, R., Burger, A., Luecke H, Karshikov, A., *Annexin V-crystal structure and its implications on function.* Behring Institute Mitteilungen, 1992. **91**: p. 107-25.
25. Burger, A., et al., *A Rapid and Efficient Purification Method for Recombinant Annexin-V for Biophysical Studies.* Febs Letters, 1993. **329**(1-2): p. 25-28.
26. Wang, F., et al., *Non-fusion expression in Escherichia coli: Single-step purification of recombinant human annexin A5 for detection of apoptosis.* Protein Expression and Purification, 2006. **45**(1): p. 80-87.
27. Mira, J.P., et al., *Inhibition of cytosolic phospholipase A(2) by annexin V in differentiated permeabilized HL-60 cells - Evidence of crucial importance of domain I type II Ca2+-binding site in the mechanism of inhibition.* Journal of Biological Chemistry, 1997. **272**(16): p. 10474-10482.
28. Brush, M.D., *Recourse to Death - A bevy of new products harnesses the power of flow cytometry for detecting apoptosis.* The Scientist, 2000. **14**(16): p. 25.
29. Thiagarajan, P. and J.F. Tait, *Binding of Annexin-V Placental Anticoagulant Protein I to Platelets - Evidence for Phosphatidylserine Exposure in the Procoagulant Response of Activated Platelets.* Journal of Biological Chemistry, 1990. **265**(29): p. 17420-17423.
30. Thiagarajan, P. and J.F. Tait, *Collagen-Induced Exposure of Anionic Phospholipid in Platelets and Platelet-Derived Microparticles.* Journal of Biological Chemistry, 1991. **266**(36): p. 24302-24307.
31. Tait, J.F., et al., *Prourokinase-Annexin-V Chimeras - Construction, Expression, and Characterization of Recombinant Proteins.* Journal of Biological Chemistry, 1995. **270**(37): p. 21594-21599.
32. Tait, J.F., C. Smith, and D.F. Gibson, *Development of annexin V mutants suitable for labeling with Tc(I)-carbonyl complex.* Bioconjugate Chemistry, 2002. **13**(5): p. 1119-1123.
33. DeFrancesco, L., *The death of a cell: a profile of apoptosis kits and reagents.* The Scientist, 1997. **11**(24): p. 22.
34. DeFrancesco, L., *Dead Again: Adventures in Apoptosis.* 1999. **13**(5): p. 17.
35. Ran, S., A. Downes, and P.E. Thorpe, *Increased exposure of anionic phospholipids on the surface of tumor blood vessels.* Cancer Research, 2002. **62**(21): p. 6132-6140.
36. Huang, X.M., M. Bennett, and P.E. Thorpe, *A monoclonal antibody that binds anionic phospholipids on tumor blood vessels enhances the antitumor effect of docetaxel on human breast tumors in mice.* Cancer Research, 2005. **65**(10): p. 4408-4416.
37. Verkleij, A.J., et al., *Asymmetric Distribution of Phospholipids in Human Red-Cell Membrane - Combined Study Using Phospholipases and Freeze-Etch Electron-Microscopy.* Biochimica Et Biophysica Acta, 1973. **323**(2): p. 178-193.

38. Gordesky, S.E., G.V. Marinetti, and R. Love, *Reaction of Chemical Probes with Erythrocyte-Membrane.* Journal of Membrane Biology, 1975. **20**(1-2): p. 111-132.
39. Zwaal, R.F.A., et al., *Organization of Phospholipids in Human Red-Cell Membranes as Detected by Action of Various Purified Phospholipases.* Biochimica Et Biophysica Acta, 1975. **406**(1): p. 83-96.
40. Marinetti, G.V. and R.C. Crain, *Topology of Amino-Phospholipids in Red-Cell Membrane.* Journal of Supramolecular Structure, 1978. **8**(2): p. 191-213.
41. Diaz, C. and A.J. Schroit, *Role of translocases in the generation of phosphatidylserine asymmetry.* Journal of Membrane Biology, 1996. **151**(1): p. 1-9.
42. Schönthal, A.H., *Checkpoint Controls and Cancer*, ed. A.H. Schönthal. Vol. 281. 2004: Humana Press.
43. Seigneuret, M. and P.F. Devaux, *Atp-Dependent Asymmetric Distribution of Spin-Labeled Phospholipids in the Erythrocyte-Membrane - Relation to Shape Changes.* Proceedings of the National Academy of Sciences of the United States of America-Biological Sciences, 1984. **81**(12): p. 3751-3755.
44. Daleke, D.L. and W.H. Huestis, *Incorporation and Translocation of Aminophospholipids in Human-Erythrocytes.* Biochemistry, 1985. **24**(20): p. 5406-5416.
45. http://www.springboard4health.com/books_online/ps/phosphatidylserine.html.
46. Ran, S. and P.E. Thorpe, *Phosphatidylserine is a marker of tumor vasculature and a potential target for cancer imaging and therapy.* International Journal of Radiation Oncology Biology Physics, 2002. **54**(5): p. 1479-1484.
47. Beck, A.W., et al., *Combination of a monoclonal anti-phosphatidylserine antibody with gemcitabine strongly inhibits the growth and metastasis of orthotopic pancreatic tumors in mice.* International Journal of Cancer, 2006. **118**(10): p. 2639-2643.
48. Verhoven, B., R.A. Schlegel, and P. Williamson, *Mechanisms of Phosphatidylserine Exposure, a Phagocyte Recognition Signal, on Apoptotic T-Lymphocytes.* Journal of Experimental Medicine, 1995. **182**(5): p. 1597-1601.
49. Blondelle, S.E., *Understanding Biology Using Peptides: Proceedings of the 19th American Peptide Symposium*, ed. S.E. Blondelle. 2006, New York: Springer.
50. Yuan, H., X. Yang, and Z.C. Hua, *Optimization of expression of an Annexin V-Hirudin chimeric protein in Escherichia coli.* Microbiological Research, 2004. **159**(2): p. 147-156.
51. Bevers, E.M., P. Comfurius, and R.F.A. Zwaal, *Changes in Membrane Phospholipid Distribution during Platelet Activation.* Biochimica Et Biophysica Acta, 1983. **736**(1): p. 57-66.
52. Rao, L.V.M., J.F. Tait, and A.D. Hoang, *Binding of Annexin-V to a Human Ovarian-Carcinoma Cell-Line (Oc-2008) - Contrasting Effects on Cell-Surface Factor-Viia/Tissue Factor Activity and Prothrombinase Activity.* Thrombosis Research, 1992. **67**(5): p. 517-531.
53. Qu, J.M., et al., *Phosphatidylserine-mediated adhesion of T-cells to endothelial cells.* Biochemical Journal, 1996. **317**: p. 343-346.

54. Vangeelen, A.G.M., et al., *Membrane Related Effects in Endothelial-Cells Induced by Human Cytomegalovirus.* Archives of Virology, 1995. **140**(9): p. 1601-1612.
55. Lupu, F., et al., *Intrinsic Procoagulant Surface-Induced by Hypercholesterolemia on Rabbit Aortic Endothelium.* Blood Coagulation & Fibrinolysis, 1993. **4**(5): p. 743-752.
56. Demo, S.D., et al., *Quantitative measurement of mast cell degranulation using a novel flow cytometric annexin-V binding assay.* Cytometry, 1999. **36**(4): p. 340-348.
57. Herrmann, A. and P.F. Devaux, *Alteration of the Aminophospholipid Translocase Activity during In vivo and Artificial Aging of Human Erythrocytes.* Biochimica Et Biophysica Acta, 1990. **1027**(1): p. 41-46.
58. Vogt, E., A.K. Ng, and N.S. Rote, *A model for the antiphospholipid antibody syndrome: Monoclonal antiphsophatidylserine antibody induces intrauterine growth restriction in mice.* American Journal of Obstetrics and Gynecology, 1996. **174**(2): p. 700-707.
59. Blankenberg, F.G., et al., *In vivo detection and imaging of phosphatidylserine expression during programmed cell death.* Proceedings of the National Academy of Sciences of the United States of America, 1998. **95**(11): p. 6349-6354.
60. Bombeli, T., et al., *Apoptotic vascular endothelial cells become procoagulant.* Blood, 1997. **89**(7): p. 2429-2442.
61. Adler, R.R., A.K. Ng, and N.S. Rote, *Monoclonal Antiphosphatidylserine Antibody Inhibits Intercellular Fusion of the Choriocarcinoma Line, Jar.* Biology of Reproduction, 1995. **53**(4): p. 905-910.
62. Sessions, A. and A.F. Horwitz, *Myoblast Aminophospholipid Asymmetry Differs from That of Fibroblasts.* Febs Letters, 1981. **134**(1): p. 75-78.
63. Utsugi, T., et al., *Elevated Expression of Phosphatidylserine in the Outer-Membrane Leaflet of Human Tumor-Cells and Recognition by Activated Human Blood Monocytes.* Cancer Research, 1991. **51**(11): p. 3062-3066.
64. Utsugi, T., et al., *Elevated expression of phosphatidylserine in the outer membrane leaflet of human tumor cells and recognition by activated human blood monocytes.* Cancer Research, 1991. **51**(11): p. 3062.
65. Bianco, A., et al., *Biomedical applications of functionalized carbon nanotubes.* Chemical Communications, 2005(5): p. 571-577.
66. McDonald, D.M. and P. Baluk, *Significance of blood vessel leakiness in cancer.* Cancer Research, 2002. **62**(18): p. 5381-5385.
67. Shaughnessy, S.G., et al., *Walker Carcinosarcoma Cells Damage Endothelial-Cells by the Generation of Reactive Oxygen Species.* American Journal of Pathology, 1989. **134**(4): p. 787-796.
68. Liu, Z., et al., *In vivo biodistribution and highly efficient tumor targeting of carbon nanotubes in mice.* Nature Nanotechnology, 2007. **2**(1): p. 47-52.
69. Wang, X., et al., *Fabrication of Ultralong and Electrically Uniform Single-Walled Carbon Nanotubes on Clean Substrates.* Nano Letters, 2009. **9**(9): p. 3137-3141.

70. Lin, Y., et al., *Advances toward bioapplications of carbon nanotubes.* Journal of Materials Chemistry, 2004. **14**(4): p. 527-541.
71. Bachilo, S.M., et al., *Narrow (n,m)-distribution of single-walled carbon nanotubes grown using a solid supported catalyst.* Journal of the American Chemical Society, 2003. **125**(37): p. 11186-11187.
72. Cherukuri, P., et al., *Mammalian pharmacokinetics of carbon nanotubes using intrinsic near-infrared fluorescence.* Proceedings of the National Academy of Sciences of the United States of America, 2006. **103**(50): p. 18882-18886.
73. Liu, Y. and H. Wang, *Nanotechnology tackles tumors.* Nature Nanotechnology, 2007. **2**.
74. http://www.azonano.com/details.asp?ArticleID=980, *Carbon Nanotube Applications.*
75. http://www.cheaptubesinc.com/applications.htm. *Properties and Applications of Carbon Nanotubes*.
76. Kohli, P. and C.R. Martin, *Smart nanotubes for biotechnology.* Current Pharmaceutical Biotechnology, 2005. **6**(1): p. 35-47.
77. Fu, K., Huang, W., Lin, Y., Zhang, D., Hanks, T. W., Rao, A. M., and Sun, Y., *Functionalization of Carbon Nanotubes with Bovine Serum Albumin in Homogeneous Aqueous Solution.* Journal of Nanoscience and Nanotechnology, 2002. **2**(5): p. 457-461.
78. Huang, W., Taylor, S., Fu, K., Lin, Y., Zhang, D., Hanks, T. W., Rao, A. M., and Sun, Y., *Attaching Proteins to Carbon Nanotubes via Diimide-Activated Amidation.* Nanoletters, 2002. **2**(4): p. 311-314.
79. Kam, N.W.S., et al., *Carbon nanotubes as multifunctional biological transporters and near-infrared agents for selective cancer cell destruction.* Proceedings of the National Academy of Sciences of the United States of America, 2005. **102**(33): p. 11600-11605.
80. Lolli, G., et al., *Tailoring (n,m) structure of single-walled carbon nanotubes by modifying reaction conditions and the nature of the support of CoMo catalysts.* Journal of Physical Chemistry B, 2006. **110**(5): p. 2108-2115.
81. Buffa, F., H. Hu, and D.E. Resasco, *Side-wall functionalization of single-walled carbon nanotubes with 4-hydroxymethylaniline followed by polymerization of epsilon-caprolactone.* Macromolecules, 2005. **38**(20): p. 8258-8263.
82. Moore, V.C., et al., *Individually Suspended Single-Walled Carbon Nanotubes in Various Surfactants.* Nano Letters, 2003. **3**(10): p. 1379-1382.
83. Graff, R.A., et al., *Achieving individual-nanotube dispersion at high loading in single-walled carbon nanotube composites.* Advanced Materials, 2005. **17**(8): p. 980-+.
84. Shao, N., et al., *Integrated molecular targeting of IGF1R and HER2 surface receptors and destruction of breast cancer cells using single wall carbon nanotubes.* Nanotechnology, 2007. **18**: p. 315101.
85. Chakravarty, P., et al., *Thermal ablation of tumor cells with antibody-functionalized single-walled carbon nanotubes.* Proceedings of the National Academy of Sciences, 2008. **105**(25): p. 8697.

86. Wang, C.H., et al., *In vitro photothermal destruction of neuroblastoma cells using carbon nanotubes conjugated with GD2 monoclonal antibody.* Nanotechnology, 2009. **20**: p. 315101.
87. Marches, R., et al., *The importance of cellular internalization of antibody-targeted carbon nanotubes in the photothermal ablation of breast cancer cells.* Nanotechnology, 2011. **22**: p. 095101.
88. Fisher, J.W., et al., *Photothermal response of human and murine cancer cells to multiwalled carbon nanotubes after laser irradiation.* Cancer Research, 2010. **70**(23): p. 9855.
89. Zhou, F., et al., *Cancer photothermal therapy in the near-infrared region by using single-walled carbon nanotubes.* Journal of biomedical optics, 2009. **14**: p. 021009.
90. Moon, H.K., S.H. Lee, and H.C. Choi, *In vivo near-infrared mediated tumor destruction by photothermal effect of carbon nanotubes.* ACS Nano, 2009. **3**(11): p. 3707-3713.
91. Robinson, J.T., et al., *High performance in vivo near-IR (> 1 μm) imaging and photothermal cancer therapy with carbon nanotubes.* Nano research, 2010. **3**(11): p. 779-793.
92. Ghosh, S., et al., *Increased Heating Efficiency and Selective Thermal Ablation of Malignant Tissue with DNA-Encased Multiwalled Carbon Nanotubes.* ACS Nano, 2009. **3**(9): p. 2667-2673.
93. Burke, A., et al., *Long-term survival following a single treatment of kidney tumors with multiwalled carbon nanotubes and near-infrared radiation.* Proceedings of the National Academy of Sciences, 2009. **106**(31): p. 12897-12902.
94. Liu, X., et al., *Optimization of surface chemistry on single-walled carbon nanotubes for in vivo photothermal ablation of tumors.* Biomaterials, 2011. **32**(1): p. 144-151.
95. Tatke, S., V. Renugopalakrishnan, and M. Prabhakaran, *Interfacing biological macromolecules with carbon nanotubes and silicon surfaces: a computer modelling and dynamic simulation study.* Nanotechnology, 2004. **15**: p. S684.
96. Mittal, V., *Carbon nanotubes surface modifications: An Overview*, in *Surface modification of nanotube fillers*, V. Mittal, Editor. 2011, Wiley-VCH Verlag GmbH & Co. KGaA. p. 1-23.
97. Chen , R.J., Zhang , Y. , Wang , D. , and Dai , H., *Spectroscopic evidence and molecular simulation investigation of the pi-pi interaction between pyrene molecules and carbon nanotubes.* Journal of the American Chemical Society, 2001. **123**: p. 3838.
98. *http://upload.wikimedia.org/wikipedia/commons/e/e1/Sodium_laurylsulfonate_V.1.svg*.
99. http://www.creativepegworks.com/heterobifunctional%20PEG.html.
100. *http://www.sunbio.com/peg-shop/peg-shop-pegylation06.asp*.
101. Thomas-Tikhonenko, A., *Cancer Genome and Tumor Microenvironment*. Vol. 3. 2009: Springer Verlag.

102. Folkman, J., *Tumor Angiogenesis*, in *Holland-Frei Cancer Medicine*, K.D. Bast RC Jr, Pollock RE, et al., Editor. 2000.
103. *http://www.angioworld.com/cancer.htm*.
104. Maeda, H., *The Enhanced Permeability and Retention (EPR) Effect in Tumor Vasculature: The Key Role of Tumor-Selective Macromolecular Drug Targeting.* Advances in Enzyme Regulation, 2001. **41**: p. 189-207.
105. *http://jaxmice.jax.org/strain/000651.html*.
106. *http://jaxmice.jax.org/images/jaxmicedb/featuredImage/000651_lg.jpg*.
107. *http://jaxmice.jax.org/images/jaxmicedb/weights/000651-lg.gif*.
108. *http://www2.healthsci.tufts.edu/saif/4T1.htm*.
109. *http://www.ncbi.nlm.nih.gov/pubmedhealth/PMH0000570/*.
110. Moore, M.J., *Clinical pharmacokinetics of cyclophosphamide.* Clinical pharmacokinetics, 1991. **20**(3): p. 194.
111. Takimoto, C.H. and E. Calvo, *Principles of oncologic pharmacotherapy.* Cancer Management: A Multidisciplinary Approach, 1998. **11**.
112. Chabner, B.A. and D.L. Longo, *Cancer chemotherapy and biotherapy: principles and practice*. 2010: Lippincott Williams & Wilkins.
113. Taieb, J., et al., *Chemoimmunotherapy of tumors: cyclophosphamide synergizes with exosome based vaccines.* The Journal of Immunology, 2006. **176**(5): p. 2722-2729.
114. Barbon, C.M., et al., *Consecutive low doses of cyclophosphamide preferentially target Tregs and potentiate T cell responses induced by DNA PLG microparticle immunization.* Cellular immunology, 2010. **262**(2): p. 150-161.
115. Amir, S. and H.G. Nechama, *Immune Recovery after Cyclophosphamide Treatment in Multiple Myeloma: Implication for Maintenance Immunotherapy.* Bone marrow research, 2011. **2011**.
116. Castano, A.P., et al., *Photodynamic therapy plus low-dose cyclophosphamide generates antitumor immunity in a mouse model.* Proceedings of the National Academy of Sciences, 2008. **105**(14): p. 5495.
117. Fernandez, J.M., *Gene Expression Systems*, ed. J.M. Fernandez. 1999, California: Academic Press.
118. Palwai, N.R., *Fill this info Naveen Thesis*. 2007.
119. Scopes, R., *Protein Purification: Principles and practice*. 1982, New York: Springer-Verlag.
120. Bao, L., et al., *Increased expression of P-glycoprotein is associated with doxorubicin chemoresistance in the metastatic 4T1 breast cancer model.* The American journal of pathology, 2011. **178**(2): p. 838.
121. Chakrabarti, R., et al., *Tranilast inhibits the growth and metastasis of mammary carcinoma.* Anti-cancer drugs, 2009. **20**(5): p. 334.
122. http://www.invitrogen.com/site/us/en/home/brands/Molecular-Probes/Key-Molecular-Probes-Products/alamarBlue-Rapid-and-Accurate-Cell-Health-Indicator.html.
123. *http://science.nayland.school.nz/graemeb/images/2010/animals/Cut_Rat%5B1%5D.jpg*.

124. Liu, Z., et al., *Circulation and long-term fate of functionalized, biocompatible single-walled carbon nanotubes in mice probed by Raman spectroscopy.* Proceedings of the National Academy of Sciences, 2008. **105**(5): p. 1410-1415.
125. Tait, J.F., D.F. Gibson, and C. Smith, *Measurement of the affinity and cooperativity of annexin V-membrane binding under conditions of low membrane occupancy.* ANAL BIOCHEM, 2004. **329**(1): p. 112-119.
126. Zhou, F., et al., *Mitochondria Targeting Single Walled Carbon Nanotubes for Cancer Photothermal Therapy.* Small, 2011.
127. Palwai, N.R., et al., *Retention of biological activity and near-infrared absorbance upon adsorption of horseradish peroxidase on single-walled carbon nanotubes.* Nanotechnology, 2007. **18**: p. 235601.
128. Liu, Z., et al., *Carbon materials for drug delivery & cancer therapy.* Materials Today, 2011. **14**(7-8): p. 316-323.
129. Palwai, N.R., et al., *Retention of biological activity and near-infrared absorbance upon adsorption of horseradish peroxidase on single-walled carbon nanotubes.* Nanotechnology, 2007. **18**(23).
130. Malik, S., et al., *Physical chemical characterization of DNA–SWNT suspensions and associated composites.* Composites science and technology, 2007. **67**(5): p. 916-921.
131. *Southwest Nanotechnologies SG 65 Single-wall Carbon Nanotubes Data Sheet.*
132. Choi, N., et al., *Atomic force microscopy of single-walled carbon nanotubes using carbon nanotube tip.* Japanese Journal of Applied Physics, 2000. **39**(part 1): p. 3707-3710.
133. Van Rite, B.D. and R.G. Harrison, *Annexin V-targeted enzyme prodrug therapy using cytosine deaminase in combination with 5-fluorocytosine.* Cancer Letters, 2011.
134. Demaria, S., et al., *Immune-mediated inhibition of metastases after treatment with local radiation and CTLA-4 blockade in a mouse model of breast cancer.* Clinical cancer research, 2005. **11**(2): p. 728-734.
135. Chen, L., et al., *Rejection of metastatic 4T1 breast cancer by attenuation of Treg cells in combination with immune stimulation.* Molecular Therapy, 2007. **15**(12): p. 2194-2202.
136. Huang, X., M. Bennett, and P.E. Thorpe, *A monoclonal antibody that binds anionic phospholipids on tumor blood vessels enhances the antitumor effect of docetaxel on human breast tumors in mice.* Cancer Research, 2005. **65**(10): p. 4408.
137. Lee, B., N. Mukhi, and D. Liu, *Current management and novel agents for malignant melanoma.* Journal of Hematology & Oncology, 2012. **5**(1): p. 3.
138. Zhou, F., et al., *Immunostimulatory properties of glycated chitosan.* Journal of X-Ray Science and Technology, 2011. **19**(2): p. 285-292.
139. Chen, W.R., et al., *Effect of different components of laser immunotherapy in treatment of metastatic tumors in rats.* Cancer Research, 2002. **62**(15): p. 4295.
140. Joo, S., et al., *Bioimaging for the monitoring of the in vivo distribution of infused mesenchymal stem cells in a mouse model of the graft-versus-host reaction.* Cell Biology International, 2011. **35**: p. 417-421.

141. Zhou, M., et al., *A chelator-free multifunctional [64Cu] CuS nanoparticle platform for simultaneous micro-PET/CT imaging and photothermal ablation therapy.* Journal of the American Chemical Society, 2010.
142. Ausubel, F.M., Brent, R., Kingston, R. E., Moore, D. D., Seidman, J. G., Smith, J. A., Struhl, K., *Current Protocols in Molecular Biology*, ed. F.M. Ausubel. Vol. 1. 1987, New York: John Wiley & Sons.
143. Novagen, I., *Novagen Catalog.* 2006.
144. http://us.expasy.org/tools/pi_tool.html.
145. Grabarek, Z.a.G., J., *Zero-length crosslinking procedure with the use of active esters.* Analytical Biochemistry, 1990. **185**: p. 131-5.
146. Staros, J.V., et al., *Enhancement by N-hydroxysulfosuccinimide of water-soluble carbodiimide-mediated coupling reactions.* Analytical Biochemistry, 1986. **156**: p. 220-2.
147. Timkovich, R., *Detection of the stable addition of carbodiimide to proteins.* Analytical Biochemistry, 1977. **79**: p. 135-43.
148. *http://www.atcc.org/ATCCAdvancedCatalogSearch/ProductDetails/tabid/452/Default.aspx?ATCCNum=CRL-2472&Template=cellBiology*.
149. http://www.atcc.org.
150. http://www.innovativecelltech.com/.
151. http://www.hausserscientific.com/products/reichert_bright_line.html.
152. *http://www.sigmaaldrich.com/etc/medialib/docs/Sigma/Bulletin/tox8bul.Par.0001.File.tmp/tox8bul.pdf*.
153. http://www.atcc.org/attachments/4889.pdf.
154. http://media.wiley.com/CurrentProtocols/IM/im0106/im0106-fig-0008-1-full.gif.
155. Hedrich H., B.G., *The Handbook of Experimental Animals*, in *The Laboratory Mouse*, H. Hedrich, Editor. 2004, Elsevier Academic Press: Italy.

APPENDICES

APPENDIX A

Laboratory Protocols

A.1. Laboratory Protocols

A.1.1. Luria Bertani (LB) medium

Table A.1: LB medium composition [142].

Component	Amount
Tryptone	10 g
Yeast extract	5 g
NaCl	5 g
1N NaOH	1 ml
Add dH_2O to 1.0 L and autoclave (25 mins).	

A.1.2. LB agar

Table A.2: LB Agar / SOC medium composition (per Liter).

Component	Amount
Tryptone	10 g
Yeast extract	5 g
NaCl	5 g
Agar	15 g
Add dH_2O to 1.0 L Adjust pH to 7.0 with 5 N NaOH Autoclave Pour into Petri dishes (~25 ml/100-mm plate)	

A.1.3. Additives:

Antibiotic: Kanamycin ($C_{18}H_{36}N_4O_{11}\cdot H_2SO_4$)

Galactosides: IPTG to 0.1 mM

Table A.3: Kanamycin properties [142].

Antibiotic [a]	Stock conc. (mg/ml)	Final conc. (µg/ml)	Mode of action	Mode of resistance
Kanamycin	10	30	Bactericidal; inhibits protein synthesis; inhibits translocation and elicits miscoding.	Aminoglycoside phosphotransferase also known as neomycin phosphotransferase, aminoglycoside acetyltransferase, and aminoglycoside nucleotidyltransferase; inactivates kanamycin.

[a] Kanamycin should be stored at 4 ºC, since it loses potency at room temperature [142].

A.1.4. Kanamycin preparation

To prepare kanamycin (10 mg/ml) 25 ml of deionized water and 250 mg of kanamycin (Sigma, St. Louis, MO) were mixed, and stored in the freezer (-20 ºC).

A.1.5. IPTG preparation (10 mg/ml)

0.4 g of IPTG (stored at -20 ºC)

40 ml of sterile and distilled water

A.1.6. Sonication buffer preparation

0.05 mM N-p-tosyl-L-phenylalanine chloromethyl ketone (TPCK)
1 mM phenylmethylsulfonyl fluoride (PMSF)
1 % of ethanol (ethyl alcohol)
0.01 % β-mercaptoethanol
0.02 M of sodium phosphate

The pH was adjusted to 7.4.

A.1.7. Sonication protocol (4 ºC)

The sonication equipment (Sonic Dismembrator 550 (Fisher Scientific, USA)) is turned on to the position 4/5 (power of 76.5 W). The tip of the sonicator (Sonic Dismembrator 550 (Fisher Scientific, USA)) is immersed in the solution to disrupt the cell membranes for 30 seconds. After that, the sonicator is turned off for another 30 seconds (with the beaker placed on ice). This procedure is repeated 4x corresponding to a total sonication time of 2.5 minutes. After the sonication, the solution is centrifuged at 12,000 x *g* for 30 min.



Figure A.1.1.: Sonication process.

A.1.8. HRV 3C protease

Recombinant type 14 3C protease from human rhinovirus (HRV 3C) is a recombinant restriction-grade protease. HRV 3C is a highly purified recombinant 6X His-fusion protein, that recognizes the same cleavage site as the native enzyme: Leu Glu Val Leu Phe Gln ↓ Gly Pro. The small, 22-kDa size of the protease, optimal activity at 4 ºC, high specificity, and His·Tag® fusion make HRV 3C protease an ideal choice for rapid removal of fusion tags [143].

Components

- 500 U HRV 3C Protease (2000 U/ml in 150 mM NaCl, 50 mM Tris-HCl, 1 mM EDTA, 0.5 mM THP, 50% glycerol, pH 8.0)
- 10 µg HRV 3C Cleavage Control Protein (in 100 mM NaCl, 50 mM Tris-HCl, 10 mM EDTA, 50% glycerol, pH 7.4)
- 10 ml 10X HRV 3C Protease Cleavage Buffer (1.5 M NaCl, 0.5 M Tris-HCl, pH 7.5)

Unit definition: One unit will cleave > 95 % of 100 µg His·Tag fusion control protein in 50 mM Tris-HCl, 150 mM NaCl, pH 7.5 at 4 ºC for 16 hours.

A.1.9. Tris-HCl

1.5 M Tris-HCl pH 8.8 (TRIS – Electrophoresis purity reagent (Tris(hydroxymethyl)-aminomethane) (CA, USA))
1 M Tris-HCl pH 6.8 (TRIS – Electrophoresis purity reagent (Tris(hydroxymethyl)-aminomethane) (CA, USA))

A.1.10. Acrylamide (29%) Bis (1%)

Mix 29.0 g acrylamide and 1.0 g N-N'-methylene-bisacrylamide in a total volume of 100 ml H_2O. Store at 4 ºC in the dark. Discard after 30 days, since acrylamide gradually hydrolyzes to acrylic acid and ammonia.
CAUTION: *Acrylamide monomer is neurotoxic. Gloves should be worn while handling the solution, and the solution should not be pipetted by mouth.*

A.1.11. Electrophoresis buffer

10% Bio-Rad 10x Tris/Glycine/SDS Buffer (Bio-Rad Laboratories (Hercules, CA))
90% H_2O

A.1.12. Ammonium persulfate preparation

10 g ammonium persulfate
H_2O to 100 ml total volume
Store refrigerated ~ 2 weeks.

A.1.13. Cell Medium Preparation

In order to prepare a new bottle of cell medium for the human endothelial cells mix the following:
- F12K medium (1 flask, 500 ml);
- 50 ml of fetal bovine serum;
- 5 ml of antibiotic (penicillin and streptomycin);
- 3 ml of heparin (0.1 mg/ml) and,
- 1.5 ml of ECGS (endothelial cell growth supplement; 0.03 mg/ml).

For the 4T1 cells mix the following:
- RPMI-1640 medium (1 flask, 500 ml);

- 50 ml of fetal bovine serum;
- 5 ml of antibiotic (penicillin and streptomycin).

Due to the fact that the medium contains proteins, it can be stored only for approximately 2-3 weeks at 4 ºC.

A.1.14. PBS preparation

Mix:
8 g of NaCl
0.2 g of KCl
1.44 g of Na_2HPO_4
0.24 g of KH_2PO_4
1 L of deionized water.

A.2 Experimental Protocols

A.2.1. Transformation Protocol

Transformation

NovaBlue GigaSingles™ Competent Cells (Cat. No. 71127) are provided in the Ek/LIC vector kits and should be used for initial cloning with all Ek/LIC Vectors. NovaBlue is a convenient host for initial cloning of target DNA into the Ek/LIC vector due to its high transformation efficiency and the high yields and excellent plasmid DNA that results from *rec*A *endA* mutations. Single-use NovaBlue GigaSingles Competent Cells are provided in 50 µl aliquots. The pET, pCDF-2, pRSF-2, and pTriEx™ Ek/LIC vector kits also receive expression host strains in standard, 0.2 ml aliquots.

The standard transformation reaction calls for 20 µl of cells, so each tube contains enough cells for 10 transformations. The following protocol is appropriate for transformations using either GigaSingles or Standard Competent Cells with noted differences for the steps effected.

Note: Upon receipt of competent cells from Novagen, verify that the cells are frozen and that dry ice is present in the shipping container. Immediately place the competent cells at –70 °C or below. For optimal results, do not allow the cells to thaw at any time prior to use. Handle only the very top of the tube and the tube cap to prevent the cells from warming. Keep the cells on ice whenever possible. To mix cells, flick the tube 1–3 times. NEVER vortex competent cells.

1. Remove the appropriate number of competent cell tubes from the freezer (include on extra sample for the Test Plasmid positive control, if desired). Immediately place the tubes on ice, so that all but the cap is immersed in ice. Allow the cells to thaw on ice for 2–5 min.
2. Visually examine the cells and gently flick the cells 1–2 times to evenly resuspend the cells.
3. *GigaSingles Kits:*

If a Test Plasmid sample is included, proceed to Step 4, if not go directly to Step 5.

Standard Kits:

Place the required number of 1.5 ml snapcap polypropylene tubes on ice to pre-chill. Pipet 20 µl aliquots of cells into the prechilled tubes.

4. (Optional) To determine transformation efficiency, add 1 µl (0.2 ng) Test Plasmid to one of the tubes containing cells. Gently flick the tube to mix and return to the ice.

5. Add 1 µl of the annealing reaction directly to the cells. Stir gently to mix and return to the ice.

Repeat for additional samples.

6. Incubate on ice for 5 min.

7. Heat the tubes for exactly 30 s in a 42 °C water bath; do not shake.

8. Place the tubes on ice for 2 min.

9. *GigaSingles Kits:*

Add **250 µl** of room temperature SOC medium to each tube. Keep the tubes on ice until all have received SOC.

Standard Kits:

Add **80 µl** of room temperature SOC medium to each tube. Keep the tubes on ice until all have received SOC.

10. Incubate at 37 °C while shaking at 250 rpm for 60 min prior to plating on selective medium.

11. Selection for transformants is accomplished by plating on medium containing antibiotic for the plasmid encoded drug resistance (50 µg/ml carbenicillin or ampicillin for the Amp resistance marker, 30 µg/ml kanamycin for the kan resistance marker, and 50 µg/ml of streptomycin and/or spectinomycin for the *aadA* gene). Additional host-specific antibiotics may also be appropriate to ensure maintenance of the host-encoded feature(s).

When plating less than 25 µl, first pipet a "pool" of SOC onto the plate and then pipet the cells into the SOC. The appropriate amount of transformation mixture to plate varies with the efficiencies of the annealing process and of the competent cells (see certificate of analysis for efficiency). For recombinants in NovaBlue, expect 105–107 transformants/µg plasmid, depending on the particular insert and the ligation efficiency. For the Test Plasmid, plate only 5 µl of the NovaBlue transformation mix or 10 µl of any strain with a 2×10^6 efficiency in a "pool" of SOC on an LB agar plate containing 50 µg/ml carbenicillin or ampicillin (because the Test Plasmid carries the ampicillin resistance gene, *bla*).

12. Set plates on the bench for several minutes to allow excess liquid to be absorbed, and then invert and incubate overnight at 37 °C.

Transformation Protocol for Experienced Users

Note: See the next section for a detailed protocol.

1. Thaw the required number of tubes of cells on ice and mix gently to ensure that the cells are evenly suspended.

2. *Standard Kits:*

Place the required number of 1.5 ml polypropylene microcentrifuge

tubes on ice to pre-chill. Pipet 20 µl aliquots of cells into the pre-chilled tubes.

Singles™ Kits:

Proceed to Step 3.

3. Add 1 µl of the DNA solution directly to the cells. Stir gently to mix.

4. Place the tubes on ice for 5 min.

5. Heat the tubes for exactly 30 s in a 42 °C water bath; do not shake.

6. Place on ice for 2 min.

7. *Standard Kits:*

Add **80 µl** of room temperature SOC medium to each tube.

Singles Kits:

Add **250 µl** of room temperature SOC medium to each tube.

8. Selection for transformants is accomplished by plating on medium containing antibiotic for the plasmid-encoded drug resistance. Additional host-specific antibiotics may also be appropriate to insure maintenance of the host-encoded feature(s).

When using NovaBlue strain: if selecting for ampicillin or chloramphenicol resistance, plate 5–50 µl cells directly on selective medium (plus IPTG/X-gal for plasmids that permit blue/white screening). If selecting for kanamycin or streptomycin/spectinomycin resistance, shake at 37 °C (250 rpm) for 30 min prior to plating on selective medium.

When using strains other than NovaBlue, incubate at 37 °C while shaking at 250 rpm for 60 min prior to plating on selective medium.

A.2.2. Bradford protein assay

Principle

This assay is a dye-binding assay in which a differential color change of dye occurs in response to various concentrations of protein. The Coomassie blue dye binds to primarily basic and aromatic amino acid residues, especially arginine.

Materials

1x dye reagent (Bio-Rad, Hercules, CA, USA) and the standard were acquired from Biorad. A Shimadzu UV-2101 PC UV-Vis spectrophotometer (Shimadzu, Japan) spectrophotometer was used to measure the absorbance.

Protocol

1. Remove the 1x dye reagent from 4 ºC storage and let it warm to ambient temperature. Invert the 1x dye reagent a few times before use.
2. Use a standard in order to obtain a standard curve.
3. Pipet each standard and unknown sample solution into separate clean test tubes or microplate wells (the 1 ml assay may be performed in disposable cuvettes). Add the 1x dye reagent to each tube (or cuvette) and vortex (or invert).

   Assay: 1,020 µl
   Volume of standard and sample: 20 µl
   Volume of 1x dye reagent: 1 ml

4. Incubate at room temperature for at least 5 minutes. Samples should not be incubated longer than 1 hour at room temperature.

5. Set the spectrophotometer to 595 nm. Zero the instrument with the blank sample (not required for microplate readers). Measure the absorbance of the standards and unknown samples.
6. Using the calibration curve, determine the concentration of the protein.

Spectrophotometry is the experimental technique that analyzes and quantifies the absorbance (light absorption). This technique requires a spectrophotometer, which can quantify intensity as a function of the light wavelength. The spectrophotometers can be classified as single beam or double beam. In this experimental work, a double beam spectrophotometer was used, that measures the absolute light intensity. Usually they are equipped with a monochromator that analyses the spectrum. Basically, the spectrophotometer quantifies the fraction of light that passes through a given solution. The intensity of the remaining light is determined using a photodiode, and the transmittance of the wavelength is calculated automatically.

Standard curve

Use the standard below to calculate the protein concentration.

$y = 0.05831 x + 0.1154$
$R^2 = 0.9315$

y – OD (595 nm)
x – Protein concentration (mg/ml)

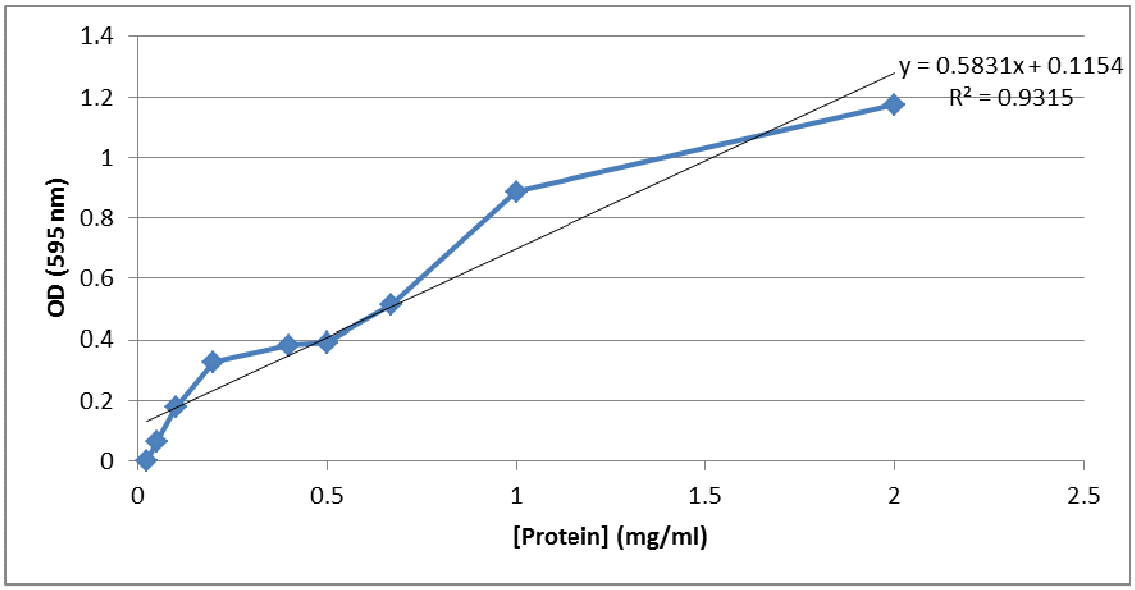


Figure A.2.2.1.: Bradford protein assay.

Focusing on the first part of the graph, we can determine another equation suitable for samples with lower concentration values:

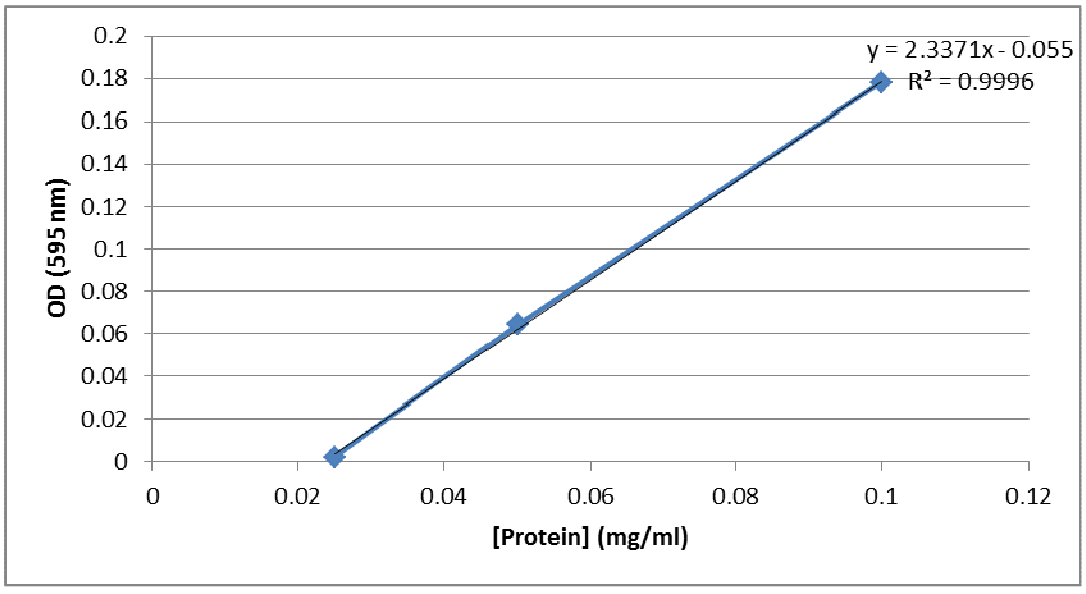


Figure A.2.2.2.: Bradford protein assay.

A.2.3. SDS-PAGE analysis of proteins

Table A.4: Reagents required for the casting of mini-SDS-PAGE (sodium dodecyl sulfate-polyacrylamide gel electrophoresis) gels.

Components	Stacking gel	Separating gel	
	4 %	12 %	15 %
dH_2O	3.63 ml	3.34 ml	2.34 ml
1.5 M Tris-HCL pH 8.8	-	2.5 ml	2.5 ml
1 M Tris-HCL pH 6.8	625 µl	-	-
10 % (w/v) SDS	50 µl	100 µl	100 µl
Acrylamide (29 %) Bis (1 %)	667 µl	4 ml	5 ml
Ammonium persulfate 10 %	25 µl	50 µl	50 µl
TEMED	5 µl	10 µl	10 µl
Total	5 ml	10 ml	10 ml

- Assemble the glass plates on the gel casting stand and fill with water to ensure that they are sealed.
- Mix the components of separating gel, adding the TEMED (N, N, N',N' – Tetramethylethylene-diamine, for electrophoresis, approx. 99 % $C_6H_{16}N_2$) last. Mix well and immediately fill the glass plates, leaving a 1.5 cm gap at the top (for the stacking gel).
- Immediately add 1 ml of isopropanol on top of the gel to prevent oxygen from inhibiting the polymerization. Wait 20 minutes for solidification.
- Pour off the isopropanol and rinse with dH_2O to remove any residual isopropanol. Mix the components for the 4 % staking gel and pour on top of the separating gel. Insert the well-comb and wait 20 minutes for solidification.
- Preheat a water bath to 100 ºC.
- Prepare the SDS-PAGE loading buffer by diluting β-mercaptoethanol 20 X (1:20) with the SDS-blue buffer.

- For a 4 ml culture with an approximate OD_{600} of 0.8, add 600 µl of SLB to the cold, centrifuged pellet. Suspend pellet in the SLB by vortexing.
- Immediately heat the sample to 100 ºC for 2 minutes.
- Allow the samples to cool down for at least one minute before loading the gel.
- Assemble the solidified gels in the buffer chamber. Fill the chamber with running buffer.
- Load 10 µl of each protein sample into the wells. Run the gel at a constant voltage of 165 V for about 1 hour, or until the dye reaches the bottom of the gel.
- Cut off the stacking gel and discard it.
- Stain the separating gel with a staining solution containing 45 % (w/v) dH_2O, 45 % (w/v) methanol, 10 % (v/v) acetic acid and 0.25 % (w/v) Coomassie Brilliant Blue R250. Stain for 1 hour with gentle shaking. If shaking is not possible, an overnight incubation will be sufficient.
- Pour the stain back into its container (it can be re-used several times) and rinse the tray with water. To remove the extra stain on the gel, use a destain solution (same as the staining solution, but without the Coomassie Blue). Protein bands will be visible immediately on a light table.

Table A.5: Marker molecular weights (BIO-RAD Laboratories (Hercules, CA)).

Protein	Calibrated MW (daltons)	Calibrated MW (daltons)	Calibrated MW (daltons)
Myosin	202,816	196,496	196,373
β-galactosidase	115,556	109,828	112,519
Bovine serum albumin	98,223	59,375	70,546
Ovalbumin	51,366	41,485	42,798
Carbonic anhydrase	37,240	28,224	31,635
Soybean trypsin inhibitor	29,003	20,261	
Lypozyme	19,748	15,013	
Aprotinin	6,658	6,494	

A.2.4. Freeze dryer protocol

1. Make sure that there is ethanol in the freezing well vacuum trap.
2. Turn on the vacuum trap and wait till red lights turns to green, indicating that ethanol in freezing well reached the appropriate temperature (~ -110 ºC) (approx 1 h).
3. Turn on the vacuum pump. (Make sure there's oil in the pump)
4. Turn on the freeze dryer wait till the pressure drops (approx. 1 h).
    a. Top light in the gauge reads higher pressures
    b. Bottom light reads low pressures
    c. Drain valve is completely closed
    d. Vent valve is completely closed
5. Make sure that there is no leak in the freeze dryer. Presently only one vent is used to dry the samples, stoppers close all other vents.
6. Make sure there is ice in the small Styrofoam box and place this box in the big Styrofoam box.
7. Place the filter paper under the freeze dryer cap (freeze dryer cap is connected to freeze dryer by a long tube).
8. Place the sample in the 20 ml freeze dryer vials (either in centrifuge tubes or other long tubes).
9. Place the 20 ml freeze dryer vial in the small Styrofoam box containing ice (make sure vial is completely immersed in ice).
10. Close the vial with black cap containing filter paper.
11. Open the vent valve on the freeze dryer.
12. Wait until the sample is completely freeze dried.
13. After complete drying, turn off all the equipment.
14. Open the drain valve on the freeze dryer, slowly to release the pressure.
15. Take the sample vial and store.

Note. Sometimes if the sample volume is large, sample will melt after few hours, if this is the case, use dry ice instead of ice in the Styrofoam box (This can happen due to inefficiency of the whole system).

FREEZE DRYING

FREEZE DRYING WITH RUBBER VALVES

1. Start the vacuum pump.
   The start switch is placed on top of the pump.
2. Open the gas ballast valve on the pump.
3. Check the oil level in the vacuum pump.
   The oil level glass must be ½ to 1/1 full.
4. Check the oil level in the oil mist filter.
   Drain the oil if the oil level glass is more than ½ full.
5. Check that the ice condenser is free from ice and water.
6. Check that the rubber valves are all closed, and that the grey cone is inserted in the top of the unit.
7. Check that the drain valve is closed.
8. Start the freeze dryer.
   WAIT.
   The cooling unit and vacuum pump should be allowed to run for 30 minutes before the freeze drying is started.
9. Open the vacuum valve.
   Wait for the pressure to drop below 0.5 mbar and for the temperature to drop below -30 ºC.
10. Connect the flask with the frozen material to the rubber valve, and slowly open the valve, turning your face away from the flask.
    The freeze drying (sublimation) is now running.
    Before connecting the next flask, wait for the pressure to drop below 0.5 mbar.

STOPPING THE FREEZE DRYING

11. Turn the rubber valve handle 180º to pressure equalize the pressure in the flask, and remove the flask.
12. Close the vacuum valve after removal of the last flask.
13. Switch off the freeze dryer.

A.2.5. Determination of the SWNT calibration curve

Principle

The assay aims to determine a generic calibration curve that can be used to determine the concentration of a specific sample where the concentration is not known. Due to the fact that there is not a relevant peak of absorption at 800 nm, that wavelength was chosen as standard to determine the absorbance of any sample.

Protocol

A suspension of SWNTs was prepared using the standard procedures already presented in the experimental section of this dissertation. The sample was then diluted using 4 different dilution factors. An UV-VIS-NIR spectrum was obtained for each sample. The absorbance values at 800 nm were then recorded on a table. Those values were then matched with the respective sample concentrations, and a curve was plotted based on the data. A linear regression was applied and an equation was generated.

Standard

Use the standard below to determine the SWNT concentration.

$y = 0.0176\ x + 0.0218$
$R^2 = 0.9959$

y – OD (800 nm)
x – SWNT concentration (mg/L)

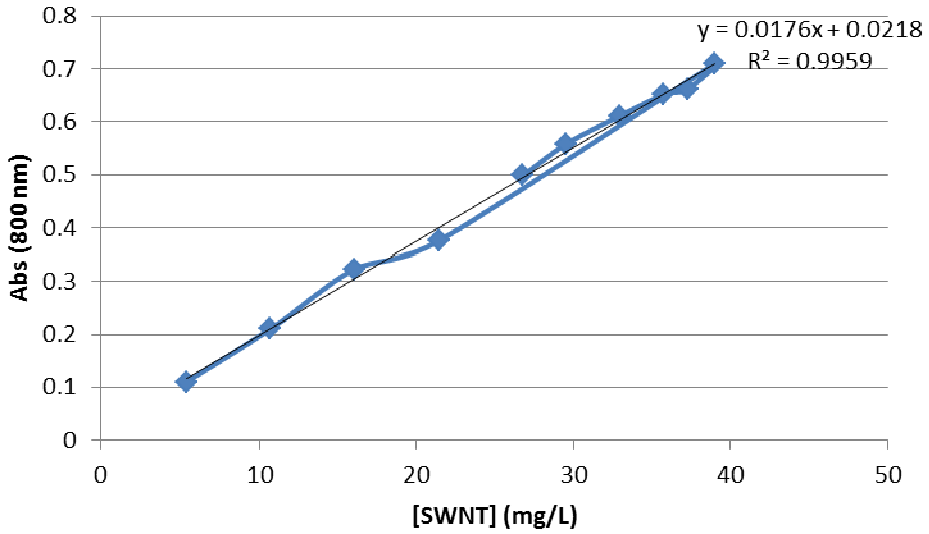


Figure A.2.5.1.: SWNT calibration curve.

APPENDIX B

Annexin V protein structure

Theoretical pI/Mw (average) for the user-entered sequence:

```
        10         20         30         40         50         60
MAQVLRGTVT DFPGFDERAD AETLRKAMKG LGTDEESILT LLTSRSNAQR QEISAAFKTL

        70         80         90        100        110        120
FGRDLLDDLK SELTGKFEKL IVALMKPSRL YDAYELKHAL KGAGTNEKVL TEIIASRTPE

       130        140        150        160        170        180
ELRAIKQVYE EEYGSSLEDD VVGDTSGYYQ RMLVVLLQAN RDPDAGIDEA QVEQDAQALF

       190        200        210        220        230        240
QAGELKWGTD EEKFITIFGT RSVSHLRKVF DKYMTISGFQ IEETIDRETS GNLEQLLLAV

       250        260        270        280        290        300
VKSIRSIPAY LAETLYYAMK GAGTDDHTLI RVMVSRSEID LFNIRKEFRK NFATSLYSMI

       310        320
KGDTSGDYKK ALLLLCGEDD
```

Theoretical pI/Mw: 4.94 / 35936.77

[144]

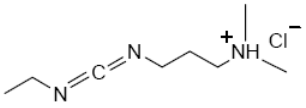
APPENDIX C

EDC (Pierce Catalog)

Number	Description
22980	**EDC** (1-ethyl-3-[3-dimethylaminopropyl]carbodiimide hydrochloride), 5 g
22981	**EDC,** 25 g
77149	**EDC,** 10 mg

Molecular Weight: 191.7

CAS # 25952-53-8



Storage: Upon receipt store Product No. 22980 and 22981 desiccated at - 20 °C. Store Product No. 77149 at 4 °C. EDC is shipped at ambient temperature.

Introduction

EDC is a carboxyl and amine-reactive zero-length crosslinker. EDC reacts with a carboxyl group first and forms an aminereactive *O*-acylisourea intermediate that quickly reacts with an amino group to form an amide bond and release of an isourea by-product (see the Additional Information Section). The intermediate is unstable in aqueous solutions, and therefore, two-step conjugation procedures require *N*-hydroxysuccinimide for stabilization [145, 146]. Failure to react with an amine will result in hydrolysis of the intermediate, regeneration of the carboxyl and release of an *N*-substituted urea. A side reaction is the formation of an *N*-acylurea, which is usually restricted to carboxyls located in hydrophobic regions of proteins [145, 147].

APPENDIX D

Procedure for Two-step Coupling of Proteins Using EDC and NHS or Sulfo-NHS

The following protocol is adapted from a procedure described by Grabarek and Gergely [145] and allows sequential coupling of two proteins without affecting the second protein's carboxyls by exposing them to EDC. This procedure requires quenching the first reaction with a thiol-containing compound.

Materials Required

- Activation Buffer: 0.1 M MES, 0.5 M NaCl, pH 6.0
- Protein # 1: Prepared in Activation Buffer at 1 mg/ml
- Protein # 2
- NHS or Sulfo-NHS (Product No. 24500 and 24510, respectively)
- 2-Mercaptoethanol (Product No. 35600)
- (Optional) Zeba™ Desalt Spin Column (Product No. 89891) or other gel filtration column
- Hydroxylamine•HCl (Product No. 26103)

Procedure

1. Equilibrate EDC and NHS to room temperature before opening bottles.
2. Add 0.4 mg EDC (~2 mM) and 0.6 mg of NHS or 1.1 mg of sulfo-NHS (~5 mM) to 1 ml of protein #1 solution and react for 15 minutes at room temperature.
3. Add 1.4 µl of 2-mercaptoethanol (final concentration of 20 mM) to quench the EDC.
4. Optional: Separate the protein from excess reducing agent and inactivated crosslinker using a desalting column. Equilibrate the column with Activation Buffer.
5. Add protein #2 to the activated protein at an equal molar ratio with protein #1. Allow the proteins to react for 2 hours at room temperature.
6. To quench the reaction, add hydroxylamine to a final concentration of 10 mM. This method hydrolyzes nonreacted NHS present on protein #1 and results in regeneration of

the original carboxyls. Other quenching methods involve adding 20-50 mM Tris, lysine, glycine or ethanolamine; however, these primary amine-containing compounds modify carboxyls on protein #1.

7. Remove excess quenching reagent using a desalting column.

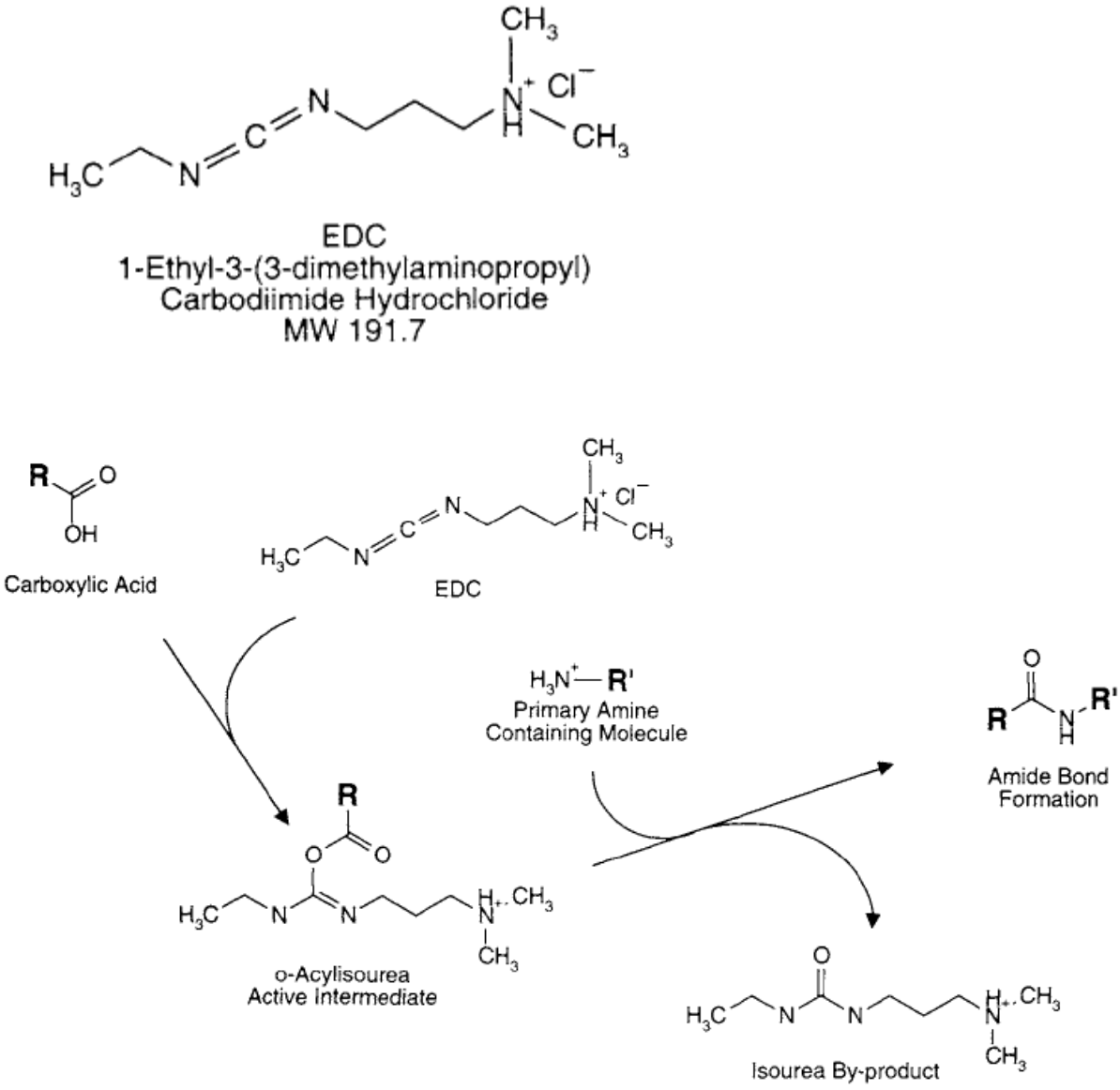


Figure D.1: EDC reacts with carboxylic acids to create an active-ester intermediate. In the presence of an amine nucleophile, an amide bond is formed with release of an isourea by product.

APPENDIX E

o-Phenylenediamine

Product Number: **P 5412**
Storage Temperature: 2-8 ºC

Product Description
Molecular Formula: $C_6H_8N_2$
Molecular Weight: 108.1
CAS Number: 95-54-5

Synonyms: 1,2-Benzenediamine, [1] OPD

o-Phenylenediamine (free base) is a chromogenic substrate suitable for use in ELISA procedures which utilize horseradish peroxidase conjugates.[2,3] This substrate produces a soluble end product that is orange-brown in color and can be read spectrophotometrically at 450 nm. The OPD reaction may be stopped with 3 N HCl or 3 M H_2SO_4, and read at 492 nm.

This product is supplied as 50 or 100 tablets per box, individually foil wrapped for ease of use, storage, and safety. Each tablet weights approximately 45 mg (range 40-50 mg) and contains 20 mg of substrate. One tablet, dissolved in 10 ml of water, gives a solution with a pH of 9.0 (range 8.5-9.5). The background absorbance of this solution cannot be more than 0.04.

Precautions and Disclaimer
For Laboratory Use Only. Not for drug, household or other uses.

Storage/Stability

Store tablets at 2-8 ºC. Protect from heat, light and moisture. Allow to reach room temperature before use. Solutions should be freshly prepared.

Procedure

Dissolve one tablet in 0.05 M phosphate-citrate buffer, pH 5.0, to the desired concentration (typically an OPD concentration of 0.4 mg/ml is used). Add 40 µl of fresh 30 % hydrogen peroxide (Product No. H 1009) per 100 ml of substrate buffer solution, immediately prior to use.

To prepare 0.05 M phosphate-citrate buffer, pH 5.0: Add 25.7 ml of 0.2 M dibasic sodium phosphate, (Product No. S 0876), 24.3 ml of 0.l M citric acid (Product No. C 7129) and 50 ml of water. Adjust the pH to 5.0, if necessary. Alternatively, use phosphate-citrate buffer capsules containing sodium perborate (Product No. P 4922). If these capsules are used, it is not necessary to add H_2O_2 to the substrate solution since sodium perborate is a substitute for hydrogen peroxide.

Troubleshooting

If the background is too high:

1. Use a blocking step prior to the application of the primary antibody. Normal serum (5 % v/v) from the same species as the host of the second antibody generally produces the best results.
2. Additional blocking agents for an ELISA are:
   a. 0.05 % TWEEN® 20 in 50 mM TBS, pH 8.0.
   b. 1 % BSA containing 0.05 % TWEEN 20 in 50 mM TBS, pH 8.0.
   c. 3 % nonfat-dried milk in 0.01 M TBS (Product No. P 2194). Do not use milk as a blocking agent when using avidin-biotin systems.
3. Use 0.05 % TWEEN 20 in all washing and antibody diluents buffers.
4. Run control wells without the primary antibody to check for non-specific reactivity of the secondary antibody.
5. Titer the primary antibody and the conjugate to optimize working dilutions.

If no color develops or the color is too faint:

1. Adjust the concentration of the primary antibody.
2. Adjust the concentration of the secondary antibody.
3. Determine if the enzyme conjugate is active by mixing a small sample of substrate and conjugate together in a test tube.
4. Increase the reaction time or temperature.
5. Adjust the concentration of the coating antigen.
6. Consider using an amplifying system such as avidin-biotin.

References

1. The Merck Index, 11th ed., Entry# 7355.
2. Wolters, G., et al., Solid-phase enzyme-immunoassay for detection of hepatitis B surface antigen. J. Clin. Path., **29(10)**, 873-879 (1976).
3. Bovaird, J. H., et al., Optimizing the o-phenylenediamine assay for horseradish peroxidase: effects of phosphate and pH, substrate and enzyme concentrations, and stopping reagents. Clin. Chem., **28(12)**, 2423-2426 (1982).

TWEEN is a registered trademark of Uniqema, a business unit of ICI America, Inc.

CMH/RXR 3/03

APPENDIX F

General Information about Human Endothelial Cells [148]

ATCC Information about the Human Endothelial Cells

Cell Biology ATCC® Number: **CRL-2472™**

Designations:	HAAE-1 [Part of the Wistar Special Collection]
Depositors:	EM Levine, Wistar Institute
Biosafety Level:	1
Shipped:	frozen
Medium & Serum:	See Propagation
Growth Properties:	Adherent
Organism:	*Homo sapiens* (human)
Morphology:	endothelial
Source:	**Organ:** aorta, abdominal **Disease:** normal **Cell Type:** endothelial
Permits/Forms:	In addition to the MTA mentioned above, other ATCC and/or regulatory permits may be required for the transfer of this ATCC material. Anyone purchasing ATCC material is ultimately responsible for obtaining the permits. Please click here for information regarding the specific requirements for shipment to your location.
Restrictions:	Distribution of this cell line is governed by the Wistar

	Special Collection Material Transfer Agreement.
DNA Profile (STR):	Amelogenin: X,Y CSF1PO: 11 D13S317: 8 D16S539: 13 D5S818: 12,13 D7S820: 10 THO1: 8,9.3 TPOX: 9,11 vWA: 16,17
Age:	20 years
Gender:	male
Comments:	A frozen ampule at population doubling 16 was received at the ATCC in June, 1999. Cells have the potential to reach approximately 46 population doublings before the onset of senescence. Check product sheet to see the PDL of the current distribution stock.
Propagation:	**ATCC complete growth medium:** Ham's F12K medium with 2 mM L-glutamine adjusted to contain 1.5 g/L sodium bicarbonate and supplemented with 0.1 mg/ml heparin and 0.03 mg/ml endothelial cell growth supplement (ECGS), 90 %; fetal bovine serum, 10 % **Temperature:** 37.0°C **Growth Conditions:** Culture vessels used to propagate this line must be precoated with 0.1 % pig gelatin. To prepare, flood vessels with gelatin solution, and leave on for at least 5 to 10 minutes. Suction off excess gelatin prior to use. Vessels may be used immediately.

Subculturing:	**Protocol:** Remove medium, and rinse with 0.25 % trypsin - 0.53 mM EDTA solution. Remove the solution and add an additional 1 to 2 ml of trypsin-EDTA solution. Allow the flask to sit at room temperature (or at 37 ºC) until the cells detach. Add fresh culture medium, aspirate and dispense into new culture flasks. **Subcultivation Ratio:** A subcultivation ratio of 1:2 to 1:3 is recommended **Medium Renewal:** Every 2 to 3 days
Preservation:	**Freeze medium:** culture medium 95 %; DMSO, 5 % **Storage temperature:** liquid nitrogen vapor phase
Related Products:	recommended serum:ATCC 30-2020
References:	46534: Levine EM, et al. Process and medium for cloning and long-term serial cultivation of human endothelial cells. US Patent 4,994,387 dated Feb 19 1991 46535: Levine EM, et al. Process and medium for cloning and long-term serial cultivation of adult human endothelial cells. US Patent 5,132,223 dated Jul 21 1992

APPENDIX G

Kaighn's Modification of Ham's F-12 Medium Formulation [149]

ATCC

F-12 K Medium

Kaighn's Modification of Ham's F-12 Medium

Formulation

Catalog No. 30-2004

Inorganic Salts	**(g/liter)**	**Vitamins**	**(g/liter)**
$CaCl_2 \cdot 2H_2O$	0.13524	D-Biotin	0.0000733
$CuSO_4 \cdot 5H_2O$	0.0000025	Choline Chloride	0.01396
$FeSO_4 \cdot 7H_2O$	0.000834	Folic Acid	0.00132
$MgCl_2 \cdot 6H_2O$	0.10572	Hypoxanthine	0.00408
$MgSO_4$ (anhydrous)	0.19264	myo-Inositol	0.01802
KCl	0.28329	Nicotinamide	0.0000366
KH_2PO_4 (anhydrous)	0.05852	D-Pantothenic Acid (hemicalcium)	0.000477
$NaHCO_3$	1.50000	Putrescine·2HCl	0.000322
Na_2HPO_4 (anhydrous)	0.11502	Pyridoxine·HCl	0.0000617
NaCl	7.59720	Riboflavin	0.0000376
$ZnSO_4 \cdot 7H_2O$	0.000144	Thiamine·HCl	0.000337
		Thymidine	0.000727
		Vitamin B-12	0.001355

Amino Acids	**(g/liter)**	**Other**	**(g/liter)**
L-Arginine (free base)	0.42140	D-Glucose	1.26000
L-Alanine	0.01782	Phenol Red. Sodium Salt	0.00332
L-Asparagine·H_2O	0.03020	Sodium Pyruvate	0.22000
L-Aspartic Acid	0.02662	Lipoic Acid	0.00021
L-Cysteine·HCl·H_2O	0.07024		
L-Isoleucine	0.02942		
L-Leucine	0.29220		
L-Lysine·HCl	0.01501		
L-Methionine	0.04192		
L-Phenylalanine			
L-Proline			
L-Serine			
L-Threonine			
L-Tryptophan			
L-Tyrosine (free base)			
L-Valine			

F-12 K Medium, Modified
Kaighn's Modification of Ham's F-12 Medium
CATALOG NO. 30-2004, 500 Ml

Storage
Store medium at 2 to 8 ºC in the yellow plastic bag when not in use. The yellow bag minimizes the effect of light on some of the components in the medium.

Quality Control Testing
Sterility tests are performed on each lot of medium using current USP methods. ATCC also checks each lot of medium for its ability to support the growth of several different cell lines using both sequential subcultures and plating efficiencies. Additional test results are listed below in the Specification Certificate.

Formulation
Contains 2 mM L-glutamine and 1500 mg/L sodium bicarbonate.
NOTE: This reduced level of sodium bicarbonate ($NaHCO_3$, 1.5 g/L) is intended for use in 5 % CO_2 in air. Additional sodium bicarbonate may be required for use in incubators containing higher percentages of CO_2.

Terms and Conditions
Please refer to the Material Transfer Agreement and Packing Slip enclosed with the product.

SPECIFICATION CERTIFICATE

Test/Method	**Specification**	**Results**
pH	7.0 to 7.4	See lot specific data
Osmolality	275 to 357 mOsm/kg	See lot specific data
Sterility Testing	Pass	See lot specific data
Endotoxin	≤0.25 EU/mL	See lot specific data

Mycoplasma	Not Detected	See lot specific data
Growth Promotion	Pass	See lot specific data

Lot number: 3000608
F-12K Medium, Modified
Kaighn's Modification of Ham's F-12 Medium

ATCC Catalog No.: 30-2004, 500 mL
Lot No.: 3000608 Expiration Date: FEB/2009

pH: 7.2
Osmolality: 336 mOsm/kg
Sterility Testing: Pass
Endotoxin: < 0.0050 EU/Ml
Mycoplasma: Negative
Growth Promotion: Pass

Trypsin-EDTA
0.25 % Trypsin/0.53 mM EDTA Solution
In Hank's BSS without Calcium or Magnesium
CATALOG NO. 30-2101, 100 Ml

Storage
Store Trypsin-EDTA solution frozen, between -5 and -20 ºC. Avoid repeated freeze-thaws by dispensing and storing in aliquots.

Application
For the dissociation of cell monolayers. NOTE: Each cell line responds to ATCC® Trypsin-EDTA solution in a unique manner. For optimum results, observe the cells during the dissociation process to avoid over-trypsinization. For more information, please refer to the General Protocol for Using ATCC® Trypsin-EDTA Solution. For cell

line-specific information, please refer to the product sheet supplied with the cell line, or contact ATCC® Technical Service. ATCC ® Trypsin-EDTA solution is suitable for most but not all adherent cell lines.

SPECIFICATION CERTIFICATE

Test/Method	**Specification**	**Results**
pH	7.0 to 7.4	See lot specific data
Osmolality	283 to 313 mOsm/kg	See lot specific data
Sterility Testing	Pass	See lot specific data
Cell Culture Tests – MRC-5 (CCL-171)	Pass	See lot specific data
Cell Culture Tests – Vero (CCL-81)	Pass	
Source	Pass (Porcine)	See lot specific data
Porcine Parvovirus (PPV)	Not Detected	See lot specific data
Mycoplasma	Not Detected	See lot specific data

APPENDIX H

General Protocol for Using ATCC® Trypsin-EDTA Solution [149]

Catalog No. 30-2101

Storage

Store ATCC® Trypsin-EDTA solution frozen between -5 and -20 ºC. Avoid repeated freeze-thaws by dispensing and storing in aliquots.

General Procedures for Adherent Cell Lines

NOTE: Each cell line responds to ATCC® Trypsin-EDTA in a unique manner. For optimum results, continually observe the cells by microscopy during the dissociation process to prevent damage by the Trypsin-EDTA solution. For cell-line-specific information, please refer to the product sheet supplied with the cell line, or contact ATCC® Technical Service.

The amounts used in this procedure are for a 75-cm^2 flask. Adjust volumes as appropriate for different sized vessels.

1. Bring ATCC® Trypsin-EDTA solution to the appropriate temperature (see cell line product sheet). This may be 4 ºC, room temperature, or 37 ºC depending upon the cell type. You may also need to use a balanced salt solution [e.g., ATCC® Dulbecco's Phosphate Buffered Saline (PBS) without Ca or Mg, Catalog number 30-2200] to rinse the cells. If so, bring this to the same temperature. Finally, bring fresh, complete cell culture medium to the appropriate temperature for cell growth (e.g., 37 ºC).
2. Remove and discard the cell culture medium from the flask.
3. Depending upon the cell line, rinse the cell monolayer with either 5 mL of ATCC® Trypsin-EDTA solution or ATCC® Dulbelcoo's PBS (for more trypsin-sensitive cells) and remove.

4. Add 2 to 3 mL of ATCC® Trypsin-EDTA solution and incubate at the appropriate temperature (4 ºC, room temperature, or 37 ºC). Continually check the progress of cell dissociation by microscopy. To avoid clumping, do not agitate the cells by hitting or shaking the flask while waiting for them to detach.
5. Once the cells appear to be detached (5 to 15 minutes for most cell lines, they will appear rounded under the microscope), add 6 to 8 mL of complete growth medium to the cell suspension and with a pipette wash any remaining cells from the bottom of the flask. Check the cells with the microscope to be sure that most (> 95%) exist as single cells. If cell clusters are apparent, continue to disperse the cells with gentle pipetting (see Troubleshooting, below).
6. Add 12 to 15 mL of fresh cell culture medium to a new flask and equilibrate this medium to the appropriate pH and temperature. Collect the cell suspension, count and/or divide it, and dispense the cells into the newly prepared flask. Refer to the cell line product sheet for recommended subcultivation ratios.
7. For serum free or low serum medium, remove the ATCC® Trypsin-EDTA solution by gentle centrifugation (5 minutes at 125 x *g*) and resuspend the cells in fresh medium.

Troubleshooting

Cells are difficult to remove:

- The dissociation agent is too weak. Try incubating at higher temperatures.
- Inhibitors in the medium (e.g., serum) are inactivating the trypsin. Rinse the cell monolayer more thoroughly before incubating with ATCC® Trypsin-EDTA solution.
- Cells have been at confluent density for a too long and the cell-to-cell junctions are so tight that they are preventing the enzyme from reaching the substrate-cell interface. Subculture cells before they are 100 % confluent.

Cells clump after dissociation:

- DNA has been released from lysed cells, because the dissociation procedure was too harsh. Add a drop of sterile DNAse (1 mg/ml in water) to the cell

suspension. In the future, treat the cells more gently during pipetting, shorten the incubation period, and/or decrease the incubation temperature.

- Cells are reaggregating before subculturing. Hold the cell suspension on ice if there will be a delay between removing cells from the flask and dispersing them into them fresh cell culture medium.

Cells have difficulty reattaching:

- The dissociation enzymes may have stripped necessary attachment proteins from the cell surface. Treat the cells more gently, use less ATCC® Trypsin-EDTA solution, shorten the incubation time, and/or lower the incubation temperature.
- Not enough serum or attachment factors are in the medium (common with serum-free medium). Add attachment factors or use protein-coated plates (collagen, polylysin, gelatin, etc.).
- ATCC® Trypsin-EDTA solution was not inactivated by the cell culture medium (e.g., the serum). Add specific enzyme inhibitors or remove the ATCC® Trypsin-EDTA solution by gentle centrifugation (5 minutes at 125 x *g*) followed by a medium change.

Lot number: 3000620
Trypsin-EDTA
0.25 % Trypsin/0.53 mM EDTA Solution
in Hank's BSS without Calcium or Magnesium

ATCC Catalog No.: 31-2101, 100 mL
Lot No.: 300620 Expiration Date: 05/09

pH: 7.0
Osmolality: 288 mOsm/kg
Sterility Testing: Pass
Cell Culture Tests – MRC-5 (CCL-171): Pass
Cell Culture Tests – Vero (CCL-81): Pass

Source: Pass (Porcine)

Porcine Parvovirus (PPV): Negative

Mycoplasma: Negative

APPENDIX I

General Protocol for Using Accutase Solution [150]

ACCUTASE

CATALOG #: AT104-500 LOT: 8P1215A EXP: 3/2010

DESCRIPTION: A cell detachment solution of proteolytic and collagenolytic enzymes. Useful for the routine detachment of cells from standard tissue culture plasticware and adhesion coated plasticware. ACCUTASE does not contain mammalian or bacterial derived products.

FORMAT: 500 ml, ready to use, frozen sterile liquid.

QUALITY CONTROL:
1. Sterility testing by USP membrane filtration method.
2. Enzymatic activity tested with synthetic chromagenic tetrapeptides.
3. Cell detachment from plastic tissue culture dishes.

FORMULATION: 1X ACCUTASE enzymes in Dulbecco's PBS (0.2 g/L KCL, 0.2 g/L KH_2PO_4, 8 g/L NaCl, and 1.15 g/L Na_2HPO_4) containing 0.5 mM EDTA·4Na and 3 mg/L Phenol Red.

STABILITY: Stable when stored at -20 ºC. Refer to lot expiration date. Recommended storage upon receipt is -20 ºC. After thawing, ACCUTASE may be stored for up to 2 months at 4 ºC. DO NOT STORE AT ROOM TEMP.

PROCEDURE:
1. Thaw ACCUTASE in the refrigerator overnight, in a vessel of cool water or at room temperature. Not at 37 ºC.
2. Wash plate, flask or beads with sterile PBS.
3. Add ACCUTASE to culture dish or flask using aseptic procedures at 10 ml per 75-cm^2 surface area.
4. Incubate at room temperature and allow cells to detach 5-10 minutes.
5. Count cells and passage as usual; no additional washes or enzyme inhibitors are required.

APPENDIX J

General Protocol for the Hemacytometer [151]

Metallized Hemacytometer

Reichert Bright-Line

The Bright-Line Hemacytometer is molded from a single piece of thermal and shock-resistant glass. An H-shaped moat forms two counting areas, or plateaus. A "V" slash at the loading side of each plateau facilitates charing and reduces the possibility of overflow into the moat. Each plateau features enhanced Neubauer rulings. The ruled surface is 0.1 mm below the cover glass, limiting the volume of blood or fluid over a square mm at 0.1 cu.mm and over each of 400 squares (within the central square mm) to 0.00025 cu. mm. Contact of the flat, polished cover glass surfaces with cover glass supports produces an exact volume of fluid over the counting area. The difference in surface tension characteristics between the metallic surface on the chamber and the polished cover glass assures smooth capillarity for precise loading and more even cell distribution.

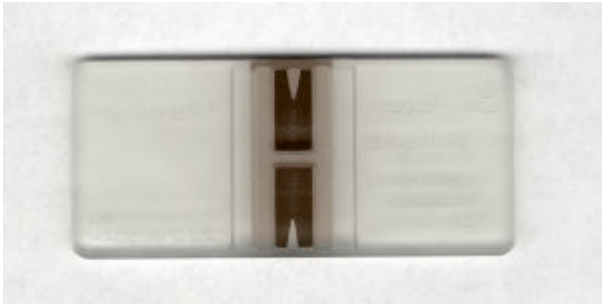


Figure J.1: Photograph of 1490

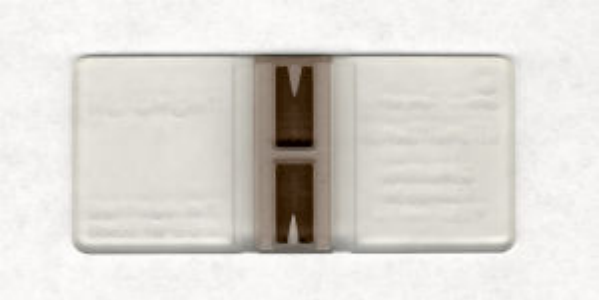


Figure J.2: Photograph of 1475

Directions for Use

Bright-Line / Dark-Line Counting Chambers

Catalog Numbers: 3100, 3110, 3200, 3500, 1490, 1492, 1475, & 1483

Usage: Cell Counts

Cell Depth: 0.100 mm +/- 2% (1/10 mm)
Volume: 0.1 Microliter
Ruling Pattern: Improved Neubauer, 1/400 Square mm

Rulings cover 9 square millimeters. Boundary lines of the Neubauer ruling are the center lines of the groups of three. (These are indicated in the illustration below.) The central square millimeter is ruled into 25 groups of 16 small squares, each group separated by triple lines, the middle one of which is the boundary. The ruled surface is 0.10 mm below the cover glass, so that the volume over each of the 16 small squares is .00025 cubic mm.

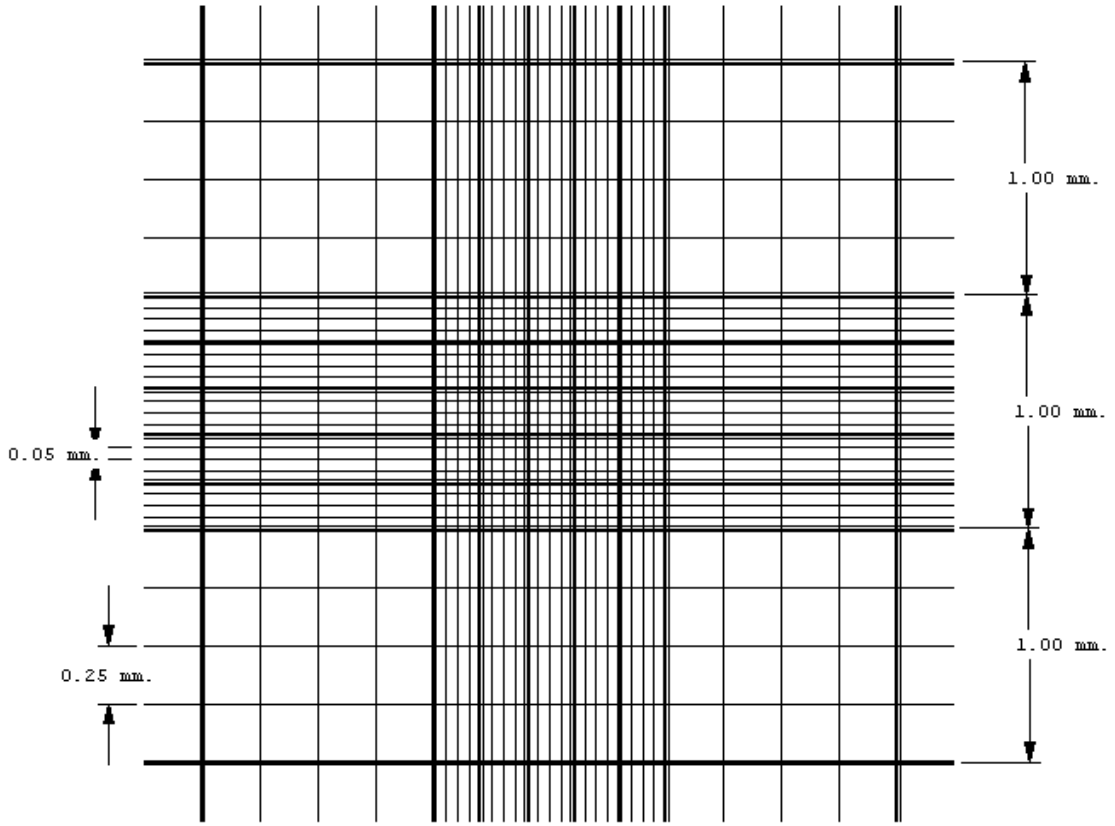


Figure J.3: Neubauer Ruling.

The number of cells per cubic millimeter =

Number of cells counted per square millimeter X dilution (if used) X 10

The number of cells per milliliter =

Number of cells counted per square millimeter X dilution (if used) X 10,000

One (1) Milliliter = 1000 cubic millimeters (cu mm)

One (1) Microliter (ul) = One (1) cubic millimeter (cu mm)

To clean the counting chamber: After completing the count, remove the cover glass and clean the counting chamber with water or a mild cleaning solution (10 % solution of bleach). Dry the counting chamber with a soft cloth or wipe, or rinse with acetone.

APPENDIX K

General Protocol for Using the Alamar Blue Assay [152]

IN VITRO TOXICOLOGY ASSAY KIT
Resazurin Based

Stock No. TOX-8

Store at 2-8 ºC

This kit is designed for fluorometrically or spectrophotometrically determining cell number as a function of metabolic activity using the dye resazurin.

IT IS RECOMMENDED THAT THE ENTIRE PROTOCOL BE REVIEWED BEFORE STARTING THE ASSAY.

Product Description

Traditionally, the toxic effects of unknown compounds have been measured in vitro by counting viable cells after staining with a vital dye. Alternative methods include the measurement of DNA synthesis by radioisotope incorporation, cell counting by automated counters and other methods which rely on dyes and cellular activity. The resazurin system measures the metabolic activity of living cells. The resazurin method is simple, accurate and reproducible. The key component is the oxidoreduction indicator dye resazurin. Solutions of resazurin, prepared in balanced salt solutions without phenol red, are dark blue in color. Bioreduction of the dye by viable cells reduces the amount of its oxidized form [blue] and concomitantly increases the amount of its fluorescent intermediate [red],indicating the degree of cytotoxicity caused by the test material. The amount of dye conversion in solution is measured fluorometrically or spectrophotometrically.

REAGENT

For Research Use Only.

Not for Use in Diagnostic Procedures.

Kit Components

Catalog No.	Item	Quantity
R-6892	Resazurin	Solution 25 ml

Procedure

The resazurin method of monitoring in vitrocytotoxicity is well suited for use with multiwell plates. For best results, use cells in the log phase of growth and a final cell density less than 10^6 cells/cm^2. Each test should include a blank containing complete medium without cells.

NOTE: Bacteria, mycoplasma and other microbial contaminants may also reduce the resazurin dye. Cultures containing microorganisms should not be assayed using this method.

1. Remove cultures from incubator into laminar flow hood or other sterile work area.
2. Add resazurin dye solution in an amount equal to 10 % of the culture medium volume.
3. Return cultures to incubator for 2-4 hours depending on cell type and maximum cell density. (An incubation period of 2 hours is generally adequate but may be lengthened for low cell densities or cells with lower metabolic activity.) Incubation times should be consistent when making comparisons.
4. Gentle mixing in a gyratory shaker will enhance distribution of the dye.
5. Samples can be measured spectrophotometrically by monitoring the decrease in absorbance at a wavelength of 600 nm. Measure the absorbance of multiwall plates at a reference wavelength of 690 nm and subtract from the 600 nm measurement.

Alternatively, samples can be measured fluorometrically by monitoring the increase in fluorescence at a wavelength of 590 nm using a excitation wavelength of 560 nm. **NOTE:** Fluorometric detection is much more sensitive than spectrophotometric detection and the number of cells used in the assay should be reduced proportionally.

6. Tests performed in multiwell plates can be read using an appropriate type of plate reader or the contents of individual wells may be transferred to appropriate size cuvettes for fluorometric or spectrophotometric measurement.

Possible Sources of Error

1. Microbial contamination will contribute to the reduction of the resazurin dye yielding erroneous results.
2. Uneven evaporation of culture fluid in wells of multiwell plates may cause erroneous results.
3. Medium and salt solutions with phenol red can be used but will contribute to higher background absorbance and can decrease sensitivity.

References

1. Dutka, B.J., N. Nyholm and J Petersen. [1983] Comparison of several microbiological toxicity screening tests. Water Research 17:1363-1367.
2. King, E.F. [1984] A comparative study of methods for assessing the toxicity to bacteria of single chemicals and mixtures. In: Toxicity Screening Procedures Using Bacterial Systems, D. Liu and B.J. Dutka eds., Decker, New York. pp. 175-194.
3. Liu, D. [1981] A rapid biochemical test for measuring chemical toxicity. Bull. Environmental Contamination Toxicology 26:145-149.
4. Strotmann, U.J., B. Butz and W-R Bias. [1993] The dehydrogenase assay with resazurin: Practical performance as a monitoring system and pH-dependent toxicity of phenolic compounds. Ecotoxicology Environmental Safety 25:79-89.

IN VITRO TOXICOLOGY ASSAY KIT
Resazurin Based
Stock No. TOX-8

APPENDIX L

Mice datasheet [105]

Mice datasheet

Strain Name: *BALB/cJ*

Stock Number: *000651*

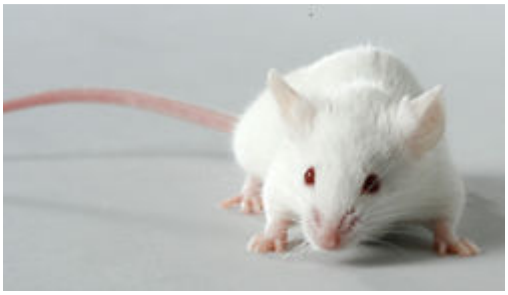
Availability: Level 1

Cell Line: BALB/cJ-PRX-BALB/cJ #9 mES cells
Cell Line: BALB/cJ-line I mES cells

Common Names: C

BALB/cJ is a commonly used inbred. Key traits include a resistance to experimental autoimmune encephalomyelitis (EAE), and a susceptibility to developing the demyelinating disease upon infection with Theiler's murine encephalomyelitis virus. The BALB/cJ substrain is susceptible to Listeria, all species of Leishmania, and several species of Trypanosoma, but is resistant to experimental allergic orchitis (EAO).

Strain Information



Type	Inbred Strain;
Mating System	Sibling x Sibling (Female x Male) 01-MAR-06
Breeding Considerations	This strain is a challenging breeder.
Species	laboratory mouse
H2 Haplotype	*D*
Generation	F230 (02-JAN-10)

Appearance

albino

Related Genotype: *A*/*A Tyrp1*^{b}/*Tyrp1*^{b} *Tyr*^{c}/*Tyr*^{c}

Description

BALB/c mice are particularly well known for the production of plasmacytomas following injection with mineral oil forming the basis for the production of monoclonal antibodies. Although not all BALB/c substrains have been examined for plasmacytoma induction, substrains derived from the Andervont (An) lineage (which includes BALB/cByJ) typically are susceptible, while those descended from BALB/cJ are resistant (see: Potter M ,1985). Mammary tumor incidence is normally low but infection with mammary tumor virus by fostering to MMTV^{+} C3H mice dramatically increases tumor number and age of onset. BALB/c mice develop other cancers later in life including reticular neoplasms, primary lung tumors, and renal tumors. Rare spontaneous myoepitheliomas arising from myoepithelial cells of various exocrine glands have been observed in both BALB/cJ and BALB/cByJ substrains.

White et al. reported a variation in thioglycolate medium-induced peritoneal leukocyte recruitment in 4 analyzed strains. The response of total leukocyte recruitment, from greatest to least, was C57BL/6J>BALB/c>CD1>129X1/SvJ. Variations were also found in the timeline of response and cell types most impacted.

Dorso-ventral vaginal septa is observed in some BALB/cJ females, and may contribute to non-productive females in this strain. (Cunliffe-Beamer T, Lab Anim Sci, 1976)

APPENDIX M

General Information about the 4T1 Cells [149]

ATCC® Number:	**CRL-2539™**
Designations:	4T1
Depositors:	BA Pulaski
Biosafety Level:	1
Shipped:	frozen
Medium & Serum:	See Propagation
Growth Properties:	adherent
Organism:	*Mus musculus* deposited as mouse
Morphology:	epithelial
Source:	**Organ:** mammary gland **Strain:** BALB/cfC3H **Disease:** tumor
Permits/Forms:	In addition to the MTA mentioned above, other ATCC and/or regulatory permits may be required for the transfer of this ATCC material. Anyone purchasing ATCC material is ultimately responsible for obtaining the permits. Please click here for information regarding the specific requirements for shipment to your location.
Applications:	4T1-induced tumors can be used as a post-operative model as well as a non-surgical model because the 4T1-induced tumor metastasizes spontaneously in both models with similar kinetics. Because 4T1 is resistant to 6-thioquanine, micro-metastatic cells (as few as 1) can be detected in many distant site organs with better accuracy that most tumor models. When injected into BALB/c mice, 4T1 spontaneously produces highly metastatic tumors that can metastasize to the lung, liver, lymph nodes and brain while the primary tumor is growing in situ.
Tumorigenic:	Yes
Comments:	4T1 is a 6-thioguanine resistant cell line selected from the 410.4 tumor without mutagen treatment. When injected into BALB/c mice, 4T1 spontaneously produces highly metastatic tumors that can metastasize to the lung, liver, lymph nodes and brain while the primary tumor is growing in situ.

	The primary tumor does not have to be removed to induce metastatic growth. The tumor growth and metastatic spread of 4T1 cells in BALB/c mice very closely mimic human breast cancer. This tumor is an animal model for stage IV human breast cancer. 4T1-induced tumors can be used as a post-operative model as well as a non-surgical model because the 4T1-induced tumor metastasizes spontaneously in both models with similar kinetics. Because 4T1 is resistant to 6-thioquanine, micro-metastatic cells (as few as 1) can be detected in many distant site organs with better accuracy that most tumor models. There is no need to count nodules or weight target organs.
Propagation:	**ATCC complete growth medium:** The base medium for this cell line is ATCC-formulated RPMI-1640 Medium, Catalog No. 30-2001. To make the complete growth medium, add the following components to the base medium: fetal bovine serum to a final concentration of 10%. **Temperature:** 37.0°C **Atmosphere:** air, 95%; carbon dioxide (CO2), 5%
Subculturing:	**Protocol:** NOTE: the cells should not be allowed to become confluent, subculture at 80% of confluence. Remove medium, and rinse with 0.25% trypsin-0.53mM EDTA solution. Remove the solution and add an additional 1 to 2 ml of trypsin-EDTA solution. Allow the flask to sit at room temperature (or at 37.0°C) until the cells detach. Add fresh culture medium, aspirate and dispense into new culture flasks. **Subcultivation Ratio:** A subcultivation ratio of 1:6 to 1:8 is recommended **Medium Renewal:** Every 2 to 3 days
Preservation:	**Freeze medium:** Complete growth medium 95%; DMSO, 5% **Storage temperature:** liquid nitrogen vapor temperature
Related Products:	Recommended medium (without the additional supplements or serum described under ATCC Medium):ATCC 30-2001 recommended serum:ATCC 30-2020
References:	49687: Pulaski BA, et al. Immunotherapy with vaccines combining MHC class II/CD80+ tumor cells with interleukin-12 reduces established metastatic disease and stimulates immune effectors and monokine induced by interferon gamma. Cancer Immunol. Immunother. 49: 34-45, 2000. PubMed: 10782864 49688: Pulaski BA, Ostrand-Rosenberg S. Reduction of established spontaneous mammary carcinoma metastases following immunotherapy with major histocompatibility complex class II and B7.1 cell-based tumor vaccines. Cancer Res. 58: 1486-1493, 1998. PubMed: 9537252 49689: Pulaski BA, et al. Cooperativity of Staphylococcal aureus

enterotoxin B superantigen, major histocompatibility complex class II, and CD80 for immunotherapy of advanced spontaneous metastases in a clinically relevant postoperative mouse breast cancer model. Cancer Res. 60: 2710-2715, 2000. PubMed: 10825145
49690: Aslakson CJ, Miller FR. Selective events in the metastatic process defined by analysis of the sequential dissemination of subpopulations of a mouse mammary tumor. Cancer Res. 52: 1399-1405, 1992. PubMed: 1540948

APPENDIX N

Formulation for RPMI-1640 Medium ATCC® 30-2001[153]

ATCC

Inorganic Salts (g/liter)		**Vitamins (g/liter)**	
Ca(NO3)2·4H2O	0.10000	D-Biotin	0.00020
MgSO4 (anhydrous)	0.04884	Choline Chloride	0.00300
KCl	0.40000	Folic Acid	0.00100
NaHCO3	1.50000	myo-Inositol	0.03500
NaCl	6.00000	Nicotinamide	0.00100
Na2HPO4 (anhydrous)	0.80000	p-Amino Benzoic Acid	0.00100
		D-Pantothenic Acid (hemicalcium)	0.00025
Amino Acids (g/liter)		Pyridoxine·HCl	0.00100
L-Arginine (free base)	0.20000	Riboflavin	0.00020
L-Asparagine·H2O	0.05682	Thiamine·HCl	0.00100
L-Aspartic Acid	0.02000	Vitamin B-12	0.000005
L-Cystine·2HCl	0.06520		
L-Glutamic Acid	0.02000	**Other (g/liter)**	
L-Glutamine	0.30000		
Glycine	0.01000	D-Glucose	4.50000
L-Histidine (free base)	0.01500	Glutathione (reduced)	0.00100
Hydroxy-L-Proline	0.02000	HEPES	2.38300
L-Isoleucine	0.05000	Phenol Red, Sodium Salt	0.00500
L-Leucine	0.05000	Sodium Pyruvate	0.11000
L-Lysine·HCl	0.04000		
L-Methionine	0.01500		
L-Phenylalanine	0.01500		
L-Proline	0.02000		
L-Serine	0.03000		
L-Threonine	0.02000		
L-Tryptophan	0.00500		
L-Tyrosine·2Na·2H2O	0.02883		
L-Valine	0.02000		

APPENDIX O

Cell Culturing

A layer of a 0.1 % porcine gelatin was used as a substrate for growing endothelial cells. The sterile gelatin solution was added to the bottom of each flask using an appropriate volume that would create a thin layer. The gelatin was then left for 10 minutes in the flask. After that time, the excess of gelatin was removed by aspirating it using a pipette connected to a vacuum system. The cells were kept in a controlled environment (37 ºC, 5 % CO_2) in an incubator. The original cells that were received from the company were replicated according to the recommended procedure sent by the seller. When kept in a T-75 flask the cells will increase their number with time.

After a certain stage, it is necessary to split the cells into more flasks in order to allow them to continue growing, without reaching full confluency. The confluency level defines the ratio between the surface area occupied by the cells and the surface area of the flask. When that ratio percentage is almost 100 %, the cells enter in a quasi-steady mode, where they basically stop or dramatically reduce their replication rates. The optimal level to split the cells used in our laboratory was between 75 to 85 %. Every time work was done with cells, the cell medium used was previously warmed in the incubator in order to have it ready at 37 ºC, minimizing the possibility of a temperature shock for the cells. The cell passage or subculturing is the designation for the transfer of the cells from one set of culture flasks to another. This cell transfer is required in order to increase the available surface area required by the cells to replicate more.

Generally, human endothelial cells reach confluence after approximately 3 to 4 days. To perform the cell passage, the medium was removed from the T-75 flasks using

Pasteur pipets that were connected to the vacuum system. The flasks were rinsed with 3 mL of phosphate buffer saline (PBS) in order to wash the flask. This step is required and very important, because it allows for the complete removal of the F12K medium which has in its composition an accutase/trypsin inhibitor. The plate was gently shaken, and the solution was aspirated with the help of the vacuum system. Each T-75 flask received 3 mL of accutase/trypsin and was incubated for 10 minutes at 37 ºC. The new T-75 flasks were previously coated with gelatin. The gelatin (3 ml) was added to the flasks in order to cover the entire surface of the flask. The gelatin constitutes an adhesion support for the cells that will further attach to it and consequently to the surface of the plate. The gelatin was incubated in the flasks for 10 minutes at 37 ºC. After the incubation, the gelatin was removed and 9 mL of F12K medium were added to each T-75 flask. The cells that received the enzymes were visualized under an optical microscope after the 10 minutes incubation. Prior to visualization it is recommend to shake the flask in order to have the cells slightly moving. Under the microscope it is expected to see all of the cells floating in suspension. The majority must be detached from the surface at this point, and their morphology should look different with a rounded appearance, instead of the traditional elongated shape. If this does not happen, there was something that did not work properly and the assay must be restarted. If the majority of the cells are floating, it means that the action of the enzymes was successful.

The T-75 flasks that had the lifted cells inside received 7 mL of warm F12K medium. The cells were mixed 3 or 4 times with the medium with the help of a pipettor. The medium was added to the cells in order to inhibit the action of the accutase/trypsin. That solution was then transferred to a 15 ml centrifuge tube. The tube was centrifuged

for 5 minutes at 1,100 rpm using a Mistral / MSE 3000 E centrifuge (Leicestershire, England). This allowed to collect all of the cells from the bottom of the tube. After centrifugation, 9 ml of the solution were carefully removed and 1 ml was left in the bottom of the tube. Eight ml of medium were added to the tube, and the solution was pipetted several times in order to resuspend all of the cells and allow for obtaining a homogeneous cell suspension. A failure on this step can result in transfer of unequal number of cells per flask. Assuming a 1:3 cell passage, each T-75 flask received 3 ml of the cells' solution. Last, the cells were incubated at 37 ºC, 5 % CO_2 in the incubator.

APPENDIX P

Cell staining

1. Grow the endothelial cells in the T-75 flasks under the appropriate conditions.
2. When the cells are approximately 75-80 % confluent, passage them into the 2-chamber slides.
3. In order to have the cells adhering to the glass cover slides it is important to pre-coat the surface with 300 µl of 0.1 % sterile pig gelatin for 10 minutes. After 10 minutes, remove the excess of gelatin and let the chambers dry for 15 minutes with the lids off.
4. Add 1,000 µl of endothelial cells to each well. Put the chamber in the incubator.
5. Wait 24 h.
6. Carefully remove the cell medium from the wells.
7. Add 1 ml of the SWNT-FITC-Annexin V conjugate at a concentration of 6 mg/L to the Petri dish. The conjugate must be diluted with cell medium and 2 mM Ca^{2+}.
8. Incubate for 2 h in the incubator.
9. Wash the wells 4x with cell medium and 2 mM Ca^{2+}.
10. Dilute the Cell Mask by placing 1.5 µl of the stock solution (5 mg/ml) in 1 ml of cell medium.
11. Add 300 µl of the diluted Cell Mask to each well and incubate in the incubator for 30 minutes.
12. Remove the staining solution.
13. Wash 4x with cell medium and 2 mM Ca^{2+}.
14. Fix the cells with 0.25 % glutaraldehyde for 5 minutes at 37 ºC.

15. Wash 4x with cell medium and 2 mM Ca^{2+}.
16. Place a drop of Fluoro-gel on a microscope glass slide.
17. Invert the glass cover slide and have the cells touching the gel.
18. Check for fluorescence using the Fluorescence microscope.

The emission and excitation wavelengths for CellMask are 649 and 666 nm, respectively. All of the dyes used for the staining are light-sensitive, and in order to preserve their fluorescence abilities, the exposure of them to the light was minimized.

APPENDIX Q

In Vitro Binding Assay

In order to perform the biotinylation, the lyophilized protein annexin V was reconstituted with 1 ml of buffer (80 mM sodium phosphate dibasic, 50 mM NaCl, pH 7.4). The vial was then stirred for 30 minutes at 4 ºC. 1 mg of biotin (SureLINK Chromophoric Biotin, KPL, Inc., Gaithersburg, MD) was dissolved in 100 µl of anhydrous DMF immediately prior to use. Using a 40-fold excess of biotin for the conjugation, 88.67 µl of biotin (20 mg/ml) were added to the protein solution. The vial was then incubated at 4 ºC for 4 hours with gentle agitation. The unconjugated chromophoric biotin was removed by dialysis using a Slide-A-Lyzer dialysis cassette with a molecular weight cut-off of 3,500 Da. The buffer used was 1 liter of 1 X modification buffer (80 mM sodium phosphate dibasic, 50 mM NaCl, pH 7.4). The dialysis was performed for 20 h at 4 ºC for with a buffer replacement at 3 and 6 h from the beginning of the dialysis. The biotinylated protein was placed in aliquots and stored in a nitrogen tank.

The dissociation constant was determined *in vitro* using 70-80 % confluent human endothelial cells cultured in 24-well plates. In order to promote the externalization of the PS molecules on the cells, 1 mM H_2O_2 was added to the cells and incubated for 1 h at 37 ºC, 5 % CO_2. For each concentration of annexin V studied, three data points were obtained and averaged. Prior to the protein incubation, the cells were fixed with 100 µl/well of PBS buffer containing 0.25 % glutaraldehyde. The excess of aldehyde groups were quenched by incubating with 100 µl/well of 50 mM NH_4Cl diluted in PBS buffer for 5 minutes at room temperature. The biotinylated annexin V

was diluted to several concentrations, and it was incubated for 2 h at 37 ºC, 5 % CO_2 in the incubator. BSA (0.5 %) diluted in PBS buffer was used to dilute the protein. For the specific binding, 2 mM CaCl was added to the PBS. For the non-specific binding, the calcium was depleted from the cells by adding 5 mM EDTA. Following the 2 h incubation, the wells were washed four times with 300 µl of 0.5 % BSA diluted in PBS buffer. Streptavidin-HRP (300 µl, 2 µg/ml) were added and incubated for 1 h at room temperature. Further wash was done four times with 300 µl of PBS buffer. O-phenylenediamine (300 µl, OPD) was then added to each well and incubated for 30 minutes at room temperature in the dark to minimize OPD color change. The absorbance was measured at 450 nm using the microtiter plate reader. A Forma Scientific incubator was also for the cell incubation (Forma Scientific, Inc., Marietta, OH).

APPENDIX R

Anesthetic Procedure

In order to anesthetize the animals, the respective cage was open from the top and without removing the top lid completely; the mouse was captured by grabbing its tail. The animal was then placed on top of the blue mat, allowing it to grab it with its front legs. The animal was then grabbed by the back of his head, and its tail was also immobilized using the left hand. This allowed for the intraperitoneal (i. p.) injection of the anesthetic. The i. p. injections were done by placing the needle a few millimeters into the body of the organism in a specific region. In order to find that region located at the lower part of the animal's abdomen, it is important to visualize two imaginary lines that will intersect. The first line can be visualized along the midsagittal plane (a vertical plane that goes through the midline of the body) of the body, while the second line will be oriented using the transverse plane (plane that passes horizontally across the body and perpendicular to the midsagittal plane). The intersection of both lines on the abdomen region and just above the lower members gives us an imaginary point, which will be used as an orientation mark. From this position, it is measured around 5 mm in diagonal towards the left or right bottom quadrant (Figure Q.1).

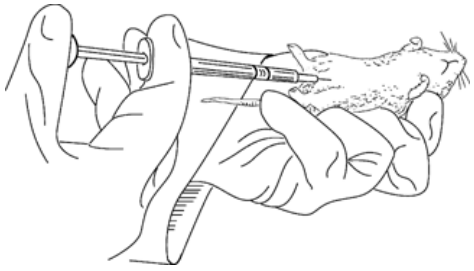


Figure R.1: Illustration showing the method used for the i.p. injections [154].

This will determine the point of injection. Changes to this location are not encouraged and can actually be hazardous and compromise vital organs. Also, the depth of penetration of the needle should not be too deep.

After injecting the entire volume of the anesthetic, the mouse was placed back in the cage allowing some time for the mouse to become completely immobilized. Generally, this occurs between 5 to 10 minutes after the i. p. injection. Multiple injections for several animals can be done sequentially in order to maximize the number of animals being immobilized during the entire session.

APPENDIX S

Tail Vein Injections

For the tail vein injections, 30 gauge needles and syringes were used. In order to facilitate this process, the tail of each mouse was placed in a 2 L beaker filled with warm water for 30 seconds. This step allows for the dilatation of the tail veins, making it easier to inject into the veins. Each mouse has 2 tail veins – left and right veins (Figure R.1).

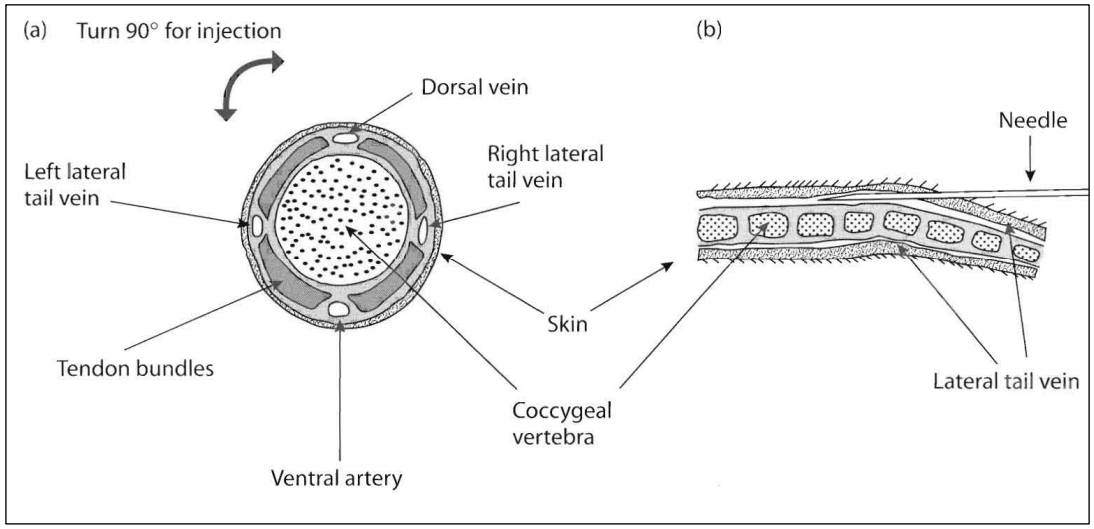


Figure S.1: Mouse tail anatomy [155].

After dilating the veins, the mouse was placed on the bench, the tail was cleaned and the solution was injected. The injection used 150 µl of the solution per animal. In case of failure to inject the solution into the vein, an accumulation of the solution was visible under the skin. When that happened, the injection on that particular site was aborted, and a different spot was chosen to inject the solution. It is not recommended to

attempt more than three times per vein, in order to maintain the integrity of the vein. When the injections are successful it is possible to see the solution entering the vein and being transported into the abdomen. It is also important to mention that all of the safety protocols were followed and for each animal, a different set of needles and syringes were used in order to avoid any contamination or disease propagation between the individuals. If bleeding occurred after injecting into the tail vein, pressure was applied on that spot for some time until the bleeding completely stopped. After injection, the animal was placed in the cage again. After a certain amount of time (which varied between individuals but never exceeded 1 hour), the animals were fully awake and restored the march completely.

APPENDIX T

Biodistribution study

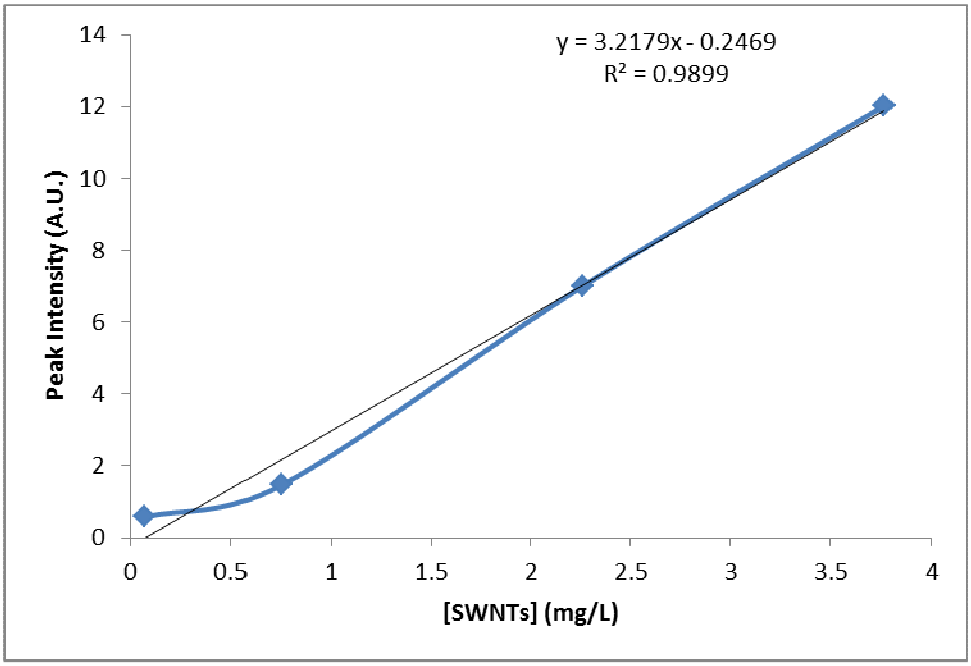


Figure T.1: Standard curve as a function of the G band peak intensity at 1,590 cm^{-1} vs. nanotube concentration. The SWNTs were suspended in lysis buffer (1% SDS, 1% Triton-X 100, 10 mM DTT, 40 mM tris-acetate-EDTA buffer). The samples were placed in a Ge metallic disk and allowed to dry. The signal was acquired using 64 scans.